UNIVERSITY OF BASILICATA

International PhD Program

"Sciences, curriculum Applied Biology"

Functional characterization of Lamin A/C mutants involved in hereditary-familial cardiomyopathies for the development of personalized diagnostic and therapeutic approaches

SSD

BIO/09 Physiology

Coordinator:

Professor Patrizia Falabella

Tutor:

Professor Monica Carmosino

Co-tutor:

Professor Andrea Gerbino

PhD candidate:

Dr. Giusy Pietrafesa

XXXVI CYCLE

Table of Contents

1. Abstract

Nuclear lamin A and C are important components of the multifunctional scaffolds that mechanically supports the inner nuclear membrane, providing nuclear and cytosolic rigidity. However, lamins escape to broader spectrum of functions beyond mere mechanics, also being associated with other physiological processes, such as modulating gene expression and intracellular signaling pathways. To further highlight its key role in cell physiology, mutations in the lamin A/C gene (*Lmna*) have been associated with a variety of pathological phenotypes with the skeletal muscles and the heart being the most affected systems. When affected, the heart can develop a wide range of phenotypes, from dilated cardiomyopathy with conduction defects (DCM-CD) to arrhythmogenic right ventricular cardiomyopathy. The variety of cardiac phenotypes is likely the consequence of the significant number of different *Lmna* mutations identified so far (1). Given the complexity of obtaining reliable genotype-phenotype correlations in *Lmna*-related diseases, it is crucial to functionally characterize each mutation to better understand its specific effects and tailor treatment strategies accordingly (personalized medicine). In this study, we analysed three different *Lmna* mutations to shed light on their specific pathogenetic mechanism at the cellular level. These mutations have been associated with different phenotypic outcome, all characterized by a consistent recurrence of dilated cardiomyopathy (DCM) with a poor prognosis.

The nonsense mutation LMNA Q517X abnormally aggregates at the nuclear envelope and within the nucleoplasm of HL-1 cardiomyocytes. In addition, LMNA Q517X-expressing cardiomyocytes are characterized by hyper-polymerized tubulin network, upregulation of acetylated α-tubulin, downregulation of Nav1.5 channels on the cell surface and significant changes in action potential parameters, indicating abnormal electrical properties. Further examination in HEK293 cells expressing LMNA Q517X with Nav1.5 shows a significant reduction in peak Na^+ current (I_{Na}) and altered channel kinetics. Treatment with colchicine, an FDA-approved tubulin assembly inhibitor, rescues cellular properties and channel kinetics in LMNA Q517X-expressing cardiomyocytes.

Then, we investigated the molecular basis of DCM associated with another nonsense mutation in *Lmna* gene, designated LMNA R321X, and explored potential pharmacological interventions that target the unfolded protein response (UPR). We demonstrated the activation of the PERK-CHOP pathway of the UPR and subsequent endoplasmic reticulum

(ER) dysfunction and apoptosis in HL-1 cardiomyocytes that stably express LMNA R321X. We assessed the effectiveness of three UPR-targeting drugs-salubrinal, guanabenz, and empagliflozin-in alleviating ER stress. Salubrinal and guanabenz function maintaining adaptive UPR state, reducing ER stress and pro-apoptotic markers, and restoring ER calcium handling. Empagliflozin suppresses apoptosis markers and inhibits the UPR by blocking PERK phosphorylation in LMNA R321X cardiomyocytes. Additionally, empagliflozin treatment restores endoplasmic reticulum (ER) homeostasis, allowing it to properly store and release intracellular calcium ions (Ca^{2+}). The study shows that various drugs targeting different stages of the UPR can effectively reduce pro-apoptotic pathways and maintain ER homeostasis in R321X LMNA-cardiomyocytes. It is noteworthy that guanabenz and empagliflozin, which are already in clinical use, offer promising therapeutic options for LMNA R321X-associated cardiomyopathies.

Finally, we investigated the molecular and cellular mechanisms underlying Emery-Dreifuss muscular dystrophy (EDMD), which is characterized by slowly progressive muscle weakness and wasting and DCM. We used a knock-in *Lmna*$^{H222P/H222P}$ mouse model carrying the LMNA p.H222P mutation, which recapitulates all the features of EDMD and also key features of cardiac laminopathies.

We observed altered tyrosinated α-tubulin network in muscle fibers of these mice compared to wild-type, indicating disrupted microtubule organization.

Here, we aim to understand how abnormal microtubule organization contributes to nuclear elongation through impaired interaction with microtubule-associated proteins (MAPs). Our investigation revealed distinct localization patterns of CLIP-170, a MAP, in the muscle fibers of *Lmna*$^{H222P/H222P}$ mice compared to wild-type. Pharmacological modulation of CLIP-170 activity with a neurosteroid restores CLIP-170 localization and nuclear morphology in the muscle fibers of mice carrying the LMNA p.H222P mutation, highlighting its therapeutic potential in improving EDMD-associated phenotypes.

Collectively, this thesis provides comprehensive insights into the pathogenic mechanisms of *Lmna*-associated cardiomyopathies and identifies potential therapeutic strategies, ranging from tubulin-targeting agents to UPR modulators and CLIP-170 regulators, offering hope for the development of effective treatments for these devastating diseases.

Riassunto

Le lamine nucleari A e C sono componenti importanti dell'impalcatura multifunzionale che sostiene meccanicamente la membrana nucleare interna, fornendo rigidità nucleare e citosolica. Tuttavia, le lamine nucleari, oltre a fornire integrità cellulare e nucleare contro segnali meccanici, sono coinvolte in notevoli processi fisiologici, quali la modulazione dell'espressione genica e la regolazione delle vie di segnalazione intracellulare. Per evidenziare ulteriormente il loro ruolo chiave nella fisiologia cellulare, le mutazioni nel gene della lamin A/C (*Lmna*) sono state associate a una varietà di fenotipi patologici, con i muscoli scheletrici e il cuore come sistemi più colpiti. Quando è colpito, il cuore può sviluppare un'ampia gamma di fenotipi, che vanno dalla cardiomiopatia dilatativa con difetti di conduzione (DCM-CD) alla cardiomiopatia aritmogena del ventricolo destro. La varietà di fenotipi cardiaci è probabilmente la conseguenza del numero significativo delle diverse mutazioni di *Lmna* identificate finora (1). Data la complessità di ottenere correlazioni genotipo-fenotipo affidabili nelle malattie correlate al gene *Lmna*, è fondamentale caratterizzare funzionalmente ogni mutazione per comprendere meglio i suoi effetti specifici e adattare di conseguenza le strategie di trattamento (medicina personalizzata). In questo studio abbiamo analizzato tre diverse mutazioni del gene *Lmna* per far luce sul loro specifico meccanismo patogenetico a livello cellulare. Queste mutazioni sono state associate a diversi aspetti fenotipici, tutti caratterizzati dall'insorgenza di cardiomiopatia dilatativa (DCM) con prognosi infausta.

La mutazione *non senso* LMNA Q517X si aggrega in modo anomalo nell'involucro nucleare e nel nucleoplasma dei cardiomiociti HL-1. Inoltre, i cardiomiociti che esprimono LMNA Q517X sono caratterizzati da una rete di tubulina iper-polimerizzata, da una sovraespressione dell'α-tubulina acetilata, da una ridotta espressione dei canali Nav1.5 sulla superficie cellulare e da cambiamenti significativi nei parametri del potenziale d'azione, che comportano anomalie delle proprietà elettriche. Inoltre, quando espressa nelle cellule HEK293 con Nav1.5, la variante mutata LMNA Q517X determina una riduzione significativa del picco di corrente Na^+ (I_{Na}) e un'alterazione della cinetica del canale. Il trattamento con colchicina, un inibitore dell'assemblaggio della tubulina approvato dalla FDA, ripristina le proprietà cellulari e la cinetica del canale nei cardiomiociti che esprimono LMNA Q517X.

Inoltre, abbiamo studiato le basi molecolari della DCM associata ad un'altra mutazione *non senso* del gene *Lmna*, denominata LMNA R321X, ed esplorato potenziali interventi farmacologici che hanno come bersaglio l'Unfolded Protein Response (UPR: risposta a proteine malpiegate). Abbiamo dimostrato l'attivazione della via PERK-CHOP dell'UPR, nonché la conseguente disfunzione del reticolo endoplasmatico (ER) e l'apoptosi nei cardiomiociti HL-1 che esprimono stabilmente LMNA R321X. Abbiamo valutato l'efficacia di tre farmaci mirati all'UPR - salubrinal, guanabenz ed empagliflozin - nell'alleviare lo stress ER. Il salubrinal e il guanabenz sono in grado di mantenere un UPR adattivo, riducendo lo stress ER, i marcatori pro-apoptotici e ripristinando la dinamica del calcio nel ER. Empagliflozin sopprime i marcatori di apoptosi e inibisce l'UPR bloccando la fosforilazione di PERK nei cardiomiociti LMNA R321X. Inoltre, il trattamento con empagliflozin ripristina l'omeostasi del ER, consentendogli di immagazzinare e rilasciare correttamente gli ioni calcio intracellulari (Ca^{2+}). Lo studio dimostra che vari farmaci che mirano a diverse fasi dell'UPR possono ridurre efficacemente le vie pro-apoptotiche e mantenere l'omeostasi dell'ER nei cardiomiociti LMNA R321X. È da notare che il guanabenz e l'empagliflozin, già utilizzati nella pratica clinica, offrono opzioni terapeutiche promettenti per le cardiomiopatie associate a LMNA R321X.

Infine, abbiamo studiato i meccanismi molecolari e cellulari alla base della distrofia muscolare di Emery-Dreifuss (EDMD), caratterizzata da debolezza e deperimento muscolare lentamente progressivi e da DCM. Abbiamo utilizzato un modello murino knock-in per $Lmna^{H222P/H222P}$ portatore della mutazione LMNA p.H222P, che ricapitola tutte le caratteristiche della EDMD e anche le caratteristiche chiave delle laminopatie cardiache.
Abbiamo osservato un'alterazione della rete dell'α-tubulina tirosinata nelle fibre muscolari isolate da questi topi rispetto ai topi wild-type, indicando un'alterata organizzazione dei microtubuli.
In questa sede, ci proponiamo di capire come l'organizzazione anomala dei microtubuli contribuisca all'allungamento nucleare attraverso un'alterata interazione con le proteine associate ai microtubuli (MAPs). La nostra indagine ha rivelato modelli di localizzazione distinti di CLIP-170, una MAP, nelle fibre muscolari isolate da topi $Lmna^{H222P/H222P}$ rispetto ai topi wild-type. La modulazione farmacologica dell'attività di CLIP-170 con un neurosteroide ripristina la localizzazione di CLIP-170 e la morfologia nucleare nelle fibre muscolari isolate dai topi portatori della mutazione LMNA p.H222P, evidenziando il suo potenziale terapeutico nel migliorare i fenotipi associati all'EDMD.

Nel complesso, questa tesi fornisce una visione completa dei meccanismi patogenetici delle cardiomiopatie associate a mutazioni del gene *Lmna* e identifica potenziali strategie terapeutiche, che vanno da agenti mirati alla tubulina a modulatori dell'UPR e regolatori di CLIP-170, offrendo una speranza per lo sviluppo di trattamenti efficaci per queste patologie devastanti.

2. Lamin A/C: from physiology to pathophysiology

2.1 Lamin A/C organization, maturation and assembly in the nuclear envelope

The nucleus of eukaryotic cell is a complex and dynamic organelle that serves as the control centre of the cell. It contains chromosomes and is responsible for DNA replication, RNA transcription and processing, and ribosome assembly. The functions of the nucleus depend on its structural organization and the formation of a membranous structure, the **nuclear envelope (NE)**, which separates the genome from the cytoplasmic environment (2,3). The NE consists of two concentric bilayers: the **outer nuclear membrane (ONM)**, and the **inner nuclear membrane (INM)**, separated by a narrow lumen, the **perinuclear space (PNS)**, which measures 20-40 nm (2,4). The INM and ONM are spanned by **nuclear pore complexes (NPCs)**, large supramolecular structures that mediate bidirectional macromolecular trafficking between the cytoplasm and the nucleus (5). The ONM is contiguous with the endoplasmic reticulum (ER) to the extent that it is considered a sub-compartment of the ER (2). In contrast, the INM is distinct because it contains a specific group of integral membrane proteins that perform tissue-specific functions (6) **(Fig.1).**

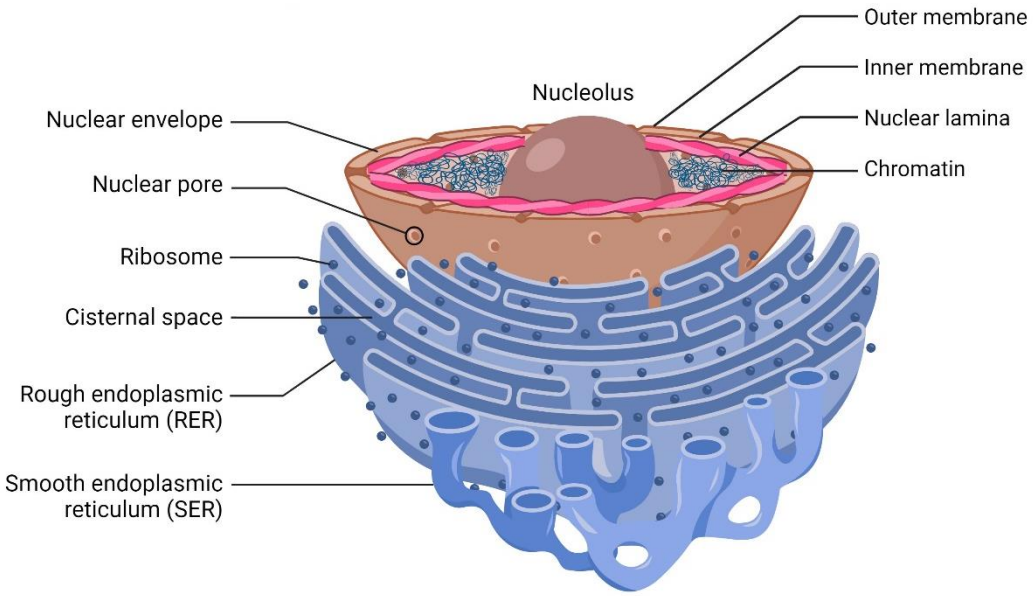

Figure 1: Nuclear Envelope Membrane (created with BioRender.com, adapted by (7)).

Under the nuclear membranes lies the **nuclear lamina**, an intricate protein meshwork that underlies the inner nuclear membrane (INM) on the nucleoplasmic side and is primarily responsible for nuclear and cytoplasmic stiffness (1,5,8,9). The nuclear lamina comprises peripheral and integral membrane proteins, such as lamins and lamina-associated proteins (10).

The **lamins** were first characterized biochemically as prominent 60 to 80 kDa proteins of the nuclear lamina and finally identified as intermediate filament (IF) proteins by sequence homology and the similar structural organization of the molecules (11,12). The name intermediate filament refers to the average diameter of the assembled intermediate fibres (10 to 12 nm), which lies between that of actin microfilaments (7 to 10 nm) and that of microtubules (25 nm). Nuclear lamins represent one (type V) of six subtypes of the IF superfamily, defined on the basis of genomic structure and nucleotide sequence. Lamins are exclusively found in metazoans and do not have any obvious homologs in the fully sequenced genomes of several lower eukaryotes, such as *Arabidopsis thaliana*, *Saccharomyces cerevisiae*, and *Schizosaccharomyces pombe* (13,14).

Based on their structural features, isoelectric points, behaviour during cell division and expression patterns in embryonic and adult tissues, lamins are typically classified into two main categories, A-type and B-type (15–17). The first group includes lamins A and C, as well as the minor isoforms AΔ10 and C2, all derived from the alternative splicing of the *Lmna* gene on chromosome 1q21.2-21.3. The second group comprises lamin B1, coded by the gene *Lmnb1*, and lamins B2 and B3 resulting from alternative splicing of the *Lmnb2* gene.

All lamins are characterized by similar amino acid sequences and molecular structure, but differ in molecular weight: *Lmna*-encoded lamins A, AD10, C correspond to 70, 66 and 61 kDa, respectively, and B-type lamin isoforms correspond to 67/68 kDa (8).

Like other intermediate filament proteins, lamins consist of three structural domains: a N-terminal head, a central coiled-coil region, and a large globular C-terminal tail. The N-terminal head is composed of an unstructured region of variable size. Instead, the central α-helical rod domain is highly structured, spanning almost half of the entire protein (approximately 350 residues), and is arranged in at least three α-helical segments (coil 1A, coil 1B, and coil 2) characterized by a typical coiled-coil heptad-repeat pattern and connected by short intermediate sub-domains termed L1 and L12 (18). The C-terminal tail domain contains an immunoglobulin-like (Ig) fold domain, the nuclear localization signal (NLS) required for their nuclear transport after synthesis in the cytoplasm, the chromatin

binding site and, except for Lamin C, a cys-aliphatic-aliphatic-any residue box (CAAX) (18–21) (**Fig.2**). The Ig-fold domain consists mainly of two β-sheets of five and four β-strands, respectively, connected by a short loop forming a compact β-sandwich (22).

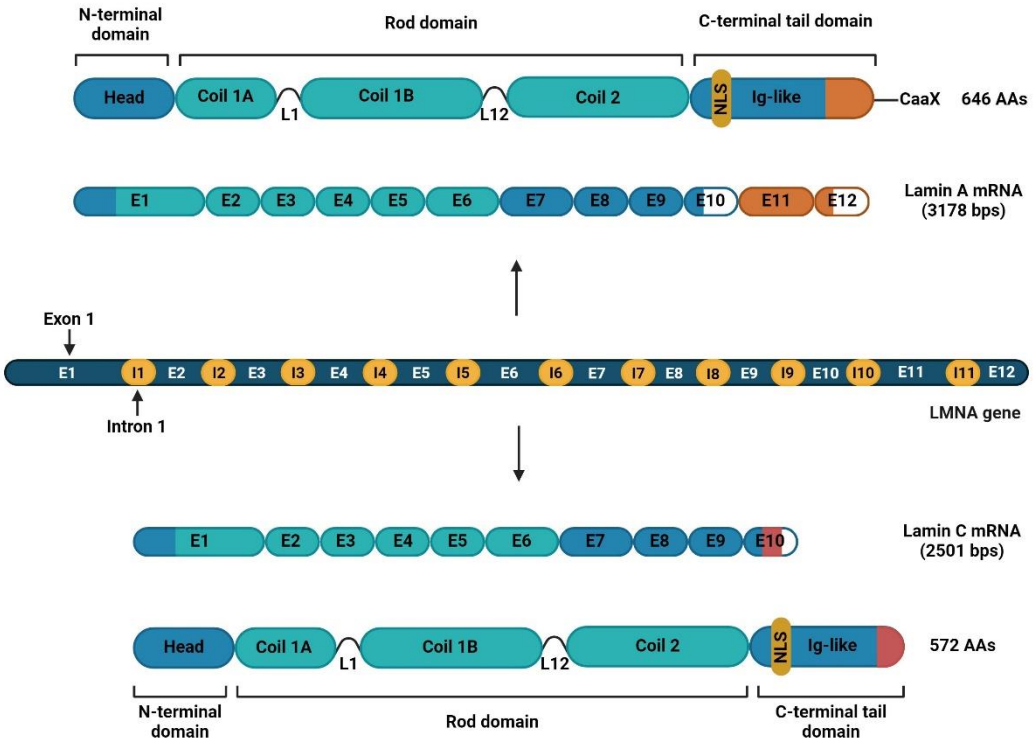

Figure 2: Structure of *Lmna* gene and its transcription variants by alternative splicing (created with BioRender.com, adapted by (8,23)).

The fundamental unit of the lamin is a dimer, consisting of two α-helical rod domains wrapped around each other, through a characteristic heptade amino acid repeat. The dimers then aggregate head-to-tail, forming antiparallel protofilaments (3,5 nm). In addition, the periodic and systematic distribution of the charged residues favours further lateral interactions of the protofilaments, resulting in intermediate filaments approximately 10 nm thick (9,18) (**Fig.3**).

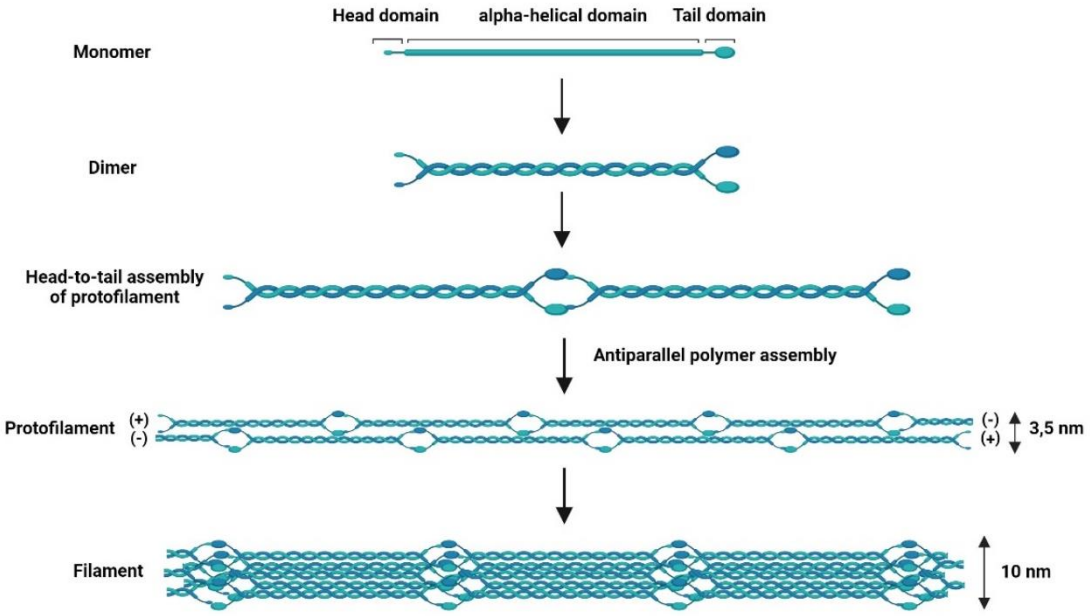

Figure3: Assembly and polymerization of lamin A/C monomers to form a 10 nm filament ((Created with BioRender.com, adapted by (13,18,24)).

Lamins A and C are identical for 566 amino acids and differ in the C-terminal domains and in the sequence of six amino acids (567-572) where GSHCSS in lamin A is replaced by VSGSRR in lamin C (25). In addition, lamin C (572 amino acids) is translated as a mature protein and lacks 98 C-terminal amino acids present in pre-lamin A, including the -CAAX box (26).

Instead, lamin A (646 amino acids) is initially translated in the pre-lamin A form characterized by a specific -CAAX box (CSIM) attached to the end of the C-terminal domain (27). Pre-lamin A undergoes post-translational modifications at the C-terminal "tail" domain to reach the mature form (26). In the first step of pre-lamin A processing, the farnesyltransferase enzyme (Ftase) adds a farnesyl group to the C-terminal cysteine. The last three residues (aaX)-peptide at the C-terminal end of lamin A are cleaved by a pair of prenyl protein–specific endoproteases: Zmpste24, also known as Farnesylated proteins-converting enzyme 1 (FACE-1) or RAS converting enzyme 1 (Rce1), also known as Farnesylated proteins-converting enzyme 2 (FACE-2). Then, the C-terminal cysteine is carboxymethylated by the isoprenylcysteine carboxy methyltransferase (ICMT). Lastly, the

carboxyterminal 15 amino acids of prelamin A, including the farnesylcysteine methyl ester, are clipped off by Zmpste24 and degraded, leaving behind mature lamin A (26,28) (**Fig.4**).

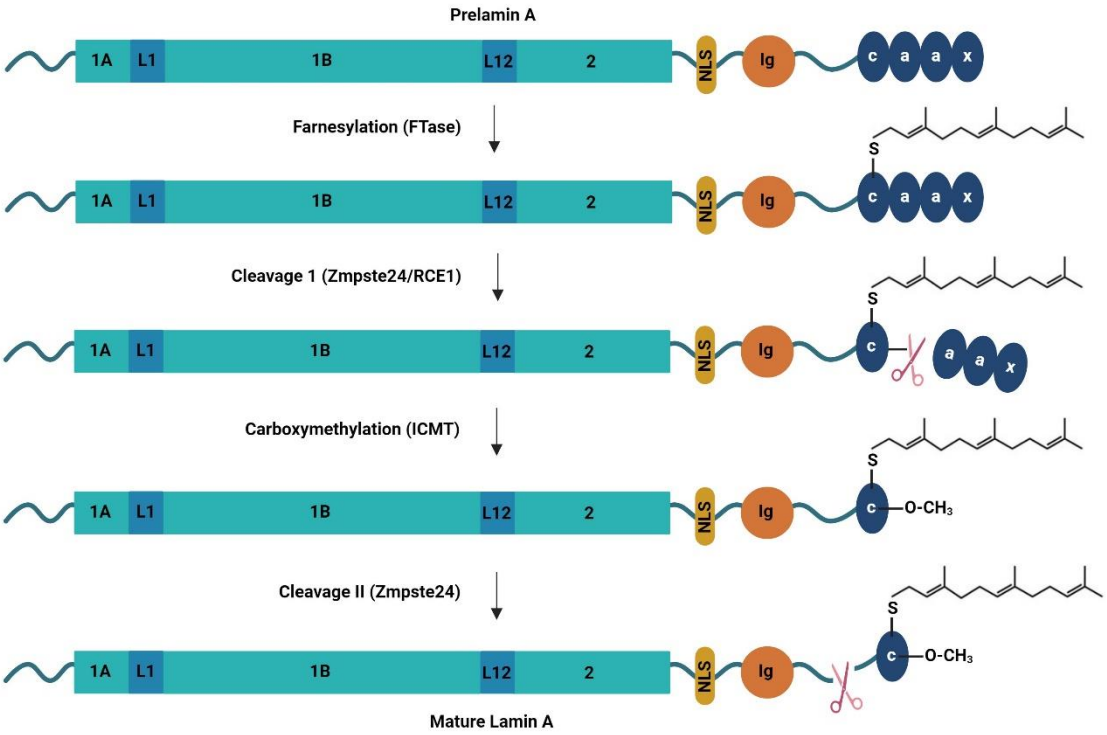

Figure 4: Prelamin A post-translational modifications during the maturation phase (created with BioRender.com, adapted by (24)).

At first glance, pre-lamin A processing could appear to be unnecessary, given that mature lamin A lacks these post-translational modifications. However, several studies have suggested that the post-translational processing steps play a role in the targeting of pre-lamin A to the nuclear envelope. The hydrophobic farnesylcysteine methyl ester probably assists in the delivery of prelamin A to the inner nuclear membrane, where Zmpste24 cleaves the C-terminus and releases mature lamin A (29).

Other post-translational modifications associated with lamins include phosphorylation, acetylation, ubiquitylation and SUMOylation (30). These modifications play an important role in maintaining nuclear structure, cellular functions and various signaling processes during the cell cycle (31). It is well documented that phosphorylation of lamins plays an

important role in the assembly and disassembly of lamins during mitosis, the regulation of nuclear import, their interaction with chromatin and the integration of signaling cascades. During mitosis, two sites on human Lamin A/C, Ser22 and Ser392, one at the N-terminal head and the other proximal to the rod domain, are phosphorylated by the protein kinase CDK-1, leading to lamin disassembly into dimers. In addition, phosphorylation of lamins at serine 22 and serine 392 renders them soluble, facilitating the formation and deformation of the lamina network and aiding in dynamic interactions with other proteins (32). Based on recent findings, it has been discovered that Ser22-phosphorylated (pS22) lamin A/C is primarily located in the nucleoplasm throughout all stages of the cell cycle. Furthermore, pS22-lamin A/C is physically associated with a specific subset of promoter-distal, enhancer-like elements, as well as with a *c-jun* transcription factor. The interaction between pS22-lamin A/C and these sites is linked to high transcriptional activity of local genes. These genes are abnormally upregulated in fibroblasts from patients affected by progeria and are responsible for most of the phenotypic aspects of this disease (33).

In addition, SUMOylation plays an emerging role in the regulation of protein function such as stability, localization and interaction with other proteins and chromatin. In familial partial lipodystrophy and familial cardiomyopathy, decreased levels of lamin SUMOylation (SUMO1 and 2) have been observed due to mutations in the *Lmna* gene (E203G and E203K) (34). Mutations in the *Lmna* gene can interfere with the correct post-translational modifications (PTMs) of lamin A, leading to its dysfunction and causing a group of inherited diseases known as laminopathies.

2.2 Expression Patterns of A- and B-Type Lamins

A-type and B-type lamins exhibit differential expression based on the cellular context and developmental stage (35,36). In human somatic cells, the primary lamins are A, C, B1, and B2. The isoforms AΔ10 are expressed in tumour cells (37), and C2 and B3 have only been detected in germ cells (38,39).

In particular, lamin B1 and B2 are ubiquitously present in embryonic and adult cell types and are essential for organogenesis and cell survival (40,41). Indeed, knockout mice for *Lmnb1* and/or *Lmnb2* die shortly after birth with severe defects in neuronal, lung and bone development (42,43). This essential role of B-type lamins in cell viability explains the limited number of mutations observed in the *Lmnb* genes and the consequent lower number of associated inherited diseases (44,45). However, lamin B1 may be involved in cellular senescence as it is lost in senescent cells (46).

In contrast, A-type lamins are mainly present in differentiated cells. During mouse embryonic development, lamin A/C expression is first detected on the 9th day in extra-embryonic tissue and on the 12th day in the embryo in muscle cells of the trunk, head, and the appendages. Three days later, it is also observed in cells of the epidermis, coinciding with the time of stratification. Lamins A/C do not appear until well after birth in lung, liver, kidney, and intestine, as well as in the heart and brain (47,48). Its expression is generally low or absent in embryonic carcinoma cells (49,50). The presence of A-type lamins in differentiated cells indicates that they may play a role in restricting developmental plasticity by preserving the differentiated phenotype of the cell (47).

While the absence of B-type lamins is incompatible with cellular life, the presence of various A-type lamin mutations causing laminopathies suggests a less critical role for A-type lamins in cell viability. However, lamin A knockout mice showed alterations in the nuclear envelope and distribution of emerin, leading to postnatal growth retardation and death within eight weeks of birth (51). Furthermore, a significant number of mice with Hutchinson-Gilford Progeria Syndrome (HGPS) mutation ($Lmna^{HG/HG}$), which express progerin, displayed human HGPS phenotypes and died at 27 weeks of age (52).

In 2013, Swift et al. demonstrated that the expression of lamin A in the nuclear envelope changes across various tissue types based on their respective levels of stiffness. Tissues subject to significant physical stress, such as muscles and bones, exhibit elevated levels of lamin A/C. Conversely, soft tissues like bone marrow and brain cells display lower

expression of lamin A due to their reduced stiffness. Furthermore, the authors showed that stem cell differentiation into fat was enhanced by maintaining low levels of lamin A/C, whereas differentiation into bone was enhanced by high levels of lamin A/C expression (53). In a separate study, it was found that lamin A/C expression was completely absent in stem cells of the adipose tissue in humans. However, after exposure to cardiomyocyte extracts, these cells differentiated into beating cardiomyocytes expressing primary markers of differentiation such as sarcomeric alpha-actinin, desmin, and cardiac troponin I, as well as lamin A/C expression. In fact, nuclear lamin A/C expression is considered a marker of terminally differentiated cells (54).

The study of the interactome of lamin A/C in different cell lines did not show any differential lamin A/C patterns of interaction dependent on tissue types (55). As demonstrated by Swift et al., the high and specific expression of lamin A/C in skeletal muscles and heart makes the physiological role of lamin A/C relevant in these tissues. Here, lamin A/C acts as a molecular mechanostat that is related to tissue stiffness and stress. It confers protection against stress-driven rupture of nuclei and systematically affects lineage determination (53).

2.3 Functional role of Lamin A/C in health and disease

Nuclear lamins are the major architectural proteins of the nuclear matrix, supporting the structural integrity and mechanical stability of the nuclear envelope. In addition, nuclear lamins enable a variety of other functions, including mechano-transduction, chromatin organization, DNA repair and replication, regulation of gene expression, regulation of mediators of various cellular signaling pathways, and cytoskeletal interactions (8,56–59). To perform these functions, lamin A/C interacts directly or indirectly with more than 100 cytosolic and intra-nuclear membrane/nucleoplasmic proteins (60). Proteomic analysis has identified several nuclear **envelope transmembrane proteins (NETs)** that interact with lamins and genomic proteins (6) (**Fig. 5**).

LaminA/C-binding partners can be divided into three groups:

1) proteins that bind lamins to the nuclear envelope, chromatin, or other subnuclear structures, providing mechanical support to the nucleus;
2) signal transduction molecules are involved in the regulation of many cellular functions, including cell differentiation and homeostasis.
3) proteins that regulate chromatin localization and gene expression (8).

The unexpected involvement of lamins in a wide range of physiological processes sparked scientific interest and these proteins became the focus of a multidisciplinary field (1).

The primary family of lamin-binding proteins are the **LEM** domain proteins: **LAP2**, **Emerin** and **MAN1** (**Fig.5**). LEM domain is a motif of approximately 40 residues (61) shared by several INM and intra-nuclear proteins that have the ability to bind a conserved metazoan chromatin protein known as **Barrier to Autointegration Factor (BAF)**. The BAF protein is involved in chromatin organisation, nuclear assembly, and gene expression. It has been shown to cross-link DNA molecules and bind histones *in vitro* (62–64). LEM-domain proteins include not only emerin, MAN1, but also several isoforms of LAP2, LEM-2/NET25 and LEM 3, 4 and 5 (65). Among these, emerin and LAP2 are the most well-characterised.

Emerin is an integral inner nuclear membrane (INM) protein that preferentially binds lamin A/C. It also binds directly to BAF, which helps to maintain chromatin close to the nuclear envelope during cell interphase, inhibiting gene expression. Loss of emerin results in Emery-Dreifuss muscular dystrophy (8,66,67).

Lamin-associated polypeptide 2 (LAP2) is a family of six alternatively spliced isoforms. LAP2α, one of its isoforms, interacts with lamins A/C in the nucleus (68). During interphase, LAP2α translocates throughout the nucleus and moves to telomeric regions during mitosis

(5). Therefore, LAP2α tethers A-type lamins to intranuclear sites and cooperates with lamins in organizing chromatin (2). Furthermore, LAP2α has dual functions in nuclear envelope assembly (69) and in binding transcriptional regulators, which directly or indirectly affect gene regulation (70).

MAN1 binds BAF directly and DNA, and it is involved in TGF-β signaling (71,72).

Therefore, the tethering of chromatin to the nuclear envelope and the organization of chromatin structure at a higher level involves a complex interplay between lamin A/C, LEM proteins, BAF and possibly other INM proteins (5).

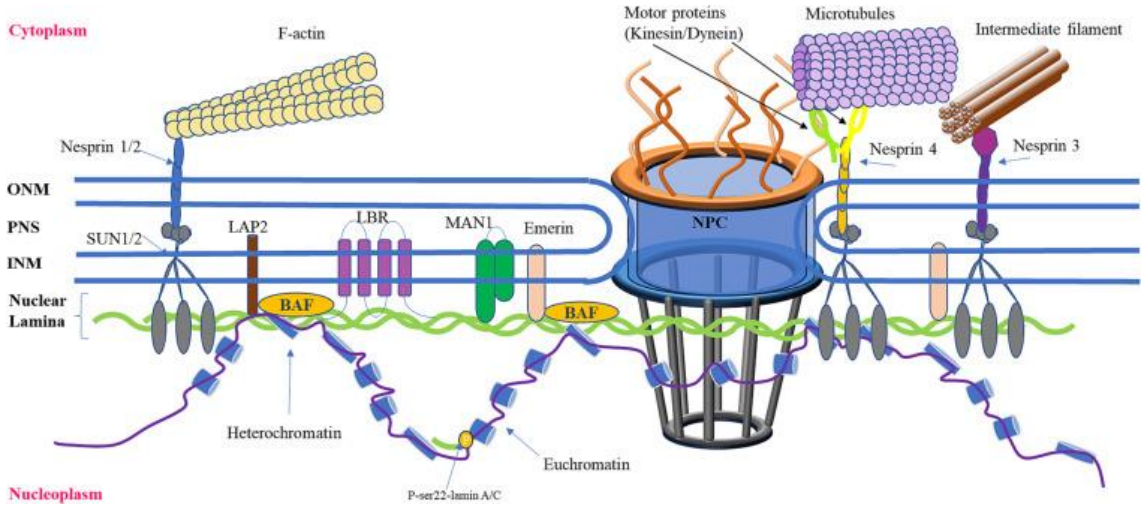

Figure 5: Lamin A/C binding-protein (4).

2.3.1 Nuclear envelope support

The focus of research on lamins has drastically changed over time. At first, lamins were primarily studied for their mechanical support role in cells and during mitosis (73,74). However, contemporary research has shifted focus, and now lamins are mostly studied for their involvement in laminopathies. According to the mechanical stress hypothesis, mutations in the gene or abnormal expression of lamin A/C can induce changes in nuclear morphology that weaken the nuclear lamina envelope, particularly in striated muscle cells that are under continuous mechanical stress (5). For instance, the heart, being a pumping organ, is subject to high mechanical stress. The α-helical coil of lamins in the nuclear lamina not only regulates downstream mechanical signaling, but also plays a crucial role in

cardiomyocyte contractile function. Moreover, it provides essential stiffness to resist nuclear deformation and protect against DNA damage (75,76).

Nikolova et al. (77) demonstrated that mice lacking the *Lmna* gene (*Lmna*$^{-/-}$) develop DCM characterized by abnormalities in nuclear shape and architecture. This confirms the importance of lamin A/C in maintaining normal nuclear shape. Additionally, these nuclei were found to be less resistant to biaxial mechanical stress applied to whole cells, indicating increased nuclear deformability and fragility in *Lmna*$^{-/-}$ cells. Impaired nuclear stability may cause nuclear rupture, leading to cell death. To investigate whether apoptosis could be responsible for cardiac dysfunction in *Lmna*$^{-/-}$ mice, serial assessment of DNA fragmentation in left ventricular tissue was performed in these mice. A significantly higher apoptotic index was found in *Lmna*$^{-/-}$ mice at 4-6 weeks of age compared to wild-type and heterozygous *Lmna*$^{-/+}$ mice (77). It has been suggested that cardiomyocyte apoptosis may play a role in disease progression, as observed in DCM and cardiac conduction disorders in humans (78,79). Furthermore, altered nuclear mechanics may also affect disease progression, in addition to the direct effect of nuclear disruption (5).

Expression of lamin A/C is high and specific in cardiac and skeletal muscle, reinforcing its physiological role in these tissues, providing protection against force-driven nuclear disruption (4).

2.3.2 Nucleo-cytoskeletal connections

Lamin A interacts with the cytoskeleton in the cytoplasm through the **LINC complex (Linker of nucleoskeleton and cytoskeleton),** a large protein complex consisting of **SUN domain proteins (Sad1, UNC-84)** and **KASH domain-containing Nesprins (Klarsicht, ANC-1, Syne Homology)** located at the inner and outer nuclear membranes, respectively (80,81) **(Fig.5).** Lamin A directly binds SUN domain proteins (SUN1 and SUN2), which, in turn, interact with a member of the Nesprin family of proteins. Nesprin-1, -2, -4 and KASH5 interact with key members of the cytoskeleton, such as intermediate filament (via plectin), actin and microtubules (via kinesin and dynein motor proteins) (82,83). This provides a link between the nucleoskeleton, the INM, the ONM, the sarcomere and the actin cytoskeleton (5).

The interaction of the LINC complex with nuclear lamins is dynamic and important for many physiological processes, including nuclear positioning, cell motility, cell division and development under both normal and pathological conditions (13,84).

Fibroblasts from mice with progeria-associated *Lmna* mutations exhibited deformed nuclei and overaccumulation of the protein Sun1, with deleterious effects on lifespan and various tissues (85). Evidence also suggests that proper expression and localisation of nuclear lamin A/C and associated LINC complex are required for proper actin-cytoskeleton function during cell differentiation (86). Studies also show that mutations in lamins A and C can disrupt LINC complex function and cause defects in skeletal and cardiac cells (87,88).

The major intermediate filament in cardiomyocytes is desmin, which connects myofibrils radially along Z-disks to sarcomeres, longitudinally to intercalated disks, and directly to the inner nuclear surface interacting with lamin A/C (5,89).

It is interesting to note that cardiomyocytes from $Lmna^{-/-}$ mice have a marked disorganisation of the desmin filaments and an increased PNS with regions in which the nucleus and the adjacent cytoskeleton are completely separated. In addition, $Lmna^{-/-}$ cardiomyocytes disproportionately increase in width when subjected to osmotic stress, suggesting that altered nuclear anchoring compromises the scaffolding function of desmin (77).

Effective mechanotransduction in cells requires intact physical and functional links between the nucleus and the cytoskeleton. Indeed, these data support a model in which altered nuclear-cytoskeletal coupling alters force transmission in cardiomyocytes, with consequent impairment of contraction and mechanical load on the nucleus (5).

Notably, consistent with the hypothesis that these changes in nuclear-cytoskeletal coupling may indeed be pathogenic is the finding of desmin disorganization in cardiac biopsy tissue from an individual with DCM and conduction system disease caused by a missense mutation in lamin A/C (90).

Furthermore, the lamin A/C N195K mutant variant, which causes DCM in transgenic mice, disrupts the organization of intercalated disks, sarcomeres, and gap junctions in mice cardiomyocytes (91). Intercalated disks are regions where the cell membranes of two adjacent cardiomyocytes are extensively intertwined and bound together by gap junctions and desmosomes. Intercalated disks play a crucial role in stabilising the positions of the cells in relation to each other, maintaining the 3D structural integrity of the tissue, and facilitating electrical signal propagation between cells. This ensures the proper functioning of the heart and efficient ejection of blood with each contraction. Disruption of intercalated disks has been observed upon expression of lamin A/C mutants. This may be responsible for the

conduction defects typically associated with DCM observed in both mutant lamin A/C transgenic models and lamin A/C mutant carriers.

Additionally, a second lamin-related protein network involving nesprins may regulate nuclear-cytoskeletal coupling. Loss of lamin A/C binding to nesprin could exacerbate desmin-induced changes in cytoskeletal tension (5).

Recently, mutations in *Lmna* gene causing DCM showed different degree of lamin A/C–Nesprin-2 interaction and causing LINC complex alterations (Yang et al., 2013), reinforcing the hypothesis that the disruption of the lamin A/C interaction with one or more elements of the LINC complex may affect the cytoskeleton-nucleus mechanotransduction (92).

2.3.3 Chromatin organization

Lamins can organize and regulate chromatin position within the nuclear envelope (93,94). Studies conducted on cardiomyocytes and mouse embryonic fibroblasts (MEFs) derived from *Lmna*$^{-/-}$ mice have shown a partial loss of peripheral heterochromatin, ectopic chromosome condensation, and mispositioned centromeric heterochromatin. This phenomenon has also been observed in cells expressing mutant lamin A proteins (51,77,95–98). Lamins contain at least two chromatin-binding regions: one in the tail region between the end of the rod domain and the Ig domain, and the other within the rod domain (99,100). Chromatin interactions are thought to be mediated by histones and **Lamin-A-associated domains (LADs)**, which contain sparsely transcribed genes (99).

The association of LADs with chromatin is known to influence gene expression regulation. LADs comprise a variety of differentiation-related genes that are either active or inactive depending on their association with chromatin. Gene expression is caused by the release of LADs from nuclear lamina, while their association with the lamina causes gene repression (101,102). However, *in vitro*, lamins bind non-specifically to DNA through contacts in the minor groove of the double helix (99,103).

In addition, lamin interacts with the epigenetic regulator **Inhibitor of Growth 1 (ING1)**. The ING proteins (ING1, 2, and 4) regulate apoptosis and remodel chromatin by binding to core histones, histone deacetylases (HDAC), and histone acetyltransferases (HAT). Han et al. (104) demonstrated that the **Lamin Interacting Domain (LID)** found in ING1 can bind and colocalize with lamin A. Disruption of this interaction contributes to the Hutchinson-Gilford Progeria Syndrome (HGPS) phenotype (104).

2.3.4 Participating in DNA repair

To investigate the role of lamins in DNA repair, researchers found that cells from patients with HGPS show delayed recruitment of the repair factor p53-binding protein (53BP1) to damaged DNA sites. These cells also show increased levels of the double-strand break marker γ-H2AX and are more sensitive to DNA damaging agents (105). Additionally, it was discovered that lamin A interacts with the DNA damage sensor, **ATR kinase**. This interaction is important for the formation of DNA repair foci in response to UV-induced DNA damage (106). Manju et al. (106) demonstrated that HeLa cells expressing mutants that cause progeria syndromes in vivo (lamin A del50, R471C, R527C and L530P) exhibit mislocalization of the ATR kinase and emerin, thereby disrupting the DNA repair machinery (106,107). *Lmna* mutations are believed to affect not only myofibers but also the efficiency of satellite cells in muscle repair and regeneration (108). This may increase nuclear fragility by disrupting the mechanical coupling between the cytoskeleton and the nucleus, leading to a greater susceptibility to physical stress, particularly in tissues exposed to mechanical strain such as skeletal and cardiac muscle (77,109,110).

2.3.5 Transcriptional regulation

Increasing evidence suggests that nuclear lamins can modulate gene expression, either by directly interacting with chromatin or by sequestering transcriptional regulators at the nuclear periphery (111–113). Lamin expression coincides with RNA polymerase II activity, which varies with developmental stage, and altering nuclear lamin organization can inhibit RNA polymerase II-dependent transcription (114). A-type lamin also associates with numerous other transcriptional regulators, such as *Rb*, *Gcl*, *Mok2*, *cFos*, and *Srebp1*, affecting gene expression by sequestering these factors or by influencing the assembly of core transcriptional complexes (113,115,116).

Retinoblastoma protein (Rb) is a transcriptional regulator that plays a central role in the control of the cell cycle and apoptosis by specifically binding to A-type lamins and LAP2α, when hypophosphorylated (117,118).

Similar to *Rb,* ***Mok2*** binds to the coil 2 region of A-type lamins. *Mok2* is a DNA-binding transcriptional repressor and competes with the cone-rod homeobox protein (*Crx*) transcription factors for binding sites and silences their activating genes (119). Additionally, *Mok2* binds RNA, suggesting that it may affect RNA processing (120). It is noteworthy that

A-type lamins have transcriptional repressor binding sites not only in their tail domain but also in their rod domain. To ensure optimal access to the sites in the rod domain, a specific oligomeric state (dimer, tetramer or octamer) or assembly (filamentous) may be necessary (70).

Instead, ***c-Fos*** is an early response transcription factor that is sequestered at the nuclear envelope by A-type lamins. During MAP kinase signaling, this association is released and *c-Fos* can regulate important cellular processes such as cell proliferation, death, survival, and differentiation (116,121–123).

Lastly, ***srebp1*** is a dual-specificity transcription factor of the basic helix-loop-helix-leucine zipper (bHLH-Zip) family involved in both the regulation of cholesterol biosynthesis and adipogenesis, including the expression of genes involved in fatty acid metabolism. *Srebp1* exists as two isoforms, *srebp1a* and *srebp1c*, produced by alternative splicing, which bind to the Ig-fold domain of the lamin A/C tail, as do many other partners. The binding of lamin A to *srebp1* was significantly reduced by familial partial lipodystrophy (FPLD) mutations. Interestingly, a mutation in autosomal dominant EDMD was also found to interfere with the interaction between lamin A and *srebp1*. While the physiological relevance of this interaction remains to be elucidated, these data raise the intriguing possibility that the fat loss seen in laminopathies may be caused, at least in part, by reduced binding of the adipocyte differentiation factor *srebp1* to lamin A (124).

2.3.6 Regulation of cellular signaling pathways

Lamin A/C is also involved in a variety of signaling pathways, including **mitogen-activated protein kinase (MAPK)**, **transforming growth factor beta-1 (TGF-β1)**, **protein kinase B/mammalian target of rapamycin complex 1 (AKT/mTORC1)**, **WNT/β-Catenin**, **myocardin-related transcription factor A/serum response factor (MRTF-A/SRF)** (1,5). The interaction of lamin A/C and associated proteins with signaling pathways is an important mechanism by which the NE regulates gene expression in cardiomyocytes. The discovery that signaling pathways are defective in several laminopathies will help us understand the role of lamin A/C in gene regulation in physiopathological states (5).

Studies in a single mouse model with a knock-in mutation in the lamin A/C gene (H222P), which causes muscular dystrophy and DCM (125), provide most of the evidence for all the pathways and specific targets modulated in striated muscle **(Fig. 6).**

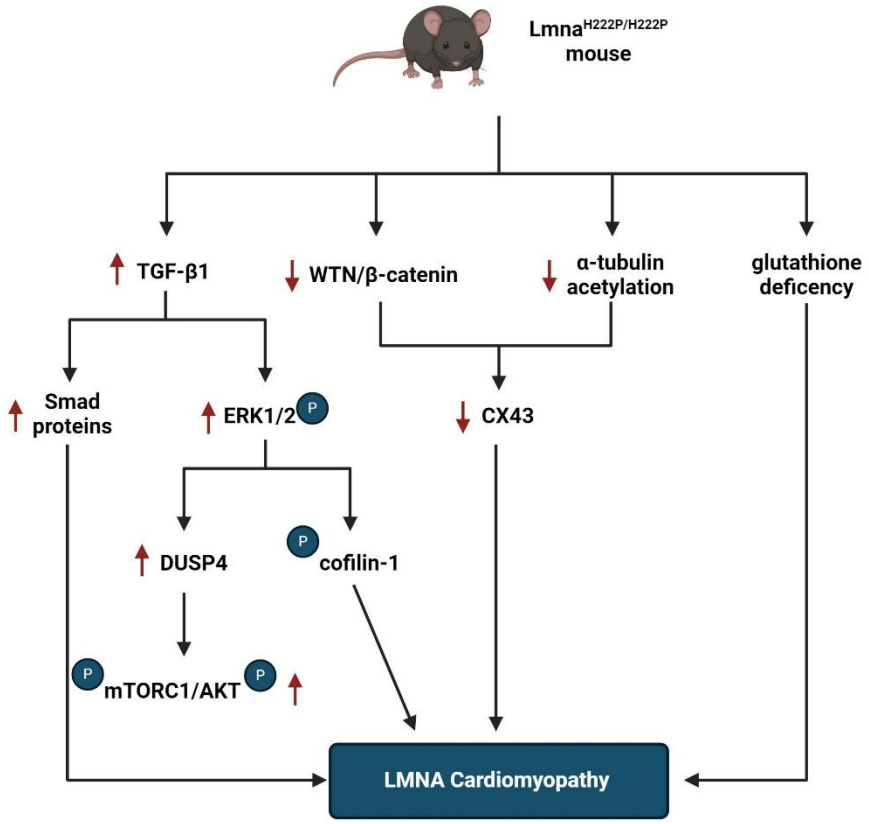

Figure 6: Diagram showing signaling mediators and cellular targets affected in hearts of *Lmna*$^{H222P/H222P}$ mice. Red arrows indicate the effects (increase/decrease) induced by the mutation in terms of expression level or activity (created with BioRender.com, adapted by (1)).

2.3.6.1 ERK1/2 Signaling

Lamins are well-known molecular scaffolds that bind to the nuclear envelope mitogen-activated protein (MAP) kinase extracellular signal-regulated kinase (ERK) 1/2 and its downstream transcription factor *c-Fos*. Changes in lamin A/C structure or function could affect nuclear envelope geometry, potentially impacting ERK1/2 activity and its downstream signaling targets. Increased ERK1/2 phosphorylation has been reported in the hearts of patients with cardiolaminopathy (126). In the hearts of *Lmna*$^{H222P/H222P}$ mice, hyperactivation of ERK1/2, JNK and P38α was reported before the onset of significant cardiac impairments (126,127). This suggests that hyperactivation of MAP kinases is a causative event of cardiac disease rather than a consequence. Genetic or pharmacological approaches to control ERK1/2 signaling in *Lmna*$^{H222P/H222P}$ mice had a beneficial effect on cardiac symptoms and

led to prolonged survival (127–130). Additionally, MAPKs activated several downstream target genes in the hearts of *Lmna*$^{H222P/H222P}$ mice (127,130,131). All these targets could potentially modulate the expression of additional genes involved in cardiac pathogenic mechanisms (132,133). The mechanisms through which LMNA H222P expression leads to hyperactivation of the ERK1/2 signaling pathway are currently under investigation. However, the activation of ERK1/2 in the heart of *Lmna*$^{H222P/H222P}$ mice was preceded by an increase in both transforming growth factor beta-1 (TGF-β1) and its nuclear effectors, the Smad proteins, which are key mediators of fibrosis and extracellular matrix deposition (131,134). Notably, treatment with a TGF-β receptor blocker decreased the amount of activated ERK1/2, suggesting increased TGF-β1 upstream ERK1/2 activation, as previously reported for other cardiac pathophysiological conditions (135).

Recently, Chatzifrangkeskou et al. (131) demonstrated that active cytosolic ERK1/2 can directly interact with and phosphorylate cofilin-1, a F-actin depolymerising factor. Phosphorylated cofilin-1 affects actin dynamics, which in turn leads to defective actin organization in sarcomeres and alterations in left ventricular contractile force generation. Left ventricular tissue from wild-type mice injected with adeno-associated viruses expressing cofilin-1 showed myofibrillar disruption similar to that observed in *Lmna*$^{H222P/H222P}$ mice. Therefore, pharmacological compounds capable of correcting defective actin dynamics could be used as a novel therapeutic approach to ameliorate left ventricular dysfunction in *Lmna*-mediated cardiomyopathy (131).

2.3.6.2 AKT/mTORC1 Signaling

ERK1/2 hyperactivation and nuclear sequestration have a direct consequence of increasing the expression of the dual-specific protein phosphatase 4 (DUSP4) in ventricular tissue of *Lmna*$^{H222P/H222P}$, along with left ventricular dilation markers (136–138). DUSP4 is an ERK1/2-specific phosphatase primarily located in the nucleus, where it regulates the ERK1/2 cascade at the nuclear level. It is worth noting that the deletion of DUSP4 gene improved heart function and prolonged survival in *Lmna*$^{H222P/H222P}$ mice (137). DUSP4 is currently the primary molecular link between MAP kinases and the hyperactivation of the protein kinase B/mammalian target of rapamycin complex 1 (mTORC1) signaling pathway in *Lmna*$^{H222P/H222P}$ mice (136). This is likely related to reduced autophagy, a physiological process in which the cell degrades damaged or excess cellular components through the lysosomal machinery. The autophagy is a key process for lifespan extension (139,140).

Strikingly, treatment with temsirolimus, a specific inhibitor of mTOR, restores autophagy and prevents cardiac defects in *Lmna*$^{H22P/H22P}$ mice (141).

Autophagy maintains cellular homeostasis by clearing damaged or toxic proteins and organelles. It promotes cell survival during periods of starvation or increased energy demand by recycling cellular components. In cardiomyocytes lacking lamin A/C, including senescent and non-functional lamin A/C-expressing cardiomyocytes, autophagy inhibition caused by m-TOR hyperactivation may lead to energy deficits or the accumulation of toxic proteins/organelles, resulting in senescence and eventual cellular death (5).

2.3.6.3 WNT/β-Catenin Signaling

Furthermore, the *Lmna*$^{H222P/H222P}$ mice exhibited reduced expression of WNT and β-catenin (126,138,142), two signaling mediators involved in several cellular mechanisms that lead to proliferation, differentiation, and apoptosis. β-catenin is typically phosphorylated, in the absence of WNT stimulation, by GSK-3β and degraded after ubiquitination by the proteasome. Upon activation of the WNT pathway, GSK-3β is inactivated, allowing β-catenin to accumulate in the cytosol and subsequently translocate to the nucleus. There, it forms a complex with transcription factors, which activate target genes. In the heart, β-catenin interacts with the gene encoding connexin-43 (Cx43), a crucial cardiac connexin, to enhance its transcription. In addition, β-catenin can interact with Cx43 as part of a multiprotein complex within the intercalated disk to stabilize its structure (138). The reduced Cx43 expression in *Lmna*$^{H222P/H222P}$ mice appears to be tightly dependent on deficient WNT/β-catenin signaling. The levels of Cx43 are restored by rescuing β-catenin pharmacologically blocking its specific inhibitor GSK-3β. Therefore, mice that lack Lamin A also exhibit decreased levels of cx43. Similarly, mutant mice homozygous for the LMNA N195K variation display conduction abnormalities due to altered expression and distribution of both cx40 and cx43, as well as misregulation of HF1b/Sp4, a transcription factor of the Sp family (91). Additionally, cx43 protein expression was reduced by approximately 40% in neonatal rat cardiomyocytes expressing LMNA E82K (143).

Furthermore, when considering the abnormal distribution of cx43 in cardiomyocytes and cardiac tissue from *Lmna*$^{H222P/H222P}$ mice, it is important to take into account the alterations of the cytoskeleton due to reduced acetylation of α-tubulin. Treatment with paclitaxel stabilised the microtubule network by increasing acetylation of α-tubulin. This, in turn,

improved the correct localisation of cx43 at intercalated disks, thereby improving conduction defects in *Lmna*$^{H222P/H222P}$ hearts (144).

Additionally, Rodriguez et al. (145) demonstrated that the cardiac phenotype associated with *Lmna*$^{H222P/H222P}$ is characterised by abnormal oxidative stress levels and glutathione deficiency. Pharmacological glutathione replenishment reduced cardiac oxidative stress damage and alleviated contractile dysfunction in *Lmna*$^{H222P/H222P}$ mice (145).

The findings from the *Lmna*$^{H222P/H222P}$ mice highlight the significant impact that a single mutation of a structural gene can have on cell signaling. This animal model emphasizes the need for the generation of new transgenic models to evaluate the impact of other mutations of lamin A/C. The collected information may aid in the discovery of the molecular mechanisms that underlie the functional complexity of this protein (1).

2.3.6.4 MRTF-A/SRF signaling

MRTF-A (also known as MAL or MKL1) is a mechanosensitive transcription factor with important roles in the cardiovascular system (146,147). The intracellular localization of MRTF-A is regulated by changes in actin polymerization (148,149). Normally, MRTF-A is localized to the cytoplasm by binding to cytoplasmic G-actin and constitutive nuclear export. Mitogenic or mechanical stimulation triggers RhoA-mediated actin polymerization, releasing MRTF-A from G-actin and exposing a NLS within the actin-binding domain of MRTF-A (150,151). Increased nuclear import, coupled with decreased export, leads to the accumulation of MRTF-A in the nucleus, where it co-activates SRF to turn on genes that regulate cellular motility and contractility, including vinculin, actin and SRF itself (152), as well as structural genes involved in conferring the myogenic phenotype, such as sarcomeric proteins (153).

Ho et al. (154) showed that heart sections from *Lmna*$^{-/-}$ and *Lmna*$^{N195K/N195K}$ mice had significantly reduced fractions of cardiomyocytes with nuclear MRTF-A, suggesting that impaired MRTF-A translocation is a general effect of lamin A/C loss (154). Furthermore, cardiac tissue from *Lmna*$^{-/-}$ mice had lower SRF and actin transcript levels than that of wild-type littermates, and activation of SRF expression in response to left ventricular pressure overload was impaired in *Lmna*$^{+/-}$ mice, demonstrating altered MRTF-A/SRF mechanosignaling *in vivo*. Notably, ectopic expression of the nuclear envelope protein emerin, which is poorly localised in LMNA mutant cells and is also associated with EDMD and DCM, restored MRTF-A nuclear translocation and rescued actin dynamics in mutant

cells. The mechanism by which lamin A/C and emerin regulate gene expression by modulating nuclear and cytoskeletal actin polymerisation may provide insights into the aetiology of the cardiac phenotype in many laminopathies (154).

2.3.6.5 Apoptosis, Endoplasmic Reticulum-Stress and Ca^{2+} Signaling

In response to mechanical or metabolic stimuli, specific *Lmna* mutations can significantly affect the dynamic equilibrium between cell death and survival. Cell death by apoptosis causes a continuous loss of myocytes and leads to altered cardiac conduction and dispersed refractoriness (155), potentially leading to sudden cardiac death (156). Furthermore, the reduction in cardiomyocyte content, likely compensated for by additional fibrosis, may provide a substrate for conduction block and re-entrant arrhythmias (155,157). Indeed, previous reports have shown that *Lmna* mutation carriers with conduction defects and arrhythmias have histopathological evidence of myocardial fibrosis involving the cardiac conduction system (158–160).

Altered expression of the lamin A/C mutation E82K in the nucleus of mouse heart tissue affected by DCM-CD compromises the integrity of the nuclear envelope, enlarges mitochondria, reducing their number of cristae, and increases the rate of apoptosis ninefold. In particular, expression of this mutant increases the expression of the first apoptosis signal receptor (FAS), leading to caspase-8/caspase-3 activation and cytochrome c caspase-9-dependent release from mitochondria into the cytosol (161).

Interestingly, the apoptotic fate seems to affect the conduction system cardiomyocytes earlier (162). Mechanical stress is unlikely to be significantly different in the myocytes that populate or surround the cardiac electrophysiological system. However, a different susceptibility to apoptosis may reflect intrinsic molecular properties that distinguish conduction system myocytes from atrial and ventricular myocytes.

Since lamin A/C sequesters *c-Fos* at the NE of fibroblasts and suppresses the DNA-binding activity of transcription AP-1 by affecting *c-Fos* and *c-Jun* dimerization (121), reduced levels of lamin A/C protein could have consequences for downstream transcription. It is possible that atrio-ventricular nodal myocytes, like other excitable neurons, are particularly sensitive to AP-1-mediated transcriptional regulation, including caspase activation and stress-induced apoptosis. Therefore, mutations that reduce lamin A/C levels may selectively activate pro-cell death signals in these specialised myocytes (163).

In addition, a heterozygous lamin A/C variant consisting of a 21-nucleotide in-frame duplication in exon 2 of the *Lmna* gene (c.418_438dup) has been identified in members of an Italian family and co-segregates with an arrhythmogenic cardiomyopathy of variable phenotype with high intrafamilial variability. In vitro characterization of this LMNA variant revealed reduced nuclear stability and altered nuclear-cytoskeletal coupling, resulting in increased susceptibility to nuclear breakage and stress-induced cardiomyocyte apoptosis as the main pathogenetic mechanism (164)

In addition, two nonsense mutations of lamin A/C (LMNA R321X and LMNA D243Gfs∗4), both segregating with cardiomyopathies with conduction defects, mislocalize and accumulate in the ER (165,166). Notably, the accumulation of LMNA R321X in the ER led to the unfolded protein response (UPR), which results in apoptosis (165,167). This pathway will be the subject of further discussion later in Chapter.5. Instead, the accumulation of LMNA D243Gfs∗4 in the ER did not induce neither UPR/ER stress nor apoptosis. The fact that the LMNA D243Gfs∗4 mutant was silent with respect to the UPR suggested that it accumulates in a more tolerated unfolded state, probably due to the absence of the entire coil 2b region involved in polymeric head-to-coil assembly of lamin monomers. However, accumulation of LMNA D243Gfs∗4 in the ER impairs intracellular Ca^{2+} oscillations in both the cardiomyocyte carrying the mutation and the cardiomyocyte directly coupled to it, indicating defective electrical coupling between these cardiac cells (166).

2.4 Laminopathies

In 1999, Bonne et al. demonstrated that mutations in *Lmna* cause the autosomal dominant form of Emery-Dreifuss muscular dystrophy, an inherited disorder that selectively affects the heart and skeletal muscles (168). Since then, over 450 mutations in the *Lmna* gene have been identified, causing 20 phenotypically distinct diseases, collectively known as laminopathies (4).

Laminopathies are classified as either "**tissue-specific laminopathies**", which affect striated muscles, peripheral nerves, or adipose tissues, or as "**systemic laminopathies**", which affect multiple tissues simultaneously, as in premature ageing syndromes (169).

Laminopathies that affect **striated muscles** comprise various clinical disorders that can manifest in childhood or adulthood. These include:

- Emery-Dreifuss muscular dystrophy (EDMD2, EDMD3);
- Limb-girdle muscular dystrophy type 1B (LGMD1B);
- Dilated cardiomyopathy with conduction defect (DCM-CD) (158,168,170,171).

Lmna mutations have also been associated with congenital muscular dystrophy in infants, with the heart often being affected (172).

Laminopathies that affect striated muscle exhibit significant phenotypic differences. However, since they all share significant myocardial alterations, they can be considered as a single disease called LMNA cardiomyopathy, with or without various types of skeletal muscular dystrophy **(Fig.7)** (173).

Lmna mutations causing striated muscle diseases are mostly missense mutations found in all exons of the gene. Mutations causing RNA splicing abnormalities, small deletions, and nonsense mutations leading to haploinsufficiency of A-type lamins have also been documented (173). Cardiomyocytes appear to be more vulnerable than skeletal muscle cells to lamin A/C haploinsufficiency in both patients and mouse models.

Genotype-phenotype correlations using the *Lmna* Universal Mutation Database (https://omim.org/entry/150330#title) indicate that 67% of nonsense and truncating mutations, which are putatively dominant and lead to lower lamin A/C levels, cause cardiac diseases without muscle involvement.

The different sensitivity to lamin A/C haploinsufficiency between the heart and skeletal muscles may be due to structural and functional differences between these two tissues. The heart contracts in a twisting manner, generating torsion, whereas skeletal muscles generate unidirectional shortening. Additionally, the cellular cytoarchitecture and nuclei positioning

are organized differently in cardiomyocytes compared to muscle cells, resulting in a unique force applied on cardiac nuclei. This is in contrast to myofibres. Furthermore, this may clarify the increased vulnerability of cardiac muscle to nuclear mechanical defects and deformations resulting from a loss of lamin A/C function (5).

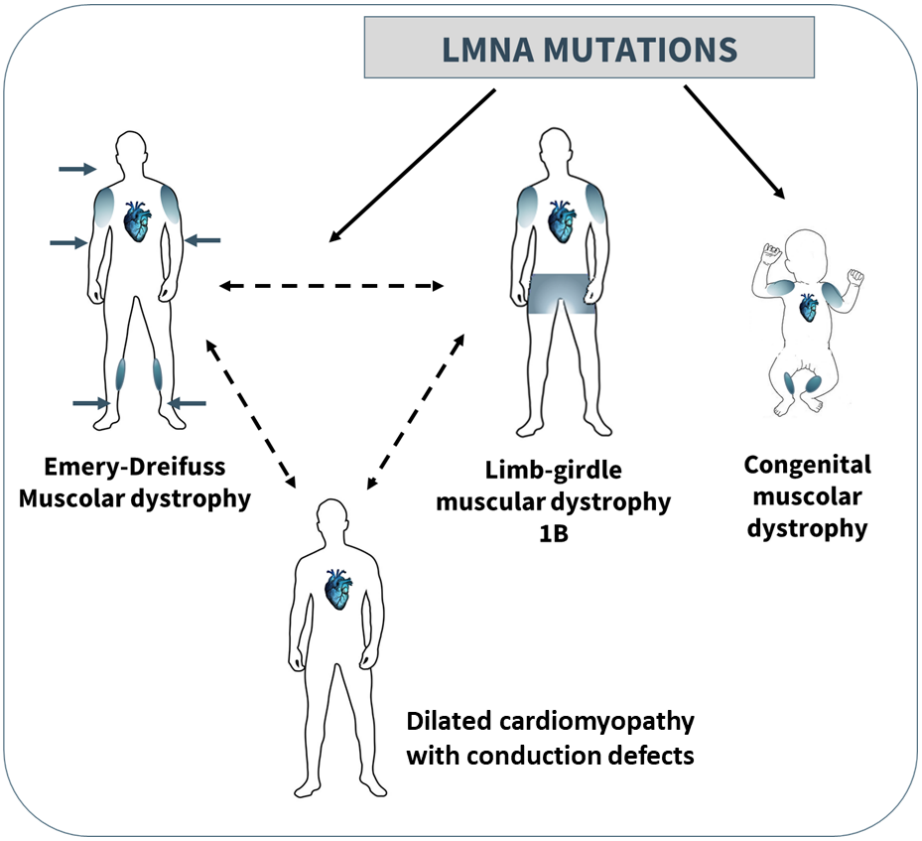

Figure 7: Laminopathies affecting striated muscles, adapted by (173).

Lipodystrophy syndromes comprise:

- Familial partial lipodystrophy type Dunnigan (FPLD2);
- Lipoatrophy with diabetes and other features of insulin resistance;
- Insulin resistance without lipoatrophy (174–176).

Forms of **peripheral neuropathy** include Charcot-Marie-Tooth disorder type 2B1 (CMT2B1) (177).

Accelerated aging disorders (progerias) comprise:

- Hutchinson-Gilford Progeria syndrome (HGPS),

- Atypical Werner syndrome (WRN-like),
- Restrictive dermopathy (DR),
- Variant progeroid disorders (173,178–182).

Additionally, there is a growing category of laminopathies that encompasses a variety of clinical scenarios in which two or more tissues are affected, including:

- striated muscles with partial lipodystrophy,
- striated muscles and peripheral nerves,
- peripheral nerves, striated muscles and lipodystrophy,
- lipodystrophy and progeroid features, such as MandibuloAcral Dysplasia (MADA) (183).

This group of disorders may be referred to as the 'overlapping laminopathies'. Due to the significant phenotypic overlap, it is suggested that the laminopathies represent a functional *continuum* of related diseases rather than separate disorders (13).

Three non-competing hypotheses could explain the etiology of laminopathies. The "**mechanical stress hypothesis**" suggests that the reduced nuclear rigidity due to Lamin A/C mutations could increase cellular susceptibility against recurrent mechanical stress and reduce mechano-transduction, especially in cells subjected to mechanical forces such as those of skeletal muscle and cardiomyocytes (5). On the other hand, the "**gene expression hypothesis**" proposes that mutation-induced defects in nuclear envelope proteins could lead to alterations in signaling pathways and abnormal control of gene expression, which in turn could be associated with skeletal muscle diseases (184) and cardiomyopathies (185). Finally, the "**chromatin hypothesis**" supports the idea that lamin A/C controls gene expression by regulating the compartmentalization of chromatin within the nucleus (186,187). Chromatin is anchored to the nuclear periphery by LADs, which are heterochromatic regions that overlap with euchromatic regions (188). Due to the role of lamin A/C in regulating chromatin compartments and dynamics, it has been proposed that certain *Lmna* mutations may alter cell type-specific chromatin interactions, leading to abnormal gene expression (189), particularly in LMNA-cardiomyopathies (102,190). However, experimental testing of this hypothesis in disease-relevant cellular models has only just begun (186,191).

2.5 LMNA cardiomyopathy: clinical features, diagnosis and treatments

Mutations in the *Lmna* gene can cause arrhythmogenic cardiomyopathies with high interfamilial heterogeneity. The most common form of this condition is DCM-CD (1).
DCM is defined as the presence of left ventricular dilatation and left ventricular systolic dysfunction in the absence of abnormal loading conditions such as hypertension, valve disease, or coronary artery disease that can cause global systolic impairment. Although right ventricular dilation and dysfunction may be present, they are not required for diagnosis (192) (**Fig. 8**).

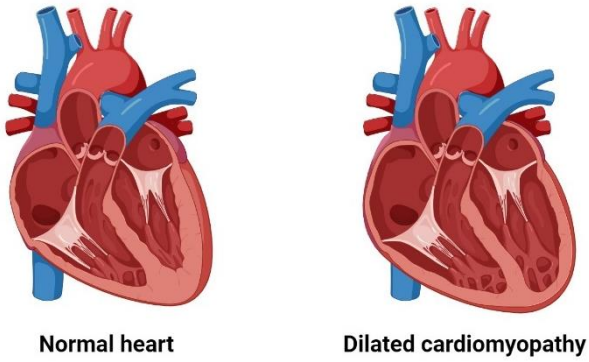

Figure 8: Morphology of normal heart and heart with left ventricular dilatation (dilated cardiomyopathy) (created with BioRender.com, adapted by (187)).

Lmna mutations occur in 6-8% of patients with DCM, and this frequency increases to 30% in patients with associated conduction defects (193). Although there are no established clinical criteria to differentiate LMNA-DCM from other DCM, the presence of conduction abnormalities or arrhythmias associated with ventricular dysfunction suggests *Lmna*-associated dilated cardiomyopathy, particularly if skeletal muscle involvement is present, regardless of degree (194). *Lmna* mutations responsible for DCM are transmitted in an autosomal dominant manner, meaning that the offspring of a patient have a 50% chance of

inheriting the genetic defect (195). However, there are also cases of autosomal recessive transmission, albeit at a very low frequency (170).

The onset age of cardiac manifestations in these diseases varies widely. The meta-analysis of 299 patients revealed that dysrhythmias tend to occur at an early age in *Lmna* carriers. Specifically, 18% of carriers experience dysrhythmias before the age of 10, rising to 36% in those aged 10-20 years, 74% in those aged 20-30 years, and 92% in those aged over 30 years. Arrhythmias were evenly distributed among carriers with either a neuromuscular or predominantly cardiac phenotype. In contrast, heart failure tends to appear later in life and less frequently than arrhythmias, with only 10% of patients experiencing it by the age of 30. However, this increases to 64% by the age of 50 (196). Penetrance is high and data suggest that 100% of mutation carriers are affected by the age of 60 years (197).

LMNA-DCM is characterized by left ventricular (LV) dysfunction and dilatation, often accompanied by arrhythmias and ECG abnormalities that precede the onset of ventricular dysfunction, as in all types of DCM. The initial symptoms of the disease may include conduction disturbances with or without symptoms of arrhythmia or heart failure, as well as thromboembolic events from ventricular mural thrombi (195).

LMNA-DCM is associated with a rapid and aggressive clinical course that can result in sudden cardiac death from malignant ventricular arrhythmias and end-stage heart failure at an earlier age than other familial cardiomyopathies (196–198). Adverse events typically occur by the fifth decade of life, with malignant ventricular arrhythmias being the most common cause of death, followed by end-stage heart failure (199). Approximately 70% of patients with LMNA-DCM will experience a cardiac adverse event within 5 years of diagnosis, primarily due to malignant arrhythmias (66%) or end-stage heart failure requiring heart transplantation (200).

In the natural course of the disease, conduction defects and rhythm disturbances may occur. These include atrioventricular block of any degree, bundle branch or fascicular blocks, minor intraventricular conduction delay, supraventricular arrhythmias such as atrial fibrillation, atrial flutter, paroxysmal supraventricular tachycardias, and supraventricular premature beats, as well as ventricular arrhythmias such as ventricular premature beats, sustained or unsustained ventricular tachycardias, and ventricular fibrillation (195).

Brodt et al. conducted an analysis of the temporal relationship between the onset of ECG changes and the onset of left ventricular (LV) dysfunction in carriers of *Lmna* mutations. The study found that the ECG changes preceded the left ventricular (LV) dysfunction by approximately 7 years. With the exception of one patient, all patients included in the study

had ECG changes at the time of diagnosis of left ventricular structural or functional abnormalities. ECG abnormalities can be an early indication of DCM caused by a *Lmna* mutation. Therefore, individuals at risk for LMNA cardiomyopathy with any ECG findings should undergo clinical surveillance at least once a year (199).

More than 90% of the carriers of a *Lmna* mutation develop dysrhythmia, including both bradyarrhythmias and tachyarrhythmias. Approximately half of these patients require either a pacemaker or an implantable cardioverter-defibrillator (ICD) to prevent sudden death (197,198). Although there is consensus regarding the efficacy of ICDs in the secondary prevention of sudden death in persons with cardiovascular disease and also in primary prevention in patients with a reduced ejection fraction (<35 percent), it is not yet known whether ICD therapy is efficacious as primary prevention in carriers of a lamin A/C mutation (201). Nearly half of the patients die suddenly before reaching the stage of overt heart failure (196,198).

According to Van Rijsingen et al. (202), male mutation carriers have a worse prognosis due to a higher prevalence of malignant ventricular arrhythmias and end-stage heart failure. Of note, the same gender correlation was found in the $Lmna^{H222P/H222P}$ mice model, displaying males more prominent abnormalities in cardiac function than females, and dying significantly earlier than female mice (203).

Lmna mutations have been associated with a combination of morpho-functional phenotypes between DCM and arrhythmogenic right ventricular cardiomyopathy (ARVC). ARVC is characterized by myocyte loss/fibro-fatty replacement, and reduction/absence of the intercalated discs of myocardium and LV noncompaction (164,204,205). *Lmna* mutation carriers are also associated with an increased risk of thromboembolic complications (206). This highlights the need for a new and broader classification of cardiac laminopathies (207).

Genetic testing is now available for DCM patients in many laboratories, using protocols for the most frequently involved genes in the disease's ethiopathogenesis. However, due to high costs and minimal influence on therapy, it is not routinely performed. Nevertheless, for *Lmna* mutations, the situation is changing due to the high risk of sudden death, making genetic analysis indispensable. Therefore, low-cost non-genetic diagnostic tests for LMNA-DCM are required (173,195). Narula et al. (208) proposed determining the expression levels of the *Lmna* gene in mRNA from peripheral blood samples. The levels were found to be significantly lower in patients carrying the mutation, with a sensitivity of 100% and a specificity of 87% in predicting *Lmna* mutation. Therefore, monitoring quantitative *Lmna*

gene expression in the peripheral blood of patients with cardiomyopathies could be a potential low-cost biomarker for the diagnosis of LMNA-DCM. (208).

At present, there is no specific treatment for laminopathies, including LMNA cardiomyopathy. The current clinical management strategies for patients with LMNA cardiomyopathy are identical to those for patients with other cardiomyopathies or heart failure. This includes symptomatic and supportive treatment with ventricular devices and pharmacologic therapies such as neurohormonal antagonists, diuretics for congestion, and vasodilators for hemodynamic unloading (209–211). Patients or carriers with LMNA-cardiomyopathy often require pacemaker implantation, and in cases where progressive conduction delays develop, an upgrade to an ICD may be considered (211–213). Although implantation of a defibrillator can prevent sudden death from arrhythmias, heart failure eventually becomes refractory to treatment, and heart transplantation is frequently necessary (209–212,214). As studies have shown that patients with LMNA cardiomyopathy have a worse clinical course compared to those without, identifying certain risk factors for sudden cardiac death among *Lmna* mutation carriers is crucial for more aggressive therapy and earlier pacemaker/defibrillator placement (197,215,216). The AHA/ACC/HRS (American Heart Association/American College of Cardiology/Heart Rhythm Society) recommends implanting a cardioverter-defibrillator (ICD) to prevent sudden cardiac death in cases of arrhythmogenic cardiomyopathy caused by an identified *Lmna* mutation, even in situations of mild left ventricular dysfunction (where LVEF is <50%) (217).

In cases of cardiomyopathy involving laminopathies, patients may require medication for seizures and spasticity due to neuropathy. Additionally, physical therapy and/or corrective orthopaedic surgery may be helpful for patients with muscular dystrophies (218–220).

These therapies increase the survival rate of affected patients. However, they only improve cardiac function and reduce the complications and secondary features of the disease without addressing the specific mutation causing the pathology. Unfortunately, the lack of insight into the underlying pathogenic mechanisms often hinders the design of patient-specific therapeutic approaches (1).

Research is being conducted to identify new targets and molecules for the treatment of laminopathy and *Lmna*-associated cardiomyopathy. This includes high-throughput drug discovery and exploring repurposed drugs.

The MAPK pathway and the mTOR pathway are the main therapeutic targets, as they are altered in *Lmna* mutation carriers (see section 2.3.6). For instance, the mTOR pathway,

which is involved in *Lmna* regulation by accelerating autophagy, can be inhibited by temsirolimus and rapamycin, leading to attenuation in DCM severity (136,141,221).

Instead, Selumetinib, developed by Array BioPharma, is a compound that targets MAPK signaling and rescues *Lmna*-associated DCM (142). Metformin is a MAPK signal-targeting compound that has been found to lower progerin levels in cells and improve the symptoms of progeria (222). Recently, a phase II trial began using ARRY-797, a selective oral inhibitor of the p38 MAPK, in patients with LMNA cardiomyopathy. The company's phase I trial demonstrated a favourable outcome for patients on ARRY-797, showing improved cardiac function on an echocardiogram. The trial's final outcome is yet to be determined. However, it exhibits a promising therapy for LMNA cardiomyopathy by reducing left ventricular dilatation and deterioration (www.ClinicalTrials.gov, Identifier NCT02057341).

Remodelin, an inhibitor of the enzyme N-acetyl transferase 10 (NAT10), has shown improvement in the phenotypes of HGPS. This suggests that NAT10 could be a potential target for HGPS (223).

Another therapeutic approach involves the use of compounds that induce translational read-through over the premature stop codon and restore the production of full-length proteins from the affected genes, such as PTC124. In this scenario, using cardiomyocytes derived from human induced pluripotent stem cells carrying different *Lmna* mutations (nonsense and frameshift), Lee et al. demonstrated that the effect of PTC124 is codon selective. A premature stop codon UGA appeared to be most responsive to PTC124 treatment (224).

Sayed et al. studied induced pluripotent stem cell–derived endothelial cells (iPSC-ECs) from a family carrying a mutation on *Lmna* causing DCM. They found down-regulation of Krüppel-like factor 2 (KLF2) as a potential transcription factor responsible for the EC dysfunction. Gain-of-function studies showed that treatment of LMNA iPSC-ECs with KLF2 agonists, including lovastatin, rescued the EC dysfunction. Patients with *Lmna*-related DCM treated with lovastatin showed improvements in clinical endothelial dysfunction as indicated by an increased reactive hyperemia index. Furthermore, iPSC-derived cardiomyocytes (iPSC-CMs) from patients exhibiting the DCM phenotype showed improvement in CM function when cocultured with iPSC-ECs and lovastatin (225).

One novel approach to treating progeria involves antisense oligonucleotide therapy (siRNA), which targets exon 11 and reduces the accumulation of prelamin A (or progerin), while promoting increased lamin C expression (226–228). Another study shows that microRNA-9 is present in the brain cells of mice to regulate lamin A expression but not lamin C (229). This suggests that miR-9 could be a potential tool to regulate prelamin A expression in other

organs, such as the heart. Some reports from in vitro and in vivo studies suggest that genome editing using CRISPR/Cas9 and Adenine Base Editors (ABE) technology could be promising for the treatment of progeria and HGPS.

Santiago-Fernández et al. and Beyret et al. independently demonstrated a reduction in progerin levels and an improvement in progeria symptoms in HGPS mice models by incorporating frameshift mutations with CRISPR/Cas9 technology via an adeno-associated virus 9 (AAV9) delivery vector (230,231). Sánchez-López et al. (232) have demonstrated that early-stage treatment can result in a cure. *In vivo* and *in vitro* applications of ABE have shown a reduction in the expression of progerin. This has resulted in an extension of the lifespan of mice and a rescue of nuclear blebbing and increased intracellular nitric oxide (NO) levels in respective studies (233,234).

Lamin A is involved in several cellular and molecular mechanisms that require further investigation to understand the cellular pathogenic mechanisms underlying *Lmna* gene mutations. This understanding is necessary to identify customised treatments for cardiolaminopathies.

3. Aim

The aim of this study is to elucidate at cellular level the molecular mechanisms associated with three *Lmna* mutations that co-segregate with DCM, characterized by a poor prognosis. This research aims to pave the way for identifying novel and patient-specific therapeutic targets. In particular, I focused my attention on the following mutations:

1. LMNA Q517X, a nonsense mutation caused by a heterozygous nucleotide substitution c.1549C > T in exon 9 of the *Lmna* gene resulting in the introduction of a premature stop codon and a truncated protein isoform. This mutation has been described in patients with severe arrhythmogenic cardiomyopathy with a history of sudden death.
2. LMNA R321X, a nonsense mutation which introduces a premature termination codon in the 6th of 12 *Lmna* exons, producing a truncated protein isoform in the central a-helical coiled-coil rod domain (coil 2B) of the lamin A protein. This mutation has been identified in several members of an Italian family affected by DCM with a poor prognosis.
3. LMNA p.H222P, a missense mutation caused by a nucleotide substitution c.665A>C in the *Lmna* gene. This mutation has been identified in a family with typical autosomal dominant Emery-Dreifuss muscular dystrophy (AD-EDMD). We used a mouse model carrying the LMNA p.H222P mutation, which develops muscular dystrophy and DCM-CD.

Using a multidisciplinary approach to functionally evaluate cardiomyocytes and muscle fibers, we unmasked the aberrant mechanisms caused by these mutations and proposed novel putative targets for patients-dependent therapeutic approaches.

This dissertation describes experimental evidence collected in collaboration with the Department of Biosciences, Biotechnologies and Environment of University of Bari "Aldo Moro," in which electrophysiological analyses were conducted on stable HL-1 clones expressing either LMNA Q517X or LMNA R321X mutation, reported in Chapters 4 and 5. The clinical description of patients carrying LMNA Q517X mutation and their genetic background was performed by our collaborators at the Department of Emergency and Organ Transplantation of University of Bari "Aldo Moro" and the ASST Grande Ospedale Metropolitano Niguarda Pathological Anatomy Center of Milano. Experiments on a mouse

model of EDMD, carrying the LMNA p.H222P mutation, were performed at the Centre de recherche en Myologie, of Paris and are reported in Chapter 6 of this dissertation.

The thesis is divided into three sections describing the background of each mutation and the methods used to collect the results. Each section concludes with a brief discussion, followed by general conclusions about the work done and future prospects.

4. Role of Nuclear Lamin A/C in the Regulation of Nav1.5 Channel and Microtubules: Lesson From the Pathogenic Lamin A/C Variant Q517X

Roberta De Zio[1], Giusy Pietrafesa[2], Serena Milano[1], Giuseppe Procino[1], Manuela Bramerio[3], Martino Pepe[4], Cinzia Forleo[4], Stefano Favale[4], Maria Svelto[1], Andrea Gerbino[1†], Monica Carmosino[2*†].

[1]Department of Biosciences, Biotechnologies and Biopharmaceutics, University of Bari, Bari, Italy

[2]Department of Sciences, University of Basilicata, Potenza, Italy

[3]ASST Grande Ospedale Metropolitano Niguarda Pathological Anatomy Center, Milano, Italy

[4]Department of Emergency and Organ Transplantation, Cardiology Unit, University of Bari Aldo Moro, Bari, Italy

Published in *Front Cell Dev Biol. 2022;10. (https://doi.org/10.3389/fcell.2022.918760)*

4.1 Abstract

In this work, we studied a *Lmna* nonsense mutation encoding for the C-terminally truncated Lamin A/C (LMNA) variant Q517X, which was described in patients affected by a severe arrhythmogenic cardiomyopathy with history of sudden death. We found that LMNA Q517X stably expressed in HL-1 cardiomyocytes abnormally aggregates at the nuclear envelope and within the nucleoplasm. Whole-cell patch clamp experiments showed that LMNA Q517X-expressing cardiomyocytes generated action potentials with reduced amplitude, overshoot, upstroke velocity and diastolic potential compared with LMNA WT-expressing cardiomyocytes. Moreover, the unique features of these cardiomyocytes were 1) hyper-polymerized tubulin network, 2) upregulated acetylated α-tubulin, and 3) cell surface Nav1.5 downregulation. These findings pointed the light on the role of tubulin and Nav1.5 channel

in the abnormal electrical properties of LMNA Q517X-expressing cardiomyocytes. When expressed in HEK293 with Nav1.5 and its β1 subunit, LMNA Q517X reduced the peak Na^+ current (I_{Na}) up to 63% with a shift toward positive potentials in the activation curve of the channel. Of note, both AP properties in cardiomyocytes and Nav1.5 kinetics in HEK293 cells were rescued in LMNA Q517X-expressing cells upon treatment with colchicine, an FDA-approved inhibitor of tubulin assembly. In conclusion, LMNA Q517X expression is associated with hyper-polymerization and hyper-acetylation of tubulin network with concomitant downregulation of Nav1.5 cell expression and activity, thus revealing 1) new mechanisms by which *Lmna* may regulate channels at the cell surface in cardiomyocytes and 2) new pathomechanisms and therapeutic targets in cardiac laminopathies.

4.2 Introduction

Lamin A/C (LMNA) are type-V intermediate filament proteins expressed by the majority of differentiated somatic cells. Both proteins are encoded by the same gene on chromosome 1q22 through alternative splicing events and targeted to the nucleus where they polymerize to form the nuclear lamina, which is a scaffold that underlies the inner nuclear membrane. This mesh of proteins plays multifunctional roles in cell biology. Nuclear lamins are pivotal for the maintenance of cellular and nuclear integrity and for correct intranuclear mechanotransduction, spatial organization of chromatin, regulation of signaling, and gene expression (1,5).

Hundreds of different mutations in the *Lmna* gene segregate with largely autosomal-dominant conditions identified as laminopathies. Mostly, these diseases affect specifically the striated muscle with a recurrent involvement of the heart. Notably, almost half of the LMNA cardiomyopathy patients succumb to sudden cardiac death as a result of a fatal arrhythmia, and conduction defects associated with LMNA mutations can substantially precede the onset of structural heart modification, meaning that subtle but fatal arrhythmias may occur before any noticeable change in the function (235).

Several hypotheses have been postulated to underlying the electrical abnormalities in the heart of laminopathy patients.

We demonstrated that either nuclear fragility or ER stress may increase the rate of apoptosis in cells expressing pathogenic LMNA variants (164,165). Recently, we also found proinflammatory cytokines deregulation in different LMNA mutant carriers with arrhythmogenic cardiomyopathies (236). Of note, either apoptosis or inflammation may in turn induce deposition of fibrotic tissue acting as an arrhythmic substrate. Moreover, the expression and the function of the connexin 43 have been found altered in cardiomyocyte *syncytia* (166,237). and mouse heart (144) expressing pathogenic variants of LMNA, thus accounting for conduction defects associated with those variants.

Electrical disturbance in the heart may also result from the defective electrical impulse generation due to ion channels remodeling of atrial and ventricular myocytes.

Some LMNA variants have been associated with changes in sodium currents. Olaopa and collaborators showed that variants R545H and A287Lfs*193 reduced the peak Na^+ current when co-expressed with Nav1.5 channel in HEK293 cells (238). The LMNA V445E mutant also reduced the peak current of I_{Na+} when co-expressed with Nav1.5 channel in HEK293 cells (239). Similarly, the expression of LMNA R399C mutant decreases the density of

cardiac sodium current in Nav1.5-expressing HEK293 cells (240). Recently, Salvarani et al. showed that iPSC-derived cardiomyocytes expressing LMNA K219T pathogenic variant have altered action potentials, reduced peak sodium current, and diminished conduction velocity (241).

On the other hand, both peak and late I_{Na+} were significantly increased in cardiomyocytes from *Lmna*$^{N195K/N195K}$ transgenic mice (242) with concomitant prolongation of Action Potential (AP) duration.

Of note, the mechanisms through which LMNA mutants may affect Nav1.5 trafficking and activity have not been always elucidated. Interestingly, an epigenetic effect of LMNA K219T variant acting through the *scn5a* gene silencing has been reported (241).

Overall, regardless of which theory better explains the etiology of cardiac arrhythmia in laminopathies, dissecting the pathogenic mechanisms at the cellular level would offer information on the mechanism by which this nuclear protein may regulate the electrical properties of cardiomyocytes and personalized therapeutic approaches in the field of laminopathies.

Here, we characterized a truncated LMNA variant, Q517X, a pathogenic LMNA variant shown to be associated with dilated cardiomyopathy with conduction abnormalities and neuromuscular disorders (243). In the family involved in our study, however, LMNA Q517X segregates with a severe cardiac phenotype and history of sudden death without any neuromuscular involvement, most likely because of the genetic background of the mutation carriers and environmental influences. The LMNA haploinsufficiency due to the non-sense-mediated decay of the messengers encoding for truncated LMNA variants has been proposed as one of the pathogenic mechanisms in carriers of *Lmna* nonsense gene mutations. However, we and others demonstrated the expression of the truncated LMNA variant in the tissues of the carriers (159,165). Accordingly, several studies performed on genotype–phenotype correlations in cardiac laminopathy demonstrated that truncation mutations are associated with more severe phenotypes and poor prognosis in LMNA mutation carriers because of the early onset of conduction disturbance, atrial fibrillation, malignant ventricular arrhythmias, and sudden death (215,244). Thus, unmasking the pathogenic mechanisms associated with the expression of C-terminal truncated LMNA variants in cardiomyocytes has high clinical relevance.

At the onset of the cardiomyopathy LMNA Q517X carriers presented sinus node dysfunction, first-, second-, and third-degree atrioventricular block and persistent atrial fibrillation. Years later DCM developed with ventricular arrhythmias and heart failure finally

occurred. Since the key pathogenetic mechanism in this cardiomyopathy seems to be the electrical disturbance in the atria, we analyzed the possible effect of LMNA Q517X expression in HL-1 cardiomyocytes. These cardiomyocytes possess a mixed phenotype between an atrial cardiomyocyte and a pacemaker cell, as evident by the ion channels expressed at the plasma membrane of these cells (245,246). Consequently, these cells can beat spontaneously in culture for the presence of If current, but the AP generation is due to Na^+ inward current through Nav1.5 channel as in adult atrial cardiomyocytes (247), thus providing a unique model to investigate the effect of this LMNA mutant in atrial automaticity.

4.3 Materials and Methods

4.3.1 Patients

The heterozygous nucleotide substitution c.1549C > T in exon 9 of the *Lmna* gene, introducing a premature stop codon (p.Q517X), was detected in a 36-year-old man referred to our Cardiomyopathy Unit, Cardiology Unit, Department of Emergency and Organ Transplantation, University of Bari Aldo Moro, Bari (Italy). He presented conduction system disorders, premature ventricular complexes, and left ventricle dilatation. Clinical evaluations and molecular analysis were proposed in all first-degree relatives of our index patient. The participants underwent a clinical workup including medical history, physical examination, 12-lead electrocardiogram (ECG), transthoracic echocardiography, and 24-h ECG monitoring. Written informed consent was provided by all participating subjects and was obtained by parents of the minor included in the study. This project was consistent with the principles of the Declaration of Helsinki and was approved by the Ethics Committee of the University Hospital Consortium, Policlinico of Bari, Italy.

4.3.2 Cell Culture

HL1 cardiomyocytes were cultured in Claycomb Medium (51800C, Sigma-Aldrich) supplemented with 10% fetal bovine serum (F2442, Sigma-Aldrich), Penicillin/Streptomycin 100 U/mL: 100 μg/ml (P4333, Sigma-Aldrich), 2 mM L-Glutamine (G7513, Sigma-Aldrich), and 0.1 mM Norepinephrine [(±)-Arterenol] (A0937, Sigma-Aldrich) in a humidified 5% CO_2, 95% O_2 incubator at 37°C.

HEK293 cells and HEK293T packaging cells were cultured in Gibco™ DMEM, high glucose, GlutaMAX™ (31966-021, Life Technologies™) supplemented with 10% Gibco™ Fetal Bovine Serum (10270-106, Life Technologies™) and 1% Penicillin-Streptomycin (10,000 U/mL,15140122, Gibco™, Life Technologies™) in a humidified 5% CO_2, 95% O_2 incubator at 37 °C.

Cell concentration and viability were assessed using Trypan Blue Stain, 0.4% with LUNA-II™ Automated Cell Counter (Logos Biosystems).

4.3.3 Generation of LMNA-Expressing HL-1 Stable Clones

HL-1 cells stably expressing LMNA WT or LMNA Q517X were obtained using Lentiviral transduction.

For viral particles production HEK293T packaging cells were plated at 30% confluence on 60-mm Petri dishes coated with Poly-L-lysine hydrobromide (2,636, Sigma-Aldrich). After 24 h, cells were co-transfected, using Invitrogen™ Lipofectamine™ 2000 Transfection Reagent (Invitrogen Corporation), with the plasmid encoding the protein of interest (either Lamin WT mCherry-tagged pLV [Exp]-Neo-CMV > mCherry (ns):hLMNA [NM_170707.4] or LMNA Q517X mCherry-tagged pLV [Exp]-Neo-CMV > mCherry (ns):hLMNA [NM_170707.4]*, Vector Builder, CA), two additional plasmids such as an envelope protein VSV-G-expressing plasmid pMD2G and a packaging plasmid pSPAX2-expressing Gag-pol and Tat viral proteins (Addgene) in OPTIMEM (Gibco™ Opti-MEM™). The day after the transfection the medium was replaced by 3 ml of fresh supplemented DMEM with penicillin–streptomycin. 24-h after, the virus-containing medium was harvested, clarified with 0.45-µm filter, and stored at −80°C, and 3 ml of fresh medium was re-added to the cells. After additional 24-h of incubation, the virus-containing medium was harvested again and pooled with that collected the day before.

For viral transduction, the HL-1 cells were plated in a 6-well plate at 30–50% of confluency, and after adhesion, they were incubated with 500 µl of virus-containing medium at 37°C in a humidified 5% CO_2 incubator for 18h. The cells were then incubated with 400 µg/ml Geneticin (G418, Gibco, Life Technologies) for 1 week to select stable clones.

4.3.4 Generation of Transfected HEK293 Cells for Patch Clamp Studies

HEK293 cells were transiently co-transfected with plasmids encoding LMNA WT or LMNA Q517X, the voltage sodium channel Nav1.5, and the Nav1.5 accessory β1 subunit using lipofection following the manufacturer's instructions (Invitrogen Corporation), 24 h before patch clamp experiments. Where described, HEK293 were transiently co-transfected with plasmids encoding LMNA WT or LMNA Q517X and the voltage K^+ channel KCNH2 (**Fig.17**).

The generation of the LMNA WT mCherry-tagged construct was previously described(165). The generation of the LMNA Q517X mCherry-tagged construct was performed by the

mutagenesis of the LMNA WT mCherry construct using the “Stratagene’s Quik Change II XL site-directed mutagenesis kit” KIT (Agilent Technologies, United States). The mutagenic primers were designed using the Quick Change Primer Design Program available online at www.agilent.com/genomics/qcpd/$. The mutation was verified by sequencing. Nav1.5 GFP-tagged and β1 subunit constructs were kindly provided by Paola Imbrici from Department of Pharmacy-Drug Sciences, University of Bari, Italy. GFP-tagged KCNH2 encoding plasmid was previously characterized by us (248).

4.3.5 Electrophysiological Recordings

Electrophysiological recordings were performed with the Patch Clamp technique in a whole-cell configuration using the Multiclamp 700B (Axon CNS-Molecular Devices, Sunnyvale, CA, United States) amplifier interfaced with the Axon Digidata 1,500 (Axon Instrument-Molecular Devices, Sunnyvale, CA, United States). Currents were sampled at 10 k Hz and low-pass filtered at 5 kHz. AxoScope 10.4 (Molecular Devices, Sunnyvale, CA, United States) and pClamp 10.4 (Molecular Devices, Sunnyvale, CA, United States) were used to acquire and analyze the data. After gigaseal formation and whole-cell access, pipette capacitance (Cp) and the membrane capacitance (Cm) were compensated adjusting the Cp fast and the Cp slow setting on the MultiClamp 700B. A Rs stable for the entire experiment and lower than 20 MΩ was considered acceptable. All recordings were performed at room temperature (26 °C) on HL-1 cardiomyocytes stably expressing either LMNA Q517X or LMNA WT and on HEK293 cells transiently co-transfected with the GFP-tagged Nav1.5 channel, its associated β1 subunit, and LMNA Q517X or WT-expression plasmids. Where described HEK293 cells were transiently co-transfected with GFP-tagged KCNH2 and LMNA Q517X or WT-expression plasmids. Fluorescent tags were used for selecting the transfected cells. Borosilicate patch pipettes were pulled to obtain tip resistances of 2–4 MΩ with the P-1000 Pipette puller (SUTTER INSTRUMENT, Novato, CA 94949, United States).

For the electrophysiological recordings on HL-1 cardiomyocytes, cells stably expressing either LMNA WT or LMNA Q517X were plated at low confluence, on 35-mm Petri dishes coated with gelatin-fibronectin (5 μg/ml Fibronectin, F1141, Sigma-Aldrich, in 0.02% Gelatin from bovine skin, G9391, Sigma-Aldrich), the day before the experiments. After complete cell adhesion, 10-μM Colchicine (C-9754 Sigma) was added to the complete

Claycomb media for an overnight treatment in a humidified 5% CO_2, 95% O_2 incubator at 37 °C, when required. HL-1 spontaneous action potentials were recorded using an extracellular solution contained (in mM): 138 NaCl, 4 KCl, 1 $MgCl_2$, 1,8 $CaCl_2$, 10 Hepes, 10 Glucose (pH of 7.4, adjusted with NaOH, and osmolarity of 290 ± 10 mmol/kg, adjusted with mannitol) and an internal pipette solution contained (in mM): 144 KCl, 2 $MgCl_2$, 10 Hepes, 5 EGTA (pH of 7.2 adjusted with KOH and osmolarity of 280 ± 10 mmol/kg, adjusted with mannitol). Spontaneous action potentials (APs) were recorded in current clamp mode without current injection and analyzed for the following parameters: amplitude (expressed in mV), overshoot (expressed in mV), upstroke (expressed as $\Delta V/\Delta t$), maximum diastolic potential (MDP, expressed in mV), and threshold (expressed in mV).

For the electrophysiological recordings on HEK293 cells transiently expressing either LMNA WT or LMNA Q517X, Nav1.5 channel and its β1 subunit were plated at low confluence the day before the experiments on 35-mm Petri dishes coated with Poly-L-lysine hydrobromide for 20 min at room temperature (2636 Sigma-Aldrich). After complete adhesion, 10-μM Colchicine (C-9754 Sigma) was added to the complete Glutamax media for an overnight treatment in a humidified 5% CO_2, 95% O_2 incubator at 37°C, when needed. The whole-cell Na^+ current (I_{Na}) in the HEK293 cells was recorded using a bath solution contained (in mM): 140 NaCl, 5 KCl, 1 $CaCl_2$, 1 $MgCl_2$, 10 HEPES, 5 Glucose (pH of 7.4, adjusted with NaOH, and osmolarity of 290 ± 10 mmol/kg, adjusted with mannitol) and an internal pipette solution contained (in mM): 140 CsCl, 10 NaCl, 10 HEPES, 1 EGTA, pH 7.4, adjusted with CsOH. The I_{Na} current was measured by 20 ms depolarizing voltage steps ranging from −90 to +60 mV in 5 mV increments after a holding potential of −120 mV to remove the possible inactivation.

The peak values of I_{Na} recorded at each voltage step were normalized to the cell capacitance and reported (as current density, in pA/pF) plotted against the membrane potential (Vm). Additionally, a scatter plot was used to show the distribution of the maximum I_{Na} peaks of each experiment (expressed as current density, in pA/pF).

The conductance (G) was determined using the modified Ohm's law equation:

$$G=I/(Vm-V_{rev}),$$

where I is the peak current Na^+ evoked at the membrane potential Vm and V_{rev} the reversal potential for the Na^+ in our experimental condition. The conductance values were normalized with respect to the maximum conductance value (G/G_{max}) and plotted against the voltage. The conductance voltage curves were fitted with the Boltzmann function

$$G_{Na}=G_{Na,max}/\{1+\exp[(V1/2-Vm)/K]\}$$

to yield the membrane potentials at half-maximal conductance (V1⁄2), and the slope factors (K). Additionally, the scatter plots were used to show the distribution of V1/2 and the K of each experiment for both experimental conditions.

Electrophysiology on KCNH2-expressing HEK293 cells was conducted as previously described (248).

4.3.6 Laser Confocal Immunofluorescence Analysis

For the immunofluorescence analysis HL-1 cardiomyocytes were plated on 12-mm diameter glass coverslips coated with gelatin-fibronectin (5 μg/ml Fibronectin, F1141 Sigma-Aldrich, in 0.02% Gelatin from bovine skin, G9391 Sigma-Aldrich). After complete cell adhesion, 10 μM Colchicine (C-9754 Sigma) was added to the complete Claycomb media for an overnight treatment in a humidified 5% CO_2, 95% O_2 incubator at 37°C, when needed. Cells were subjected to immunofluorescence analysis as previously described (249). Primary antibodies used were: anti-β-Tubulin antibody produced in mouse (1:1,000 in PBS-BSA 1%, T5293 Sigma-Aldrich), the anti-mCherry antibody (1:500 in PBS-BSA 1%, ab167453 Abcam), the anti-γ-tubulin antibody (1:200 in PBS-BSA 1%, T6557 Sigma-Aldrich). After 3 washes in PBS the cells were incubated with the appropriate Alexafluor-conjugated secondary antibodies (Life Technologies™) for 1 h at RT. The confocal images were obtained with a laser scanning fluorescence microscope Leica TSC-SP2 (HCX PL APO, ×63/1.32–0.60 oil objective); 8-bit images were saved at 1,024 × 256 and acquired using the Leica Confocal Software®. Fluorescence was quantified in a selected region of interest (ROI) using Fiji (https://imagej.net/Fiji).

For immunofluorescence analysis on cardiac biopsies, 10-μm-thick paraffine-embedded sections of heart biopsies were deparaffinized by incubation at room temperature with histolemon for 10 min and rehydrated with a graded series of ethanol. Sections were then subjected to antigen retrieval by boiling in citrate buffer (10 mM sodium citrate, pH 6) and incubated with PBS-1% SDS for 10'. After blocking with 1% bovine serum albumin in PBS for 30', the sections were incubated with anti-Lamin A/C (1:100 in PBS-BSA 1%, #2032 Cell Signaling) and then with Alexa Fluor-conjugated secondary antibodies (Life Technologies). The images were acquired as described for HL-1 cells.

4.3.7 Cell Surface Biotinylation

For biotinylation experiments, HL-1 cardiomyocytes were plated in wells of a 6-multiwell cell culture support coated with gelatin-fibronectin (5 μg/ml Fibronectin, F1141, Sigma-Aldrich, in 0.02% Gelatin from bovine skin, G9391 Sigma-Aldrich), at a density to be 100% at the time of biotinylation. When necessary cells were incubated with 10 μM colchicine overnight before biotinylation. The procedure was previously described with some modification (250). Briefly, the HL-1 cells were washed twice in cold phosphate buffer saline (PBS, pH 8) containing 1 mM Ca^{2+} and 0.5 mM Mg^{2+} (PBS-CM) and incubated for 30 min at 4 °C in 2 mg/ml Biotin 3-sulfo-N-hydroxysuccinimide ester sodium salt (B5161 Sigma-Aldrich) in PBS-CM. After three washes in PBS-CM the exceeding biotin was removed washing the cells twice, 10 min at 4 °C, with a quenching solution (50 mM NH_4 Cl in PBS). After biotin binding cells were lysed in Lysis buffer (in mM: 20 Tris-HCl pH 8, 150 NaCl, 5 EGTA, and 1% triton X-100) supplemented with 1X protease inhibitor mixture (Roche), and phosphatase inhibitor (in mM: 10 NaF, 100 orthovanadate, 15 pyrophosphate), for 30 min on ice and sonicated at 60 amplitude with Vibra-cell® (Sonics and Materials Inc.) 3 times for 15 s. After sonication, membranes were pelleted at 13000 rpm for 30 min at 4 °C and the supernatant was collected. Protein concentrations were determined by Bradford protein assay. An equal amount of total protein from each group was incubated with streptavidin-agarose beads (69203 Novogen) overnight at 4 °C in a rotating device. Beads were then washed with Lysis buffer supplemented with protease and phosphatase inhibitors, and proteins were eluted by incubation with Laemmli buffer and freshly added 100 mM DTT, for 20 min at 95 °C and 1,000 rpm. The protein samples were subjected to SDS-Page and western blot analysis as described below.

4.3.8 Cell and Tissue Lysates

HL-1 cells, 100% confluent, plated in the wells of a 6-multiwell cell culture support coated with gelatin-fibronectin (5 μg/ml Fibronectin, F1141 Sigma-Aldrich, in 0.02% Gelatin from bovine skin, G9391 Sigma-Aldrich) were placed on ice, washed in PBS, and exposed to RIPA buffer (in mM: 150 NaCl, 10 Tris/HCl, 1% Triton X-100, 0.1% SDS, 1% deoxycholate-Na, 5 EDTA; pH 7.2) supplemented with protease and phosphatase inhibitors (in mM: 10 NaF, 100 orthovanadate, 15 pyrophosphate). Cells were then sonicated at 60 amplitude with

Vibra-cell® (Sonics and Materials Inc.) and membranes pelleted at 13000 rpm for 30 min at 4°C. Protein concentrations were determined by Bradford protein assay. Proteins were denatured in 1 × Laemmli Sample Buffer (Bio-Rad), 50 mM DTT and subjected to SDS-PAGE and western blotting as described below.

Lysates were also prepared from cardiac biopsies from the index patient' transplanted heart. These biopsies were kindly provided by Niguarda Pathological Anatomy Center, Milano, Italy, where the index patient underwent heart transplantation. Twenty µm-thick paraffine-embedded sections of heart biopsies were deparaffinized by incubation at room temperature with histolemon for 10 min and rehydrated with a graded series of ethanol. The sections were then pelleted at 16000 × g for 5 min and homogenized in 500 mM Tris-HCl pH 8 and 2% SDS at 90°C for 3 h. The samples were centrifugated for 30 min at 16000 × g at 4°C and the supernatants were subjected to SDS-PAGE and western blotting as described below. Lysates from an explanted heart of a patient with heart disease not related to LMNA mutations were used as control, as previously described (165).

4.3.9 Western Blot

Protein samples were electrophoresed on 7.5% or 10% polyacrylamide SDS gel (Mini-PROTEAN TGX Stain-Free Precast Gels; Bio-Rad) and transferred on 0.2-µm PVDF membrane (Trans-Blot Turbo Mini 0.2 µm PVDF Transfer Packs #1704156; Bio-Rad) using the Trans-Blot Turbo Transfer System (Bio-Rad). After blocking at room temperature for 1 h in TBST-5% milk or in TBST-BSA 3% (TBST in mM: 50 Tris, 150 NaCl, 0.1% Tween-20; pH 7.4), blots were incubated overnight at 4°C with the following antibodies in blocking buffer: anti-Lamin A/C (1:1000 in TBST-1% BSA; 2032 Cell Signaling); anti-mCherry antibody (1:1000 in TBST-BSA 1%; ab167453 Abcam); anti-Nav1.5 (1:700 in TBST-1% BSA; S8809 Sigma-Aldrich), anti-acetylated α-tubulin antibody (1:1000 in TBST-1% BSA; T7451 Sigma-Aldrich), anti-β-tubulin antibody (1:1000 in TBST-1% BSA; T5293 Sigma-Aldrich), anti-AKT (1:2000 in TBST-1% BSA; 4691 Cell Signaling), anti-phospho-AKT (Ser473) XP® (1:4000 in TBST-1% BSA; 4060 Cell Signaling), anti-ERK1/2 p44/42 MAPK (ERK1/2) (1:1000 in Milk-5% BSA; 4695 Cell signaling), anti-phospho ERK1/2 p44/42 MAPK (ERK1/2) (1:2000 in Milk-5% BSA; 4695 Cell signaling); the anti-mCherry antibody (1:500 in PBS-BSA 1%, ab167453 Abcam. As secondary antibodies were used the goat anti-mouse IgG-HPR conjugate (1:5000 in TBST-3% BSA; Bio-Rad) and an anti-rabbit

IgG-peroxidase antibody produced in goat (1:5000 in TBST- BSA 3%; Sigma-Aldrich) depending on the primary antibodies' species. The immunoreactive bands were detected with a ChemiDoc™ System (Bio-Rad). Densitometric analysis was performed by Image Lab 6.0 software. For protein load controls, the stain-free technology from Bio-Rad was used.

4.3.10 Statistical Analysis

GraphPad Prism 6 was used for the statistical analysis and graph representation of the data. Data are given as mean ± standard error of the mean. Statistical analysis was performed using one- or two-way ANOVA test or with Student's t-test for unpaired data depending on the data set analyzed.

4.4 Results

4.4.1 Clinical Findings

The heterozygous nucleotide substitution c.1549C > T in exon 9 of the *Lmna* gene introduced a premature stop codon producing a truncated version of the Lamin A/C (LMNA) protein after amino acid 517 (Q517X). This mutation was detected in a 36-year-old man referred to our Cardiomyopathy Unit, Cardiology Unit, Department of Emergency and Organ Transplantation, University of Bari Aldo Moro, Bari (Italy). The index patient had a family history of sudden death (father's brother died suddenly at the age of 19 during his sleep). The family members available for clinical evaluations and molecular analysis were the index patient's son and sister. The 5-year-old son carried the LMNA Q517X mutant and was asymptomatic, free of arrhythmias, and showed normal cardiac function, thus suggesting incomplete and age-related penetrance of the mutation. The 43-year-old sister was LMNA mutation-negative, clinically asymptomatic, and had no arrhythmias or structural cardiac abnormalities **(Fig. 9A, 5 years)**. The index patient (the arrow in the family three) presented with conduction system disturbances such as sinus node dysfunction, first-, second-, and third-degree atrioventricular block **(Fig. 9B),** numerous repetitive premature ventricular complexes (PVCs), recurrence of persistent atrial fibrillation **(Fig. 10A)** and biatrial and biventricular dilation. Based on the electrocardiographic and echocardiographic findings, in combination with a positive family history of sudden death, he received a dual chamber implantable cardioverter-defibrillator (ICD) in primary prevention. Years later, 24-h Holter and ICD remote monitoring showed ventricular fibrillation (VF) discontinued by appropriate ICD shocks, after ineffective anti-tachycardia pacing **(Fig. 10B).** Moreover, echocardiogram showed spherical, severely dilated (LVEDVi 92 ml/m2 and LVESVi 69 ml/m2) and markedly hypocontractile (LVEF 25%) left ventricle **(Fig. 9C)** as well as highly dilated left atrium **(Fig. 9D)**. At the age of 49, the patient underwent heart transplant for both sustained VT/VF recurrences as a storm and severe impairment of left ventricular function. Western blot experiments on samples of ventricular and atrial myocardium obtained from the index patient at the time of cardiac transplantation confirmed the expression of the truncated LMNA variant in index patient's heart. As control, we used cardiac muscle tissues from a patient who experienced heart transplantation due to an ischemic heart disease not related to LMNA mutations **(Fig. 9E)**. The immunofluorescence confocal analysis using anti-LMNA

antibodies on heart biopsies showed LMNA results expressed in protein aggregates in the nuclei of LMNA Q517X carrier's heart **(Fig. 9F, IP)**.

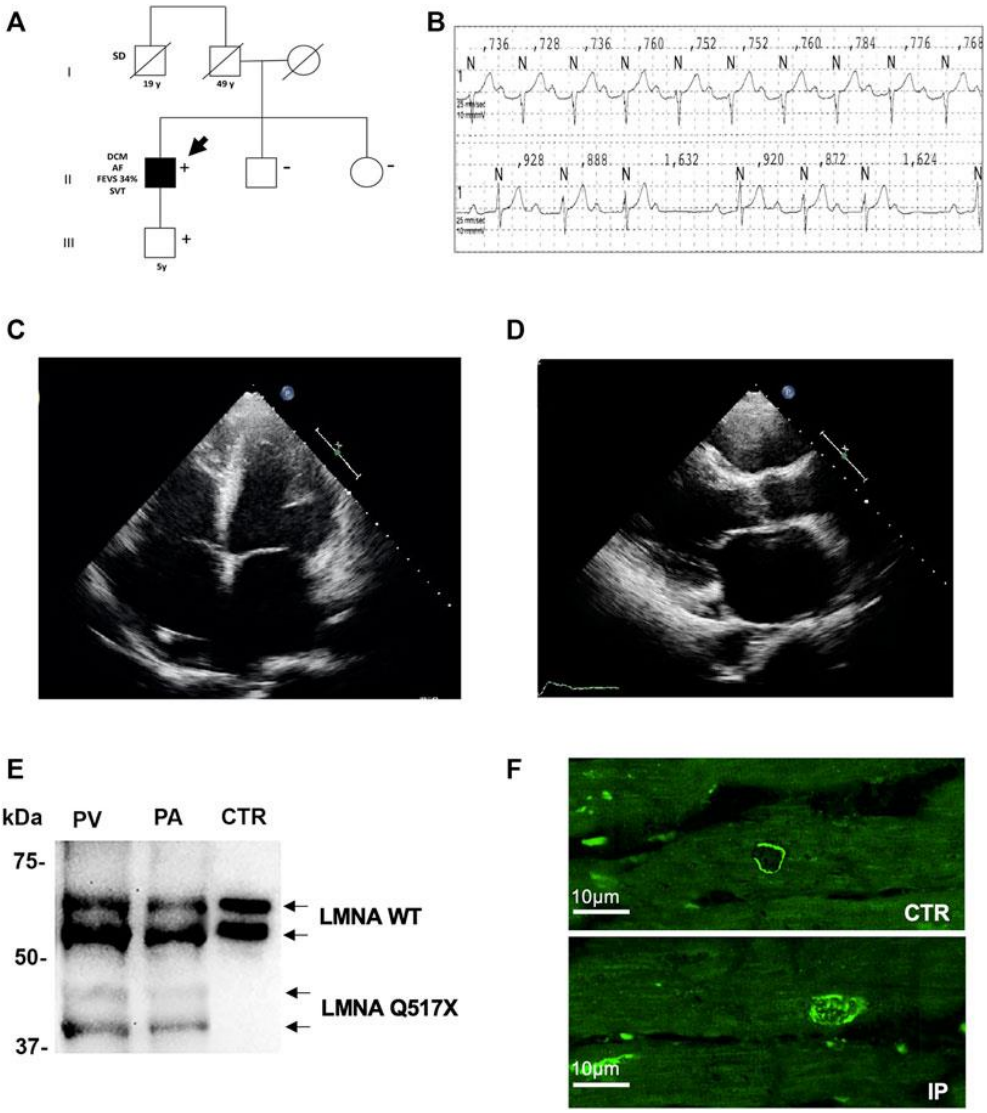

Figure 9: (A) Pedigree of the family carrying the LMNA Q517X pathogenic variant. The filled symbols indicate clinically affected individuals, the diagonal slashes indicate deceased individuals; +/− indicate positive/negative for the mutation; the arrow indicates the index patient. (B) ECG data from index patient showing sinus rhythm, first-degree atrioventricular block (upper trace), and type 1 second-degree atrioventricular block (lower trace) recorded during a 24-h ECG monitoring. (C) Apical 4C views of echocardiographic imaging from index patient showing a spherical, severely dilated, and markedly hypocontractile left ventricle. (D) In the PLAX view of echocardiographic imaging from index patient, showing a highly dilated left atrium. (E) Western blot analysis of whole lysate of left atrium (PA) and (PV) ventricular myocardial tissue from the mutant carrier (black arrow in A) and control (CTR) heart biopsies. (F) Representative confocal immunofluorescence images of

LMNA in heart biopsies from a control patient (CTR) and from the index patient (IP). ECG, electrocardiogram; PLAX view, parasternal long-axis view.

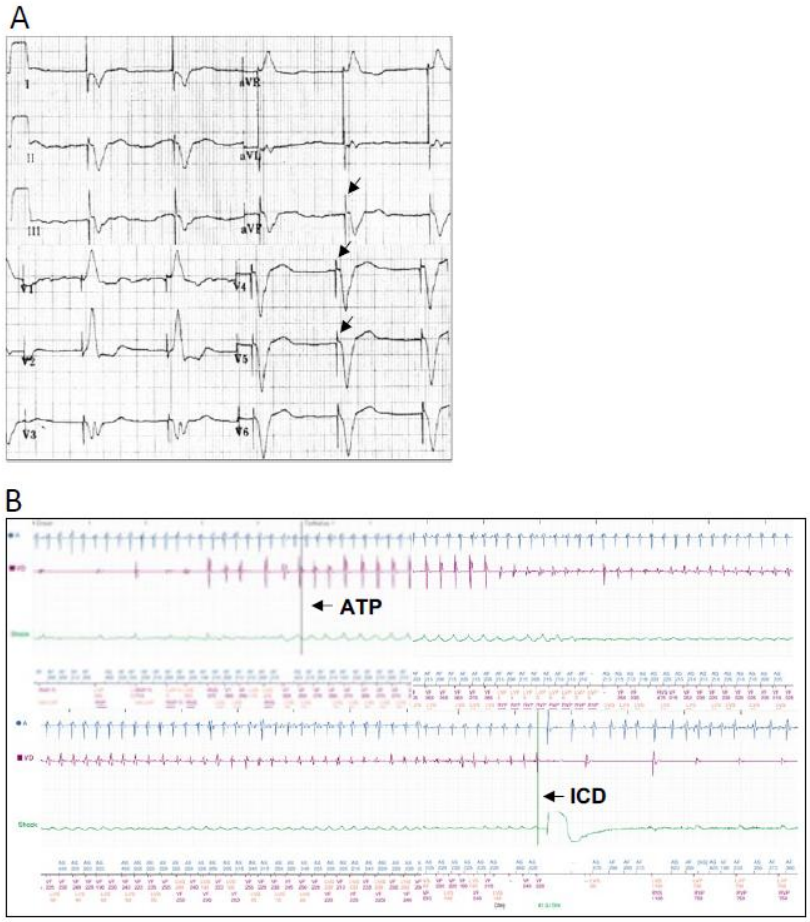

Figure 10: (A) 12-lead ECG from index patient showing atrial fibrillation and ventricular rhythm induced by a pacemaker with VVI pacing mode. Arrows indicate pacemaker spikes. (B) Typical VF episode recorded in the index patient and stopped by internal ICD shock after ineffective ATP. ATP, anti-tachycardia pacing; ECG, electrocardiogram; ICD, implantable cardioverter-defibrillator.

4.4.2 LMNA Q517X Alters Action Potential Properties in HL-1 Cardiomyocytes

When stably expressed in HL-1 cardiomyocytes, LMNA Q517X abnormally aggregated at the nuclear envelope and accumulated within the nucleoplasm as clearly shown by the

fluorescence distribution profile (**Fig. 11A**, HL-1 LMNA WT, HL-1 LMNA Q517X, insets). This peculiar nuclear distribution is consistent with that of LMNA observed *in vivo* in the index patient's heart **(Fig. 9E)**.

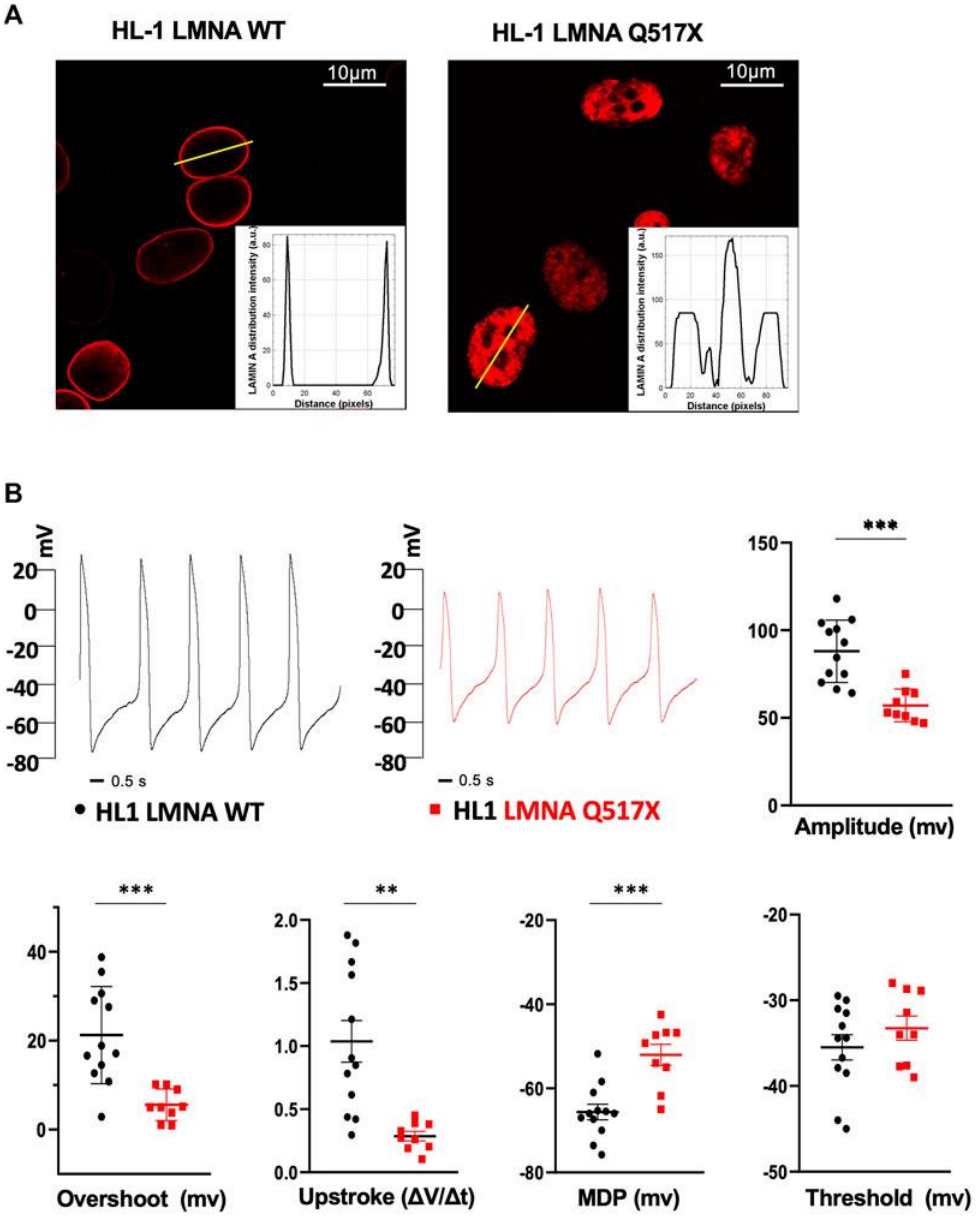

Figure 11: (A) Representative confocal immunofluorescence images of LMNA WT and Q517X in stably transfected HL-1 cardiomyocytes. The insets report the fluorescence distribution along the line (yellow line) crossing nuclei in each cell line. (B) Representative AP recordings by whole-cell patch clamp in the current clamp configuration in LMNA WT (black trace) and LMNA Q517X-expressing HL-1 cells (red trace) and scatter plots for the analysis of AP parameters in LMNA WT (black dots,

N = 12) and LMNA Q517X-expressing HL-1 cells (red squares, N = 9); ***p < 0.001; **p < 0.01; Student's t-test for unpaired data.

To evaluate the effect of LMNA Q517X expression on the membrane electrical properties in cardiomyocytes, we analyzed the biophysical properties of spontaneous action potentials in HL-1 cardiomyocytes expressing either LMNA WT (**Fig. 11B**, HL-1 LMNA WT, black trace) or Q517X (**Fig. 11B**, HL-1 LMNA Q517X, red trace) by whole-cell patch clamp recordings in current clamp. The shape of the spontaneous action potential generated by cardiomyocytes expressing the LMNA mutant variant exhibited significant reduction in Action Potentials (APs) amplitude (**Fig. 11B**, Amplitude in mV: black dots 88.04 ± 5.13 vs red squares 57.11 ± 3.11), APs overshoots (**Fig. 11B**, Overshoot in mV: black dots 21.25 ± 3.14 vs red squares 5.58 ± 1.17), maximum upstroke velocity (**Figure 11B**, Upstroke in ΔV/Δt: black dots 1.03 ± 0.16 vs red squares 0.28 ± 0.03), and maximum diastolic potential (MDP) (**Figure 11B**, MDP in mV: black dots 65.63 ± 1.86 vs red squares −52.03 ± 2.50) when compared to control cells; while no significant changes were detected in the APs' threshold between the two experimental conditions (**Fig. 11B**, threshold in mV: black dots −35.49 ± 1.48 vs red squares −33.25 ± 1.41).

4.4.3 LMNA Q517X Alters Tubulin State and Decreased the Expression of Nav1.5 at the Plasma Membrane in HL-1 Cardiomyocytes

In LMNA WT and Q517X-expressing cardiomyocytes we studied the profile of key signaling molecules, already found to be dysregulated in lamin cardiomyopathies. Specifically, enhanced phosphorylation of ERK1/2 and AKT and decreased α-tubulin acetylation have been reported in the heart of *Lmna*$^{H222P/H222P}$ mice (126,136). Here, we found that the activation profiles of ERK1/2 and AKT, quantified as the expression of their phosphorylated forms, were significantly increased in Q517X cardiomyocytes when compared with their control in accordance with the previous findings **(Fig. 12A, B)**. However, acetylated α-tubulin significantly increased in Q517X cardiomyocytes as unique feature of this mutant variant **(Fig. 12C)**. The expression of LMNA variants is comparable in the HL-1 clones used in the study **(Fig. 12D)**.

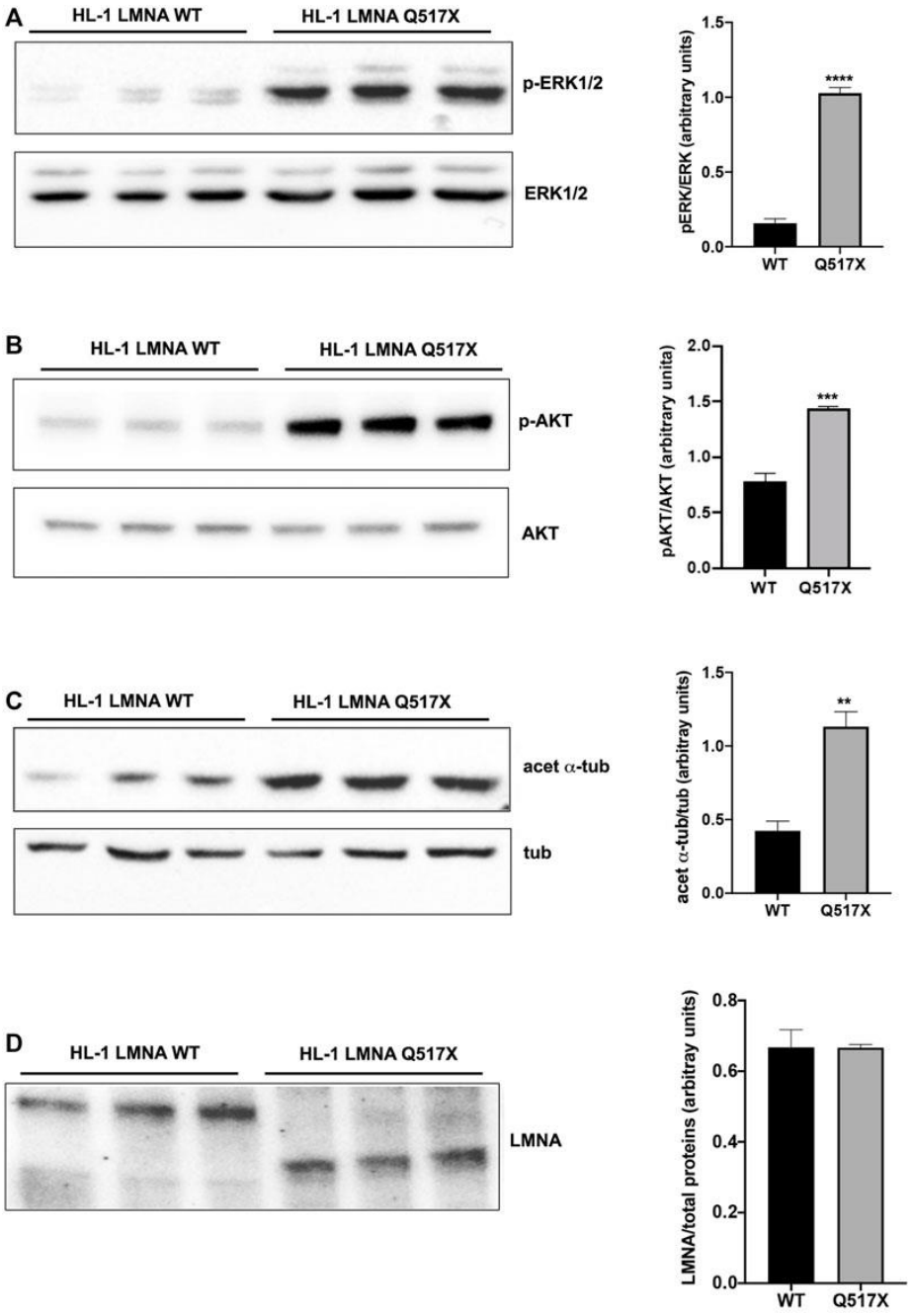

Figure 12: (A) Left panel: representative western blot of p-ERK1/2 and ERK1/2 in lysates from LMNA WT and LMNA Q517X-expressing HL-1 cells; right panel: normalized densitometric analysis of p-ERK1/2 immunoreactive bands in LMNA WT and Q517X-expressing HL-1 cells. (B) Left panel: representative western blot of p-AKT and AKT in lysates from LMNA WT and LMNA Q517X-expressing HL-1 cells; right panel: normalized densitometric analysis of p-AKT immunoreactive bands in LMNA WT and Q517X-expressing HL-1 cells. (C) Left panel: representative western blot of acetylated α-tubulin (acet α-tub) and α-tubulin (tub) in lysates from LMNA WT and LMNA Q517X-expressing HL-1 cells; right panel: normalized densitometric analysis of acetylated α-tubulin immunoreactive bands in LMNA WT and Q517X-expressing HL-1 cells. (D) Left panel: representative western blot of mCherry-tagged LMNA in lysates from LMNA

WT and LMNA Q517X-expressing HL-1 cells; right panel: normalized densitometric analysis of m-Cherry tagged LMNA immunoreactive bands. The data are means of 3 independent experiments. ****p < 0.0001 ***p< =0.001; **p < 0.01; Student's t test for unpaired data.

It has been accepted that acetyl transferase has major affinity for polymerized tubulin (251); thus, we looked at the polymerization state of tubulin meshwork by fluorescence confocal analysis and found that it underwent hyper-polymerization in Q517X-expressing cardiomyocytes compared with their controls **(Fig. 13A)**. Quantitative analysis of fluorescence intensity showed that tubulin density significantly increased by approximately 50% in LMNA Q517X-expressing cardiomyocytes compared with their controls **(Fig. 13A, right panel)**. The perinuclear positioning of microtubule-organizing center (MTOC) was not affected by the expression of LMNA Q517X variant in these cells **(Fig. 14),** thus suggesting that the physical connection between the nucleus and microtubules is preserved upon LMNA Q517X expression.

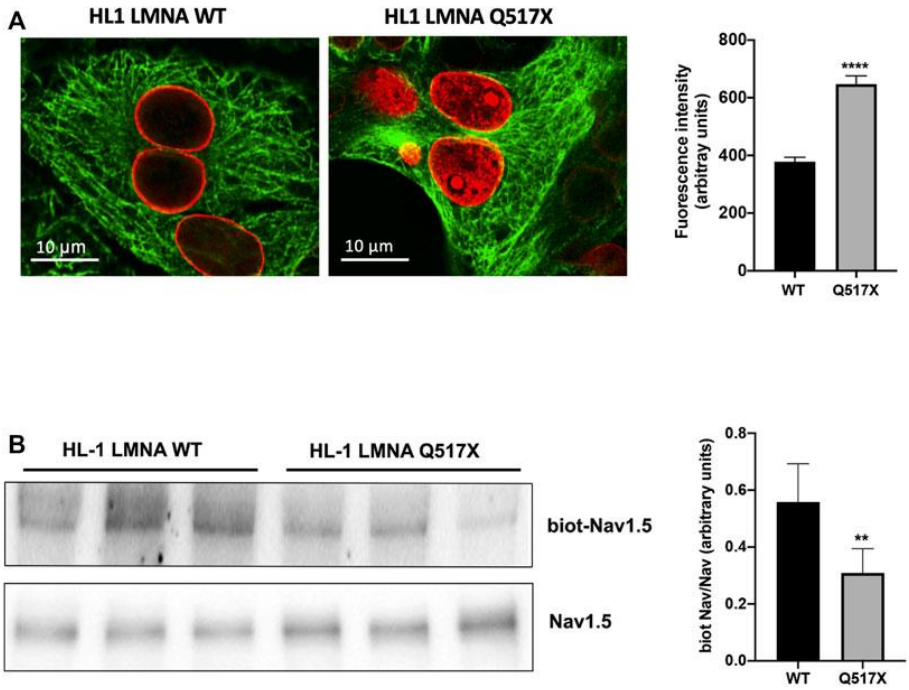

Figure 13: (A) Left panel: representative confocal laser immunofluorescence images in LMNA WT and LMNA Q517X-expressing HL-1 cells (in red LMNA, in green β-tubulin); right panel: region of interest (ROI) for tubulin fluorescence quantification in LMNA WT and Q517X-expressing HL-1

cells. N = 15 for each experimental condition. (B) Left panel: representative western blots of Nav1.5 α subunit in cell surface biotinylated proteins (biot-Nav1.5) and in cell lysates (Nav1.5) from LMNA WT and Q517X-expressing HL-1 cells; right panel: normalized densitometric analysis of biot-Nav 1.5 immunoreactive bands in LMNA WT and Q517X-expressing HL-1 cells. The data are means of 3 independent experiments. ****p < 0.0001; **p < 0.01; Student's t test for unpaired data.

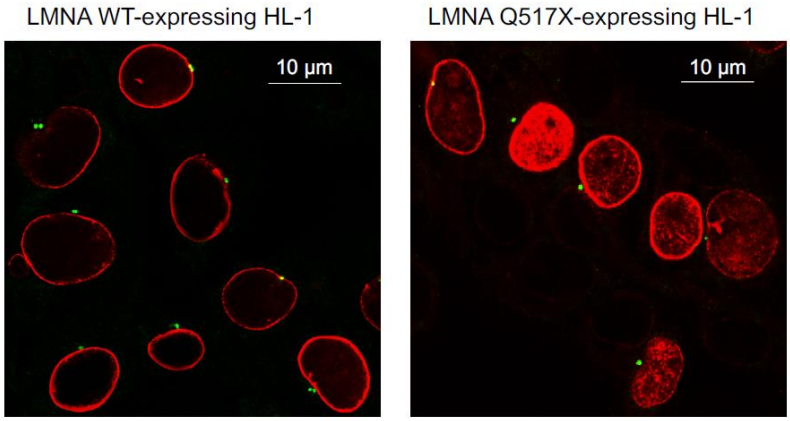

Figure 14: Representative immunofluorescence confocal images of HL-1 cells expressing either LMNA WT or LMNA Q517X (red signal) labelled with the antibody anti- g tubulin which marks the microtubule-organizing-center MTOC (green signal).

It has been previously reported that the treatment with the anticancer drug Taxol, which polymerizes the cytoskeleton protein tubulin, may evoke cardiac arrhythmias reducing both the Nav1.5 expression at the plasma membrane and the Nav1.5 activation rate (252).

We indeed semi-quantified membrane Nav1.5 expression using cell surface biotinylation experiments in cardiomyocytes expressing either LMNA Q517X or WT. We found that the cells surface expression of Nav1.5 was significantly downregulated by approximately 40% in LMNA Q517X-expressing cardiomyocytes at the plasma membrane but not in the total lysate **(Fig. 13B)**.

Currents in HL-1 cardiomyocytes have been previously shown to have genotypic, phenotypic, and electrophysiologic properties similar to adult atrial cardiomyocytes, with the upstroke phase of the AP due to I_{Na} through Nav1.5 channel (247). Accordingly, we measured a significant decrease in tetrodotoxin-sensitive inward currents in LMNA Q517X-

expressing cardiomyocytes **(Fig. 15).** Of note, outward currents were not affected by the expression of LMNA Q517X in HL-1 cardiomyocytes **(Fig. 15)**.

Indeed, the altered AP parameters registered in LMNA Q517X-expressing cardiomyocytes **(Fig. 12B)** may be actually explained by a decreased density of Nav1.5 at the plasma membrane in these cells.

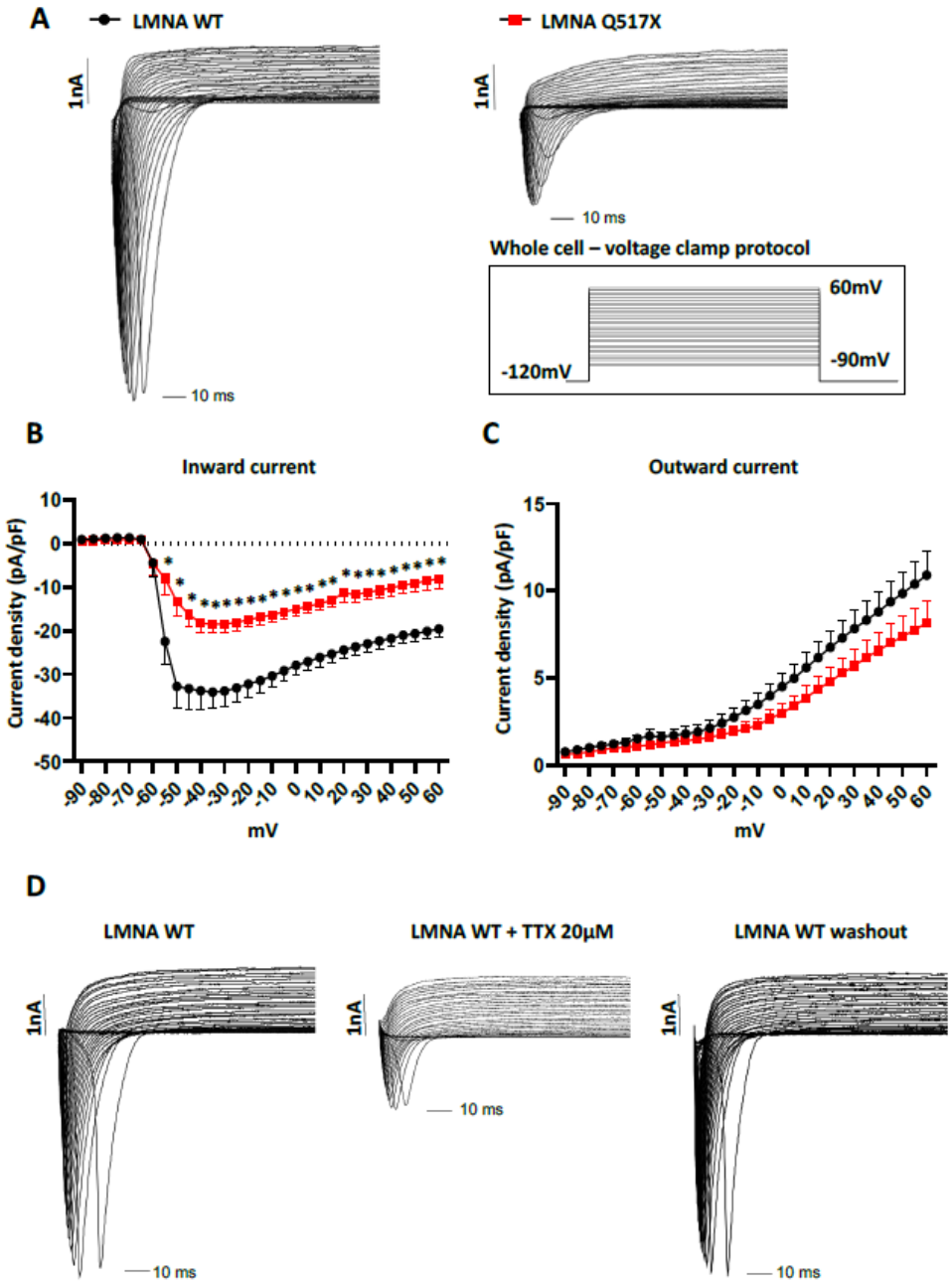

Figure 15: (A) Representative traces of currents recorded, using a voltage protocol consisting of a holding potential of −120 mV followed by depolarizing steps from −90 to +60 mV (with increments of 5 mV), in HL-1 cardiomyocytes stably expressing either LMNA Q517X (n=11) or LMNA WT

(n=14). (B) I-V plot of the inward current measured as the peak inward current evoked at each depolarizing step. The inward currents appear significantly smaller in LMNA Q517X expressing HL-1 cells compared with their control cells (with a peak current of -34,09 ± 3,71 pA/pF, in cells expressing LMNA WT and a peak current of -18,47 ± 2,02 pA/pF in cells expressing LMNA Q517X, A-nova, p-value: 0,0002). (C) I-V plot of the outward current measured as the outward current evoked at the end of each depolarizing step. No significative differences were detected between the outward current recorded in HL-1 cells expressing either LMNA Q517X or LMNA WT (with an evoked outward current at 60 mv of 10,89 ± 1,34 pA/pF in cells expressing LMNA WT and, at the same voltage, an outward current of 8,15 ± 1,2 pA/pF in cells expressing *LMNA* Q517X, Anova, p-value: 0,2). (D) Representative traces of currents recorded in HL-1 cardiomyocytes stably expressing LMNA WT (LMNA WT*),* after application of 20 µM tetrodotoxin in the extracellular solution *(*LMNA WT+ 20µM TTX) and after tetrodotoxin washout *(*LMNA WT washout).

4.4.4 LMNA Q517X Significantly Alters Nav1.5 Function in HEK293 Cells

To better analyze Nav1.5 biophysics in the presence of LMNA Q517X we moved in HEK293 cells. **Fig. 16A** shows representative Na^+ currents measured in HEK293 cells coexpressing Nav1.5, its β1 subunits (Nav1.5 + β1) and either LMNA WT or Q517X. As shown by the current–voltage curve (**Fig. 16B**; black line for Nav1.5 + β1 + LMNA WT, red line for Nav1.5 + β1 + LMNA Q517X), the peak sodium current density evoked by depolarizing steps of currents was significantly decreased in cells expressing LMNA Q517X when compared with control cells expressing LMNA WT.

The scatter plot of the maximum peak sodium currents clearly showed an up to 63% decrease in current density upon LMNA Q517X expression (peak current in pA/pF: black dots −504.46 ± 56.72 vs red squares −213.59 ± 32.380). This is consistent with the reduced expression of Nav1.5 at the plasma membrane shown above **(Fig. 13A)**. The voltage dependency of the steady-state activation for LMNA Q517X was shifted toward positive potentials with respect to WT **(Fig. 16C)**. The scatter plot of V1/2 showed a slight but significative shift of approximately 6 mV toward positive values for this parameter upon LMNA Q517X expression (**Fig. 16C**, V1/2: black dots −51 ± 4.8 mV vs red squares −45.25 ± 2.060 mV), thus indicating the need of a more intense depolarization for the activation of Nav1.5 in these cells. The slope factor of activation (K) was significantly increased upon LMNA Q517X expression (**Fig. 16C**, slope factor in mV: black dots 1.019 ± 0.22 vs red

squares 2.635 ± 0.546), suggesting an alteration in voltage dependence of Nav1.5 activation in LMNA-Q517X-expressing HEK293 cells.

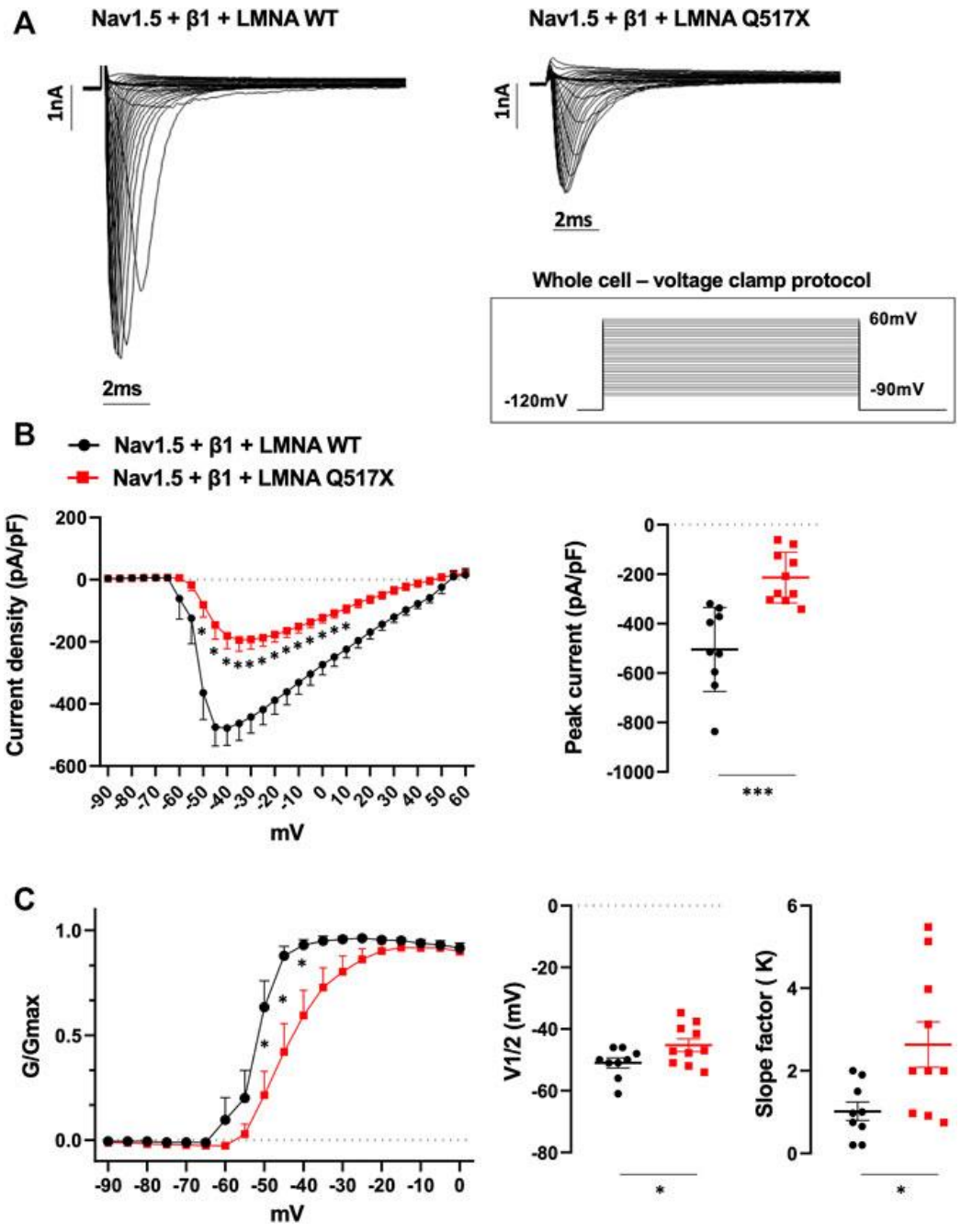

Figure 16: (A) Representative traces of inward Na^+ currents evoked in HEK293 cells expressing either LMNA WT or LMNA Q517X, under 20s depolarizing steps from −90mV to +60 mV (with 5-mV increments) starting from a holding potential of −120 mV. (B) Left panel: current density (pA/pF)–voltage relationships (I–V curve) of the Na^+ currents recorded for LMNA WT (black trace, N = 9), and LMNA Q517X-expressing HEK293 cells (red trace, N = 10); $p < 0{,}0001$ from −50 mV

to −20 mV; p-value< 0.001 at F02D15 mV an −10 mV; p-value < 0,01 at −5 mV and p-value < 0,05 at 0 mV and 5 mV, two-way Anova. Right panel: scatter plot of the maximum peak sodium currents (pA/pF) for LMNA WT (black dots) and LMNA Q517X-expressing HEK293 cells (red squares); ***p < 0.001, Student's t test for unpaired data). (C) Left panel: conductance voltage (G/Gmax) relationships of Na^+ currents (G–V curve) obtained for LMNA WT (black trace, N = 9) and LMNA Q517X-expressing HEK293 cells (red trace, N = 10); p-value < 0,0001 at −50 mV and −45 mV; < 0.001 at −40 mV, two-way Anova. Right panel: scatter plots of the half-maximal conductance (V1⁄2) and the slope factors (K) in LMNA WT (black dots) or LMNA Q517X-expressing HEK293 cells (red squares), respectively; *p < 0.01 Student's t test for unpaired data.

Interestingly, it has been also proved that a high prevalence of variants in K^+ channel encoding genes such as KCNH2 might control atrial repolarization and predispose carriers to atrial fibrillation (10.1161/circep.114.002519; 10.1093/eurheartj/ehm619). Indeed, outward K^+ currents through KCNH2 channel were analyzed in HEK293 cells transiently expressing KCNH2 together with WT or Q517X LMNA. This K^+ channel is highly expressed in HL-1 cells where it is involved in the repolarization phase of AP (253). We found that the biophysics of this channel was not affected by the expression of LMNA Q517X variant **(Fig. 17).**

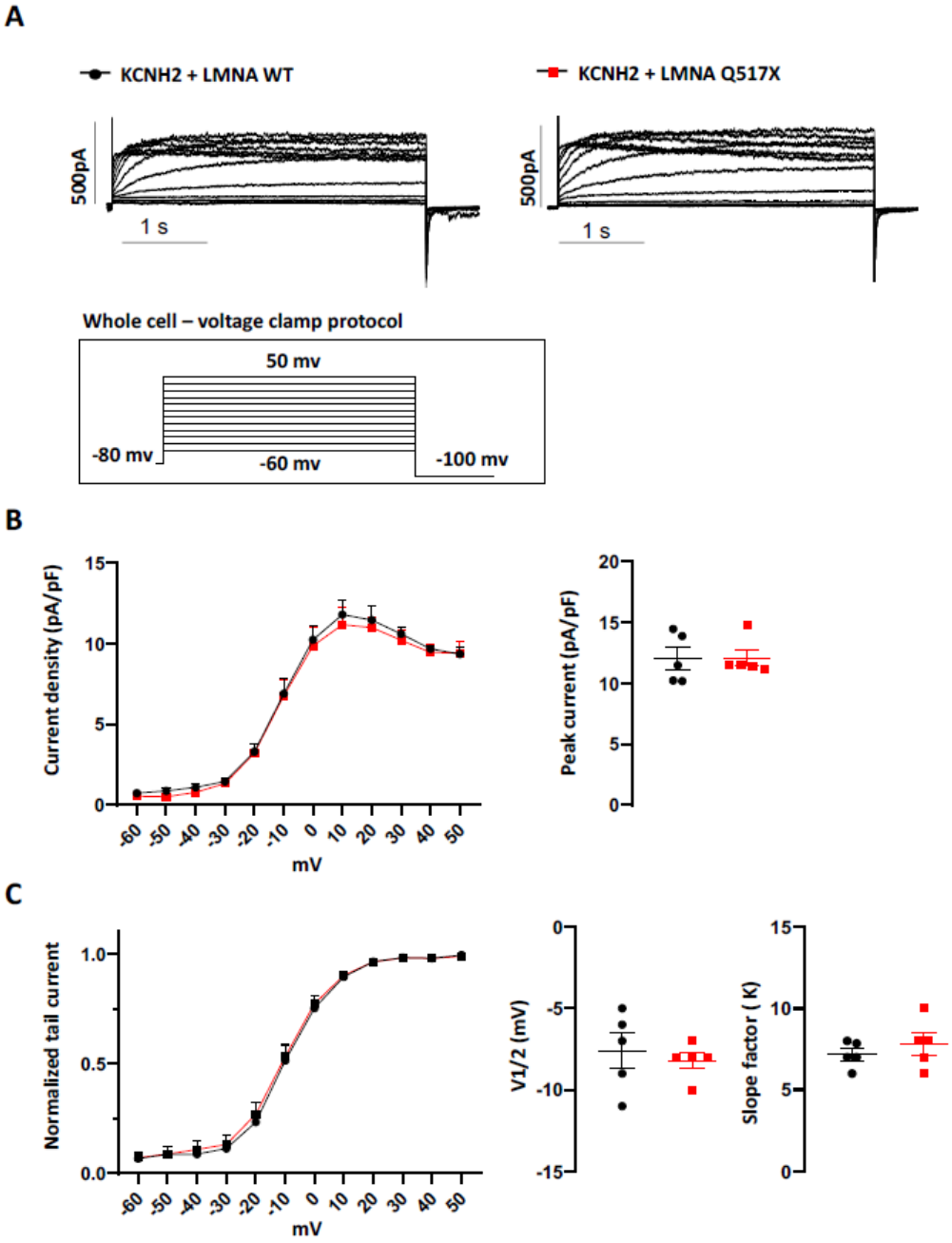

Figure 17: (A) Representative traces of the K^+ currents recorded, using a voltage protocol consisting of a holding potential of −80 mV followed by 4s depolarizing steps from −60 to +50 mV (with increments of 10 mV), in HEK293 cells transiently co-transfected with KCNH2 and either LMNA Q517X (n=5) or LMNA WT (n=5) expression plasmids. (B) I-V plot of the evoked outward K^+ current in cells described above. The K^+ current, measured at the end of the depolarizing steps, increased at each further depolarizing step until reached a similar maximum outward current amplitude in both experimental conditions at approximately 10 mv (with a peak current of 12,03 ± 0,9 pA/pF, in cells expressing LMNA WT and a peak current of 12,07 ± 0,67 pA/pF in cells expressing LMNA Q517X, t-test, p-value: 0,9749). After reaching the peak, both I-V curves quickly decreased at more positive potentials because of the voltage-dependent KCNH2 channel inactivation.

(C) Activation curves obtained fitting to a Boltzmann relationship the K^+ tail current normalized to the maximum tail current amplitude. The activation curves obtained confirmed a comparable channel kinetics in both experimental conditions (with a half-maximum activation voltage (V1/2) of −7,6 ± 1,07 mV and a slope factor (κ) of 7,1 ± 0,35 for HEK293 cells expressing LMNA WT and a half-maximum activation voltage (V1/2) of −8,2 ± 0,49 mV and a slope factor (κ) of 7,8 ± 0,66 for HEK293 cells expressing LMNA Q517X; t-test, V1/2 p-value: 0,62, K p-value: 0,42). Data were given as mean ± SEM.

4.4.5 Tubulin State Manipulation Recovers AP Parameters in LMNA Q517X-Expressing HL-1 Cardiomyocytes and Nav1.5 Biophysics in HEK293 Cells

Alpha tubulin hyper-polymerization and hyper-acetylation are the unique features of LMNA Q517X-expressing HL-1 cardiomyocytes, likely accounting for the AP abnormalities in these cells.

An FDA-approved alkaloid, colchicine, inhibits tubulin polymerization in heart (254) and depolymerizes the tubulin network of LMNA Q517X-expressing cardiomyocytes to the same extent of control cells (**Fig. 18A**, LMNA Q517X + colchi).

Concomitantly, colchicine treatment reduced the levels of acetylated α-tubulin **(Fig. 18B)** and increased the cell surface expression of Nav1.5 in LMNA Q517X-expressing cardiomyocytes **(Fig. 18C)** toward the levels of those found in LMNA WT-expressing cardiomyocytes.

Interestingly, **Fig. 19** shows that the treatment of HL-1 cardiomyocytes expressing LMNA Q517X with colchicine leads to a WT-like shape of AP when compared with untreated cardiac cells (red traces for LMNA Q517X, gray traces for LMNA Q517X + colchicine). Moreover, colchicine treatment induced a significant recovery of all AP's parameters measured in LMNA Q517X cardiomyocytes toward those found in LMNA WT-expressing cardiomyocytes. Specifically, as shown in the scatter plots (**Fig. 19**, scatter plots) AP amplitude (amplitude in mV: red squares 57.11 ± 3.11, vs gray squares 80.32 ± 7.45), AP overshoot (overshoots in mV: red squares 5.58 ± 1.17, vs gray squares 19.88 ± 4.07), maximum upstroke velocity (upstroke in mV/ms: red squares 0.28 ± 0.03, vs gray squares 0.90 ± 0.24), and the maximum diastolic potential (MDP in mV: red squares −52.03 ± 2.50, vs gray squares -61.6 ± 2.675) were all significantly increased in LMNA Q517X-treated

cardiomyocytes compared with their controls. No significant changes were observed in APs' threshold between the two experimental conditions (thresholds in mV: red squares −33.25 ± 1.41, vs gray squares −33.96 ± 1.57).

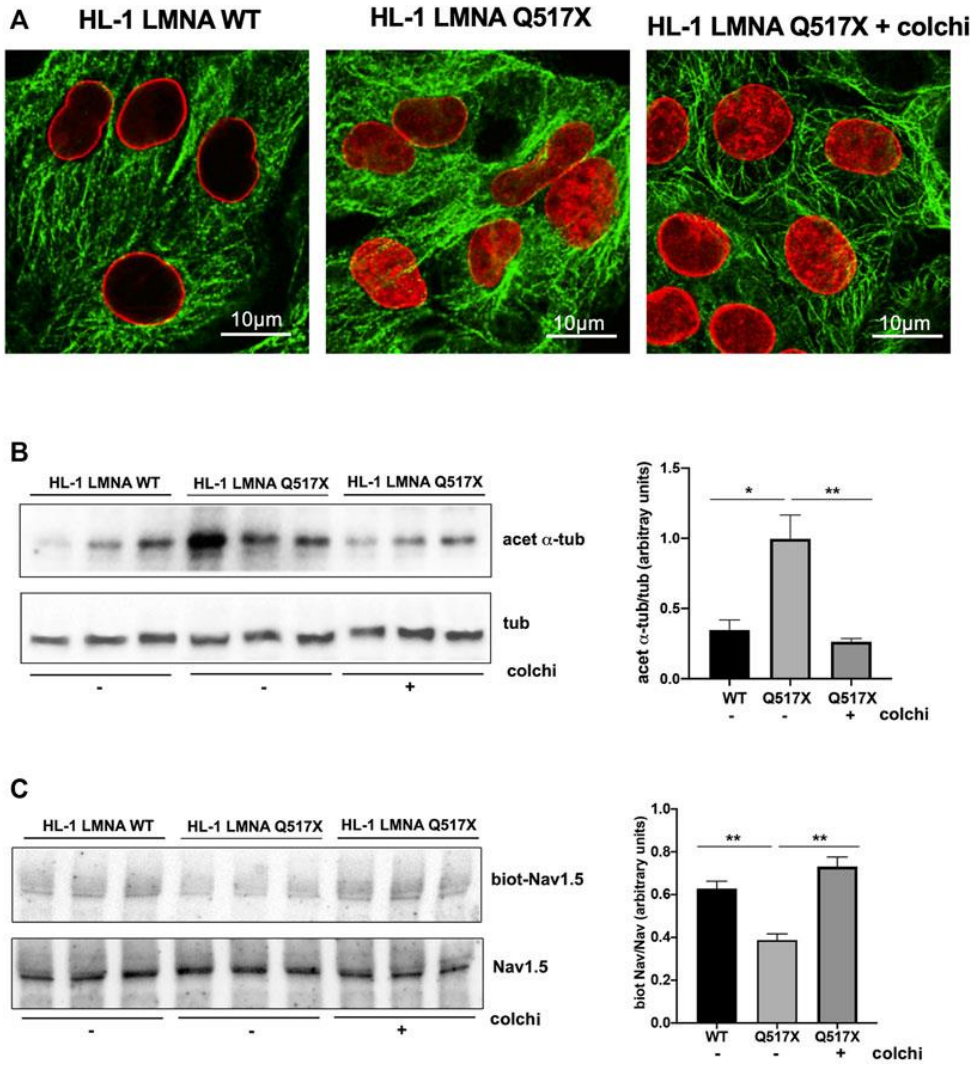

Figure 18: (A) Representative immunofluorescence confocal images of HL-1 cells expressing either LMNA WT or LMNA Q517X, the latter treated or not with colchicine (+colchi). (B) Left panel: representative western blot of acetylated α tubulin (acet α-tub) and total α tubulin (tub) in the absence (–) or the presence (+) of colchicine (colchi) in LMNA WT and LMNA Q517X-expressing HL-1 cells; right panel: normalized densitometric analysis of acetylated α-tubulin immunoreactive bands in all the experimental conditions shown in the left panel. (C) Left panel: representative western blot of cells surface biotinylated Nav1.5 (biot-Nav1.5) and Nav1.5 in cell lysates (Nav1.5) in the absence (–) or presence (+) of colchicine (colchi) in LMNA WT and LMNA Q517X-expressing HL-1 cells; right panel: normalized densitometric analysis of biot-Nav1.5 immunoreactive bands in all the

experimental conditions shown in the left panel. The data are means of 3 independent experiments *p < 0.01, **p < 0.001, one-way Anova.

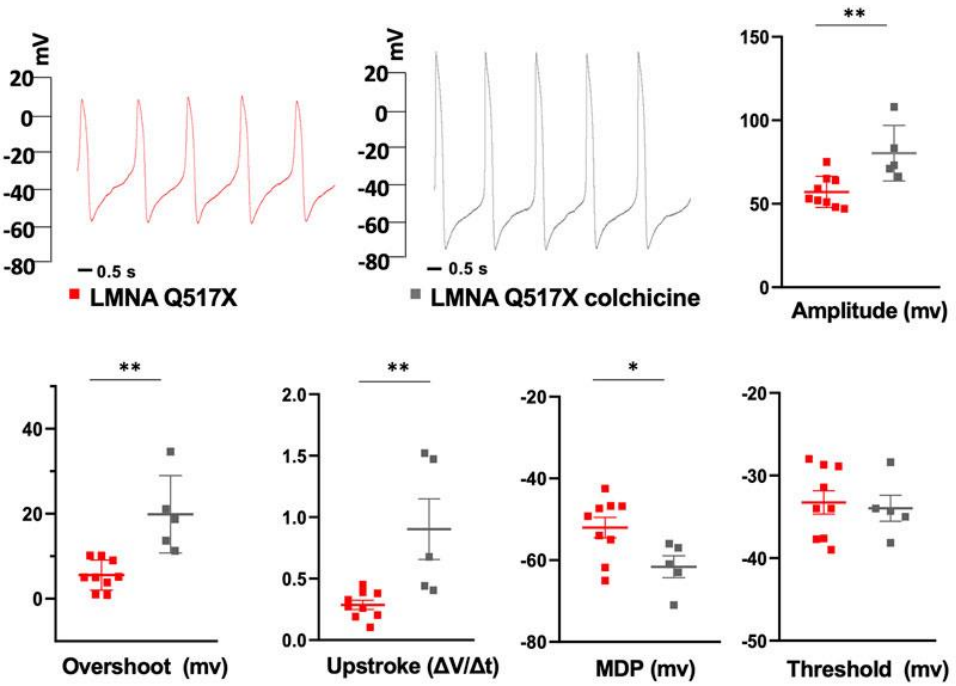

Figure 19: Representative AP recordings by whole-cell patch clamp in current clamp configuration in untreated (red traces) and colchicine-treated LMNA Q517X-expressing HL-1 cells (gray traces) and scatter plots for the analysis of AP parameters in untreated (red squares, N = 9) and colchicine-treated LMNA Q517X-expressing HL-1 cells (gray squares, N = 5). *p < 0.01, **p < 0.001, Student's t test for unpaired data.

Similarly, colchicine treatment reversed the Nav1.5 biophysical parameters measured in LMNA Q517X-expressing HEK293 cells toward those measured in LMNA WT-expressing HEK293 cells. As shown in **Fig. 20A** (representative current traces) and **20B** (current density plots: red line for Nav1.5 + β1 + LMNA Q517X, gray line for Nav1.5 + β1 + LMNA Q517X + colchicine), Na^+ currents recorded in HEK293 cells expressing LMNA Q517X significantly increased upon colchicine treatment. The peak current of Na^+ returned to that observed in LMNA WT-expressing-HEK293 cells (**Fig. 20B**, peak current in pA/pF: red squares −170.5 ± 32,942 vs gray squares −437,166 ± 33,843). Upon colchicine treatment the steady-state activation curve of Nav1.5 in LMNA Q517X-expressing cells returned to that

observed in LMNA WT-expressing cells (**Fig. 20C**, G/Gmax: red line for Nav1.5 + β1 + LMNA Q517X, gray line for Nav1.5 + β1 + LMNA Q517X + colchicine). Finally, upon colchicine treatment both V1/2 and slope factor values measured in LMNA Q517X-expressing HEK293 returned to those observed in LMNA WT-expressing cells (**Fig. 20C**; V1/2 in mV: red squares −42.68 ± 2.235 vs gray squares −49.93 ± 2.034; slope factor in mV: red squares 2.886 ± 0.650 vs gray squares 1.141 ± 0.422).

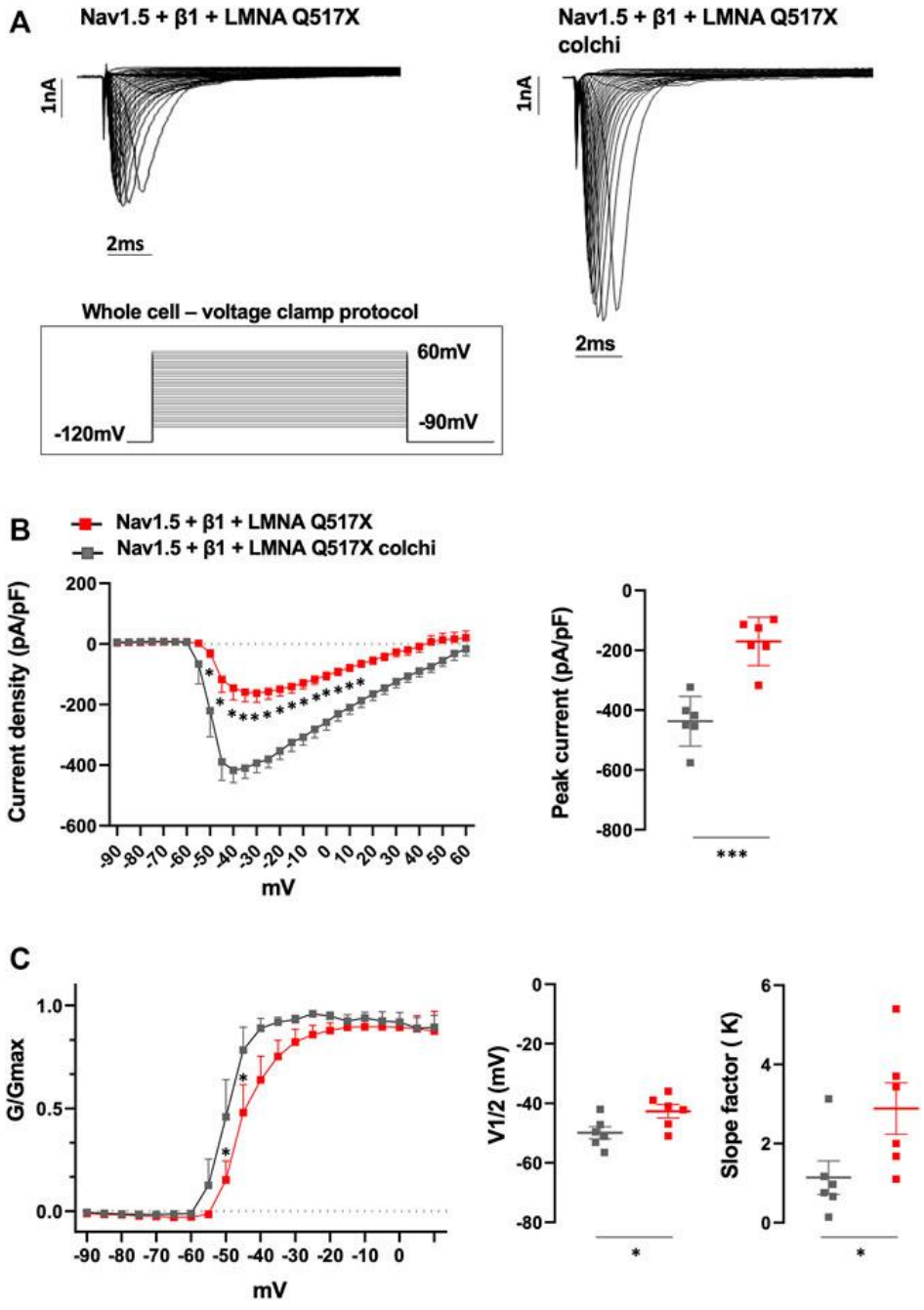

Figure 20: (A) Representative traces of inward Na^+ currents evoked in untreated (Nav1.5 + β1 + LMNA Q517X) or colchicine-treated LMNA Q517X-expressing HEK293 cells (Nav1.5 + β1 + LMNA Q517X colchi). (B) Left panel: current density (pA/pF)–voltage relationships (I–V curve) of the Na^+ currents recorded in untreated (red trace, N = 6), and colchicine-treated LMNA Q517X-expressing HEK293 cells (gray trace, N = 6); p-value < 0,0001 from −50 mV to −10 mV; p-value< 0.001 at −5 mV and at 0 mV; p-value < 0.01 at 5 mV and p-value < 0,05 at 10 mV and 15 mV, two-way Anova. Right panel: scatter plot of the maximum peak sodium currents (pA/pF) in untreated (red squares) and in colchicine-treated LMNA Q517X-expressing HEK293 cells (gray squares). (C) Left panel: conductance voltage (G/Gmax) relationships of Na^+ currents (G–V curve) obtained for untreated (red trace, N = 6), and colchicine-treated LMNA Q517X-expressing HEK293 cells (gray trace, N = 6); p-value < 0.001 at −50 mV and at −45 mV, two-way Anova. Right panel: scatter plot of the half-maximal conductance (V1⁄2) and slope factors (K) in untreated (red squares) and in colchicine-treated LMNA Q517X-expressing HEK293 cells (gray squares); *p < 0.01; **p < 0.001, Student's t test for unpaired data.

4.5 Discussion

In this work, we found that the pathogenetic LMNA Q517X variant, through a modulation of the microtubule meshwork state, impairs Nav1.5 expression and function at the plasma membrane in the murine atrial cell line HL-1, thus proving new insights into both the way how LMNA may regulate cardiac function in physiopathological conditions and the possible therapeutic approaches in the field of cardiac laminopathies.

As a consequence of the reduced Nav1.5 activity at the plasma membrane, APs have reduced amplitude, overshoot, upstroke velocity, and increased diastolic potential in LMNA Q517X-expressing cardiomyocytes compared with their controls. These AP features may decrease conduction velocity in atrial cardiomyocytes and autorhythmic cells inducing atrial fibrillation, sick sinus syndrome, and AV-block, all clinical findings of the index family carrying LMNA Q517X mutant (**Fig. 9A**, results). Atrial fibrillation is one of the most common causes for cardiac function deterioration in the setting of DCM (255,256), which also occurred in LMNA Q517X carriers. Accordingly, loss-of-function mutations in Nav1.5 encoding gene, *scn5a*, have been found associated with atrial fibrillation and conduction defects (257,258). Of note, loss of function in the Nav1.5 channel can be also associated with DCM and ventricular arrhythmias, regardless of whether the atrial fibrillation occurred, suggesting that reduction in the inward Na^+ current may affect directly electrical properties and fates of ventricular cardiomyocytes (259). Indeed, we cannot exclude that LMNA Q517X variant expressed in the whole heart of carriers may affect directly ventricular function.

The clinical history of the index family carrying LMNA Q517X mutant, however, puts the permanent atrial fibrillation and conduction defects showed at the onset of the cardiomyopathy as key events for the following heart failure.

We found that LMNA Q517X expression induced both microtubules hyper-polymerization and Nav1.5 downregulation at the plasma membrane in atrial HL-1 cardiomyocytes and significant reduction in the peak I_{Na} amplitude in Nav1.5-expressing HEK293 cells. These results are in agreement with the findings of Casini et al., showing that treatment with the anticancer drug Taxol, which polymerizes tubulin, reduces sarcolemmal Nav1.5 in neonatal cardiomyocytes, and I_{Na} amplitude in Na1.5-expressing HEK293 cells of about two-fold (252).

The density of the microtubule alters microtubule interactome not only affecting channel delivery/turnover(260), but also E-C coupling, myofilament contractility, and proteostasis (261), thus accounting also for structural cardiac abnormality.

Interestingly, the increase in α tubulin density is paralleled by a significant increase in the acetylation level of α tubulin at 40 lisine (K40) in the amino acidic sequence on α-tubulin **(Fig. 12C)**, as expected by the known higher affinity of the tubulin acetyltransferase (aTAT1) for polymerized tubulin (251). It was demonstrated that K40 acetylation weakens lateral interactions between protofilaments, thus softening the microtubules (262). As microtubules in living cells are frequently exposed to mechanical forces, an acetylation-induced increase in their flexibility would allow microtubules to better resist mechanical stress consequently making acetylated microtubules more long-lived. At the same time, longer-lived microtubules are still more likely to experience mechanical stress, thus further accumulating acetylation marks, which could reflect the notion that acetylation is a marker of microtubule age.

Indeed, it can be hypothesized that LMNA Q517X mutant impairing the mechanical nuclear–cytoskeletal coupling induces an adaptive cellular response such as microtubules polymerization and acetylation mimicking aged microtubules, with consequences on dis-regulated trafficking of Nav1.5 channel at the cell surface and the creation of pro-arrhythmic substrate.

The increasing in the α-tubulin acetylation may also account for the upregulation of AKT pathway we also found in LMNA Q517X-expressing cardiomyocytes. Interestingly, Giustiniani et al. found that tubulin acetylation recruits the chaperon protein Hsp90 to microtubules stimulating the signaling pathways of its client kinase AKT (263).

Of note, microtubules polymerization and stabilization obtained by either Taxol or Discodermolide two known chemotherapies, significantly increased ERK1/2 phosphorylation in different cell lines (264,265). Accordingly, we cannot exclude that the activation of ERK1/2 pathway we found in LMNA Q517X-expressing cardiomyocytes may be a downstream process to microtubules hyper-polymerization we found associated with this LMNA variant.

The altered tubulin state has already been found associated with some LMNA pathogenic variants. Instable microtubule network with a decrease in the acetylation of α tubulin triggered abnormal Cx43 localization and consequent electrical communication between cardiomyocytes in $Lmna^{H222P/H222P}$ and $Lmna^{N195K/N195K}$ mice (144,237). Accordingly, stabilization of microtubules using paclitaxel, a microtubule-stabilization agent commonly

used in chemotherapy, repositioned Cx43 in cardiomyocytes of *Lmna*$^{N195K/N195K}$ mice and improved intraventricular conduction defects in these mice (144). Recently, instable microtubules meshwork was also found in cardiomyocytes expressing E161K and D192G pathogenic LMNA variants with again a displacement of Cx43 (237), demonstrating a different pathogenic mechanism by which LMNA may displace a sarcolemmal protein through the microtubule network thus impairing heart electrical physiology.

To the best of our knowledge, we reported for the first time that an LMNA pathogenic variant is associated with an excess of microtubule polymerization and stabilization, which impairs Nav1.5 sarcolemmal expression and biophysics generating abnormalities in AP generation and propagation in cardiomyocytes.

Interestingly, we showed that a well-known FDA-approved alkaloid, colchicine, which depolymerizes the tubulin meshwork, reverted the altered AP properties of LMNA Q517X-expressing cardiomyocytes recapitulating those of the LMNA WT-expressing cardiomyocytes.

Similarly, when colchicine was tested on HEK293 cells expressing Nav1.5 and LMNA Q517X, I_{Na} currents and kinetics returned to those measured in control cells. The effect of colchicine non only provided evidence that the altered state of tubulin we observed is actually the key event in the electrical features of mutant expressing cardiomyocytes but also suggested a therapeutic intervention for this LMNA cardiomyopathy.

Interestingly, *in vivo* colchicine treatment significantly reduced microtubule density in cardiomyocytes of different rat models (266,267). Moreover, in the last 15 years colchicine was introduced in the field of cardiology for the treatment and prevention of different cardiovascular diseases (268), thus suggesting colchicine as a possible ready-to-use treatment for LMNA Q517X carriers.

In conclusion, our results confirm that LMNA protein at the nuclear envelope controls a chain of events involved not only in the mechanical but also in the electrical signaling transfer from the nucleus to the cell membrane in cardiomyocytes. Moreover, our findings suggest that every LMNA mutant may act with different pathogenic mechanisms in generating a common clinical phenotype in heart such as arrythmias and conduction defects. Indeed, it is very important to characterize each LMNA pathogenic variant in cardiomyocytes to gain insights on both the complexity of the cardiac cell biology, the mechanisms leading to cardiac dysfunction in laminopathies and the possible therapeutic approaches.

5. Targeting unfolded protein response reverts ER stress and ER Ca^{2+} homeostasis in cardiomyocytes expressing the pathogenic variant of Lamin A/C R321X

Giusy Pietrafesa[1], Roberta De Zio[2], Simona Ida Scorza[2], Maria Francesca Armentano[1], Martino Pepe[3], Cinzia Forleo[3], Giuseppe Procino[2], Andrea Gerbino[2], Maria Svelto[2] & Monica Carmosino[1].

[1]Department of Sciences, University of Basilicata, Potenza, Italy

[2]Department of Biosciences, Biotechnologies and Environment, University of Bari Aldo Moro, Bari, Italy

[3]Cardiology Unit, Department of Emergency and Organ Transplantation, University of Bari Aldo Moro, Bari, Italy

Published in *J Transl Med. 2023; 21(1):1–18 (https://doi.org/10.1186/s12967-023-04170-y)*

5.1 Abstract

Background

We previously demonstrated that an Italian family affected by a severe dilated cardiomyopathy (DCM) with history of sudden deaths at young age, carried a mutation in the *Lmna* gene encoding for a truncated variant of the Lamin A/C protein (LMNA), R321X. When expressed in heterologous systems, such variant accumulates into the endoplasmic reticulum (ER), inducing the activation of the PERK-CHOP pathway of the unfolded protein response (UPR), ER dysfunction and increased rate of apoptosis. The aim of this work was to analyze whether targeting the UPR can be used to revert the ER dysfunction associated with LMNA R321X expression in HL-1 cardiac cells.

Methods

HL-1 cardiomyocytes stably expressing LMNA R321X were used to assess the ability of 3 different drugs targeting the UPR, salubrinal, guanabenz and empagliflozin to rescue ER

stress and dysfunction. In these cells, the state of activation of both the UPR and the pro-apoptotic pathway were analyzed monitoring the expression levels of phospho-PERK, phospho-eIF2α, ATF4, CHOP and PARP-CL. In addition, we measured ER-dependent intracellular Ca^{2+} dynamics as indicator of proper ER functionality.

Results

We found that salubrinal and guanabenz increased the expression levels of phospho-eIF2α and downregulated the apoptosis markers CHOP and PARP-CL in LMNA R321X-cardiomyocytes, maintaining the so-called adaptive UPR. These drugs also restored ER ability to handle Ca^{2+} in these cardiomyocytes. Interestingly, we found that empagliflozin downregulated the apoptosis markers CHOP and PARP-CL shutting down the UPR itself through the inhibition of PERK phosphorylation in LMNA R321X-cardiomyocytes. Furthermore, upon empagliflozin treatment, ER homeostasis, in terms of ER ability to store and release intracellular Ca^{2+} was also restored in these cardiomyocytes.

Conclusions

We provided evidence that the different drugs, although interfering with different steps of the UPR, were able to counteract pro-apoptotic processes and to preserve the ER homeostasis in R321X LMNA-cardiomyocytes. Of note, two of the tested drugs, guanabenz and empagliflozin, are already used in the clinical practice, thus providing preclinical evidence for ready-to-use therapies in patients affected by the LMNA R321X associated cardiomyocytes.

5.2 Introduction

Lamin A/C (LMNA) are structural proteins of the nuclear envelope (NE) with a crucial role in cardiomyocytes function ((1,5). As a matter of fact, a cardiac involvement associated with mutations in the *Lmna* gene was one of the first phenotypes to be reported in humans (168). Mutations in the *Lmna* gene segregate with several cardiac phenotypes, including cardiac conduction disturbance, atrial or ventricular tachyarrhythmias, and DCM, resulting in heart failure or sudden cardiac death (269).

Cardiac laminopathies represent indeed a medical emergency being sudden cardiac death a burden impacting not only the way of life of patients and relatives but also health policies and interventions. To date, no specific therapeutic strategies are available to modify the disease progression. In fact, the clinical management of *Lmna*-related cardiomyopathy is no different from that for other forms of dilated cardiomyopathy and the implantable cardioverter-defibrillator (ICD) represents so far the unique strategy to prevent sudden death. Different disease models have been used in the field of cardiac laminopathies and several hypotheses have been postulated to underlying the electrical and structural abnormalities in the heart of laminopathy patients (102,144,241). Although the relevant advances in the knowledge of the mechanisms altering cardiac functions and structures in cardiac laminopathies, few therapeutic approaches have been proposed and developed.

The study of the $Lmna^{H222P/H222P}$ knock-in mouse, a murine model that recapitulates the dilated cardiomyopathy in humans, demonstrated upregulation of genes implicated in the MAPK signaling pathways (126). Accordingly, MEK1/2 inhibitors have been able to slow-down left ventricular dilatation progression, to improve cardiac contractility and functions and to increase survival of treated $Lmna^{H222P/H222P}$ mice (127,270,271). These findings led to the first clinical trial, still on going, on the p38α inhibitor in patients with LMNA-associated DCM (clinicaltrials.gov #NCT02057341).

We also found that the severity of the clinical manifestations in cardiac laminopathy patients harboring different pathogenic LMNA variants, correlates with the degree of inflammation in terms of numbers of pro-inflammatory cytokines upregulated, thus suggesting an immediate therapeutic approaches for each subset of patients (236).

Moreover, we recently showed that a well-known FDA-approved alkaloid, colchicine, recovered the altered tubulin polymerization state as well as the dysfunctional electrical properties in cardiomyocytes expressing a pathogenic LMNA variant (272).

The study of the pathogenic mechanisms underlying cardiac laminopathies is, indeed, an unique opportunity to identify pharmacological targets and hopefully ready-to-use therapies for these inherited cardiomyopathies.

Different cohort studies revealed that, compared with missense mutation carriers, nonsense mutation carriers had a significantly worse prognosis because of earlier onset of cardiac conduction disturbance (CCD), atrial arrhythmias, and left ventricular systolic dysfunction (215,244). This finding suggests that the pathogenetic mechanism of the cardiomyopathy in the nonsense mutation group might be related to either the dominant negative effect or cytotoxic effect of the resulting truncated LMNA protein rather than exclusively haploinsufficiency of LMNA wild type. Accordingly, we and others demonstrated that truncated pathogenic variants of LMNA were expressed into the heart of the carriers and may induce abnormal degradation of the WT LMNA [16] or interfere with cardiomyocytes homeostasis (165,166,272).

Specifically, we previously characterized nonsense *Lmna* mutation that introduces a premature termination codon within the 6th of 12 *Lmna* exons corresponding to a truncated variant in the central a-helical coiled-coil rod domain (coil 2B) of the LMNA protein, R321X. We identify this mutation in several members of an Italian family with a frequent history of sudden death and a severe DCM, confirming that this mutation is associated with a very severe cardiac phenotype and poor prognosis (165).

We have been able to detect the expression of LMNA R321X in the transplanted heart of a patient carrying this nonsense mutation. When we tried to get more insights into the disease-causing mechanisms by heterologous expression of LMNA R321X, we found that R321X was not targeted to the nuclear envelope, as expected by the absence of the nuclear localization sequence in the truncated version of LMNA, rather it accumulates in the ER. Functional studies showed that the presence of R321X into the ER caused the onset of the ER stress and the unfolded protein response (UPR). The latter triggers ER Ca^{2+} handling abnormalities and thus increased susceptibility to apoptosis (165).

The UPR is a complex signal transduction pathway that is initiated by the activation of at least three UPR stress sensors: inositol-requiring protein 1 (IRE1), protein kinase RNA-like ER kinase (PERK) and activating transcription factor 6 (ATF6). UPR signaling has distinct kinetics, intensities and downstream consequences depending on the nature and intensity of the stimuli and the cell type involved (273). In this work we provided evidence that in cardiomyocytes the expression of LMNA R321X variant induced specifically the activation

of the PERK arm of the UPR and that targeting this pathway we have been able to rescue the functional phenotype of these cardiomyocytes in terms of ER function and cell survival.

5.3 Methods

5.3.1 Cell culture

HL-1 cardiomyocytes were cultured on gelatin/fibronectin coated flasks (5 µg/mL fibronectin, F1141, Sigma-Aldrich, in 0.02% Gelatin from bovine skin, G9391, Sigma-Aldrich) using Claycomb Medium (51800C, Sigma-Aldrich) supplemented with 10% fetal bovine serum (F2442, Sigma-Aldrich), Penicillin/Streptomycin 100 U/mL: 100 µg/mL (P4333, Sigma-Aldrich), 2 mM L-Glutamine (G7513, Sigma-Aldrich) and 0.1 mM Norepinephrine [(±)-Arterenol] (A0937, Sigma-Aldrich) in a humidified 5% CO_2, 95% O_2 incubator at 37 °C.

Cell concentration and viability were assessed using Trypan Blue Stain, 0.4% with LUNA-II™ Automated Cell Counter (Logos Biosystems).

5.3.2 Generation of stable HL-1 clones expressing either WT or R321X LMNA

Lentiviral construct coding for LMNA R321X mCherry-tagged protein was produced by Stratagene's Quik Change II XL site-directed mutagenesis kit (Agilent Technologies), using the the lentiviral plasmid encoding for mCherry-tagged Lamin WT mCherry-tagged (pLV[Exp]-Neo-CMV > mCherry(ns):hLMNA[NM_170707.4], Vector Builder). Mutagenic primers were designed using Quik Change Primer Design Program as previously shown (165). The mutation was verified by sequencing.

Viral particles were produced in HEK-293T cells by simultaneously co-transfection (Invitrogen™ Lipofectamine™ 2000 Transfection Reagent) of the plasmid carrying the gene for protein of interest (mCherry-tagged-Lamin WT or mCherry-tagged-Lamin R321X), the envelope plasmid encoding VSV-G and the packaging plasmid encoding Gag/Pol and Rev, as previously reported (272).

For lentiviral transduction, HL-1 cells were plated in a 6-well plate at 30–50% of confluency, and after adhesion, they were incubated with 500 µL of virus-containing medium at 37 °C in a humidified 5% CO_2 incubator for 18 h. After viral particles removal, cells were then incubated with 400 µg/mL Geneticin (G418, Gibco, Life Technologies) for 1 week to select stable clones. Pure clones were selected by fluorescence microscopy.

5.3.3 Immunofluorescence confocal analysis

Stable transduced HL-1 cells were grown on coverslips to confluency, then were fixed in PFA with 0.1% Triton X-100 for 20 min at RT. After washes with PBS, cells were blocked in 1% bovine serum albumin (BSA) in PBS for 30 min at room temperature (RT) and incubated with anti-Calnexin (dil. 1:500; Santa Cruz Biotechnology). After three washes in PBS cells were incubated with 488 Alexafluor-conjugated secondary antibodies (Thermo Fisher Scientific) for 1 h at RT for calnexin identification. The signal corresponding to LMNA proteins was detected using their fluorescent m-Cherry tag. After removal of the secondary antibody, coverslips were mounted in PBS/glycerol (1:1) containing 1% n-propylgallate, pH 8.0.

Confocal images were acquired with a confocal laser-scanning fluorescence microscope (Leica TSC-SP2).

5.3.4 MTT assay

The in vitro cytotoxicity for salubrinal (SML0951, Sigma-Aldrich), guanabenz (G110, Sigma-Aldrich) and empagliflozin (S8022, Selleckchem) was verified by 3-(4,5-dimethylthizol-2-yl)-2,5-diphenyl tetrazolium bromide (MTT) colorimetric assay [20] (Sigma-Aldrich).

HL-1 cells were seeded in 96-well plates at the density of 1.0×104 cells/well. After complete adhesion, cells were treated for 48 h in complete grow medium with the appropriate compounds at three different concentrations (salubrinal: 100, 200, 300 µM; guanabenz: 10, 20, 30 µM; empagliflozin: 5, 10 e 50 µM). Cells were maintained in a humidified incubator (at 37 °C, 5% CO2) throughout the treatment, refreshing the medium containing the proper amount of drugs after 24 h of incubation. Cells in complete medium without treatments were used as healthy control cells, whereas 0.1% Triton x-100 for 4 h was used as positive control of cellular death.

At the end of the 48-h treatment, 5 mg/mL MTT were added to the cells and incubated for 3 h. Next, the cells were washed two times with PBS to remove detached dead cells and the formazan crystals were solubilized adding 100 µL of DMSO to each well.

Absorption was detected at 595 nm with a microplate reader (Bio-Rad) and corrected for background absorption at 620 nm.

The cytotoxicity of the drugs used in our experiments was determined by statistically comparing the absorbance measured in treated and untreated control cells.

5.3.5 Cytosolic Ca^{2+} measurements

For intracellular Ca^{2+} measurements, HL-1 cardiomyocytes, stably expressing WT or LMNA R321X protein were plated on gelatin/fibronectin coated 15-mm coverslip 96 h before the experiment. After complete cell adhesion, cells were left in complete Claycomb media or incubated with 200 µM salubrinal, 20 µM guanabenz or 10 µM empagliflozin added to the complete Claycomb media for a 48 h in a humidified incubator (5% CO_2, 95% O_2) at 37 °C. Ca^{2+} measurements were performed using 6 µM Fura-2, AM (F1221, Invitrogen). Cells were dye-loaded for 30 min at 37 °C in medium before the experiment. After the incubation, cells were washed with extracellular ringer (138 mM NaCl, 4 mM KCl, 1 mM $MgCl_2$, 10 mM Hepes, 10 mM Glucose, 1.8 mM $CaCl_2$, pH 7.4) and left in the incubator to allow de-esterification of the dye. Coverslips with dye-loaded cells were mounted in a perfusion chamber (RC quick release non-magnetic chamber, Warner Instruments), housed in a Quick Exchange Platform (QE-1, Warner Instruments) and analyzed using an inverted microscope (Nikon Eclipse TE2000-S microscope) equipped for single cell fluorescence measurements and imaging analysis. The sample was illuminated through a 40 × oil immersion objective (NA = 1.30). The Fura-2AM loaded sample was excited alternately at 340 and 380 nm every 5 s. Emitted fluorescence was passed through a dichroic mirror, filtered at 510 nm (Omega Optical) and captured by a cooled CCD camera (CoolSNAP HQ, Photometrics). Cells were stimulated with 40 µM cyclopiazonic acid (CPA, C1530, Sigma-Aldrich) in Ca^{2+}-free extracellular solution containing 50 µM EGTA (E4378, Sigma-Aldrich) to induce ER Ca^{2+} depletion. After 20 min of stimulation with CPA, re-addition of extracellular Ca^{2+} (5 mM Ca^{2+}) in the continuous presence of CPA induced capacitative calcium entry (CCE). Fluorescence measurements were performed using Metafluor software (Molecular Devices, MDS Analytical Technologies). The fluorescence ratio was recorded and normalized to the basal fluorescence ratio observed in the absence of stimulus (R/R0). Experiments were performed at room temperature.

For determination of intracellular Ca^{2+} concentration, Fura-2AM traces were corrected for the background fluorescence and fluorescence ratio (R) was calibrated according the following equation: $[Ca^{2+}]_i = Kd \times Q(R - Rmin)/(Rmax - R)$, where Kd (224 nM) indicated

the dissociation constant of Fura-2AM for Ca^{2+}_i and Q indicated the ratio of the fluorescence intensities at the minimum and the maximum Ca^{2+} concentration at 380 nm. Each sample was calibrated by the addition of 5 μM ionomycin in presence of 0.5 mM EGTA (Rmin) followed by 5 μM ionomycin in 10 mM $CaCl_2$ (Rmax).

5.3.6 Evaluation of NFAT-GFP translocation

The evaluation of NFAT translocation was performed as previously described [21]. Briefly HL-1 cells were transfected with NFATc4-GFP (kindly provided by Chi-Wing Chow (Department of Molecular Pharmacology, Albert Einstein College of Medicine, Bronx, NY, USA) with Lipofectamine 2000 according to the manufacturer's instructions. After 24 h, cells were either left untreated (CTR) or stimulated for 48 h as follows: 200 μM salubrinal, 10 μM guanabenz, 10 μM empagliflozin, in a humidified incubator at 37 °C, 5% CO_2, and 95% O_2.

Cells were fixed in PBS containing 4% paraformaldehyde and stained with DAPI for nuclear counter staining. Ten different fields for each treatment from three independent experiments were acquired blindly using the Leica DM6000B fluorescence microscope (Leica Instruments). Cells expressing NFAT-GFP were counted, and Image J was used to keep track of the nuclei vs cytosol-positive staining of the probe using DAPI colocalization to confirm NFAT nuclear translocation.

5.3.7 Western blot analysis

For protein extraction HL-1 LMNA clones were plated in a 12 wells cell culture support coated with gelatin-fibronectin until 80% of confluency. Cells were then left in complete Claycomb medium or treated adding to complete Claycomb medium either 200 μM salubrinal, 10 μM guanabenz or 10 μM empagliflozin for 48 h in a humidified incubator (5% CO_2, 95% O_2) at 37 °C.

After treatments cells were placed on ice, washed in PBS and lysed in RIPA buffer added with protease and phosphatase inhibitors (NaCl 150 mM, Tris/HCl 10 mM, 1% Triton X-100, SDS 0.1%, deoxycholate-Na 1%, EDTA 5 mM; NaF 10 mM, orthovanadate 100 mM, pyrophosphate 15 mM, pH 7.2). Cell suspensions were sonicated 3 times for 15 s at 60 Ampli

with a Vibra-cell® (Sonics & Materials Inc) and membrane debris were pelleted at 13,000 rpm for 30 min at 4 °C. Samples were quantified by Bradford protein assay and set up for the western blot analysis in 4 × Laemmli Sample Buffer (Bio-Rad) plus 50 mM DTT.

Protein samples were denatured at 60 °C for 10 min, resolved by electrophoresis on polyacrylamide SDS gel (7.5% or 12% Mini-PROTEAN TGX Stain-Free Precast Gels; Bio-Rad) and blotted on 0.2 µm PVDF membrane (Trans-Blot Turbo RTA Mini 0.45 µm LF PVDF Transfer Kit, for 40 blots #1704274, Bio-Rad) through the Trans-Blot Turbo Transfer System (Bio-Rad). Immobilized proteins were blocked at room temperature for 1 h in TBST-5% milk or in TBST-BSA 3% (TBST: 50 mM Tris, 150 mM NaCl, 0.1% Tween-20; pH 7.4) and incubated overnight at 4 °C with the following antibodies prepared in blocking buffer: anti-PARP (dil. 1:1000 in TBST-5% milk; #9542 Cell Signaling Technology), anti-Phospho-eIF2α (Ser51, dil. 1:1000 in TBST-BSA 5%; #9721 Cell Signaling Technology), anti-CHOP (dil. 1:1000 in TBST-BSA 5%; #2895 Cell Signaling Technology), anti-XBP-1s (dil. 1:1000 in TBST-5% milk; #647501 BioLegend), anti-phospho-PERK (Thr982, dil. 1:1000 in TBST-5% milk; #SAB5700521 Sigma Aldrich), anti-GRP78/BiP (dil. 1:1000 in TBST-5% BSA; #ab21685 Abcam), anti-ATF4 (dil. 1:1000 in TBST-5% milk; #11815 Cell Signaling), anti-STIM1 (dil. 1:1000 in TBST-5% milk; #66189-1 Proteintech), anti-ORAI1 (dil. 1:5000 in TBST-5% milk, #66223-1 Proteintech), anti-Na^+/K^+-ATPase α subunit (dil. 1.1000 in TBST-1% BSA; # C464.6 Millipore), anti-phospho-AKT (Ser473; dil. 1:4000 in TBST-1% BSA; #4060 Cell Signaling).

Secondary antibodies were selected depending on the host species of the primary antibodies and prepared in the relative blocking buffer (Goat anti-mouse IgG-HPR conjugate 1:5000, Bio-Rad; Goat anti-rabbit IgG-peroxidase 1:5000, Sigma-Aldrich). Chemiluminescent reactions were detected thanks to ChemiDoc™ System (Bio-Rad) using ECL substrate (Clarity western ECL substrate #1705061 or Clarity max Western ECL Substrate #1705062, Bio-Rad). Densitometric analysis was performed by Image Lab 6.0 software. Stain-free technology (Bio-Rad) allowed quantifying protein loading.

5.3.8 Statistical analysis

For both intracellular Ca^{2+} measurements and western blot analysis data are given as mean ± standard error of the mean (SEM). Student's T-test and One-way Anova were used to compare different experimental conditions. Significance was accepted for p-values < 0.05.

The software GraphPad Prism 8 allowed performing the statistical analysis and graphical representation of the data.

5.4 Results

5.4.1 Activation of the PERK arm of the UPR in LMNA R321X-expressing cardiomyocytes

We generated HL-1 cardiomyocytes stably expressing LMNA R321X to recapitulate the cellular phenotype of R321X-cardiolaminopathy. Control LMNA WT-cardiomyocytes were generated as well. As previously shown in HEK-293 cells, LMNA R321X accumulates into the ER of HL-1 cardiomyocytes in contrast with LMNA WT, which, as expected, decorates the nuclear rim (**Fig. 21A**, LMNA WT, LMNA R321X). We previously demonstrated in HEK-293 cells and in R321X carrier's heart, that R321X accumulation into the ER triggers ER stress and the activation of the PERK-CHOP branch of the UPR (165). During ER stress, PERK activation induces the phosphorylation and inhibition of the eukaryotic translation initiation factor 2 alpha (eIF2α), thus reducing the global protein synthesis and consequently ER workload. On the other hand, phosphorylation of eIF2α increases the cap-independent translation of certain mRNAs, such as activating transcription factor 4 (ATF4). ATF4 is a transcription factor that regulates a wide range of genes playing a crucial role in cell adaptation to stress conditions and cell survival, but, during long-term ER stress, ATF4 may also stimulate genes of CCAAT-enhancer-binding protein homologous protein (CHOP), which is responsible for initiation of the apoptotic cascade (for review see (273)). As shown in **Fig. 21B**, the expression of LMNA R321X in cardiomyocytes significantly increased the expression of both phospho-PERK (p-PERK) and CHOP compared to their controls, thus confirming the activation of PERK-CHOP pathway. We also checked for the expression of spliced X-box-binding protein-1 (s-Xbp1) and of (Glucose-Regulated Protein 78) GRP78 proteins whose expression levels are associated with the activation of IRE1α- and ATF-6-dependent pathways of the UPR response (274), respectively. As shown in **Fig. 21B** their expression was comparable in the two lines of cardiomyocytes.

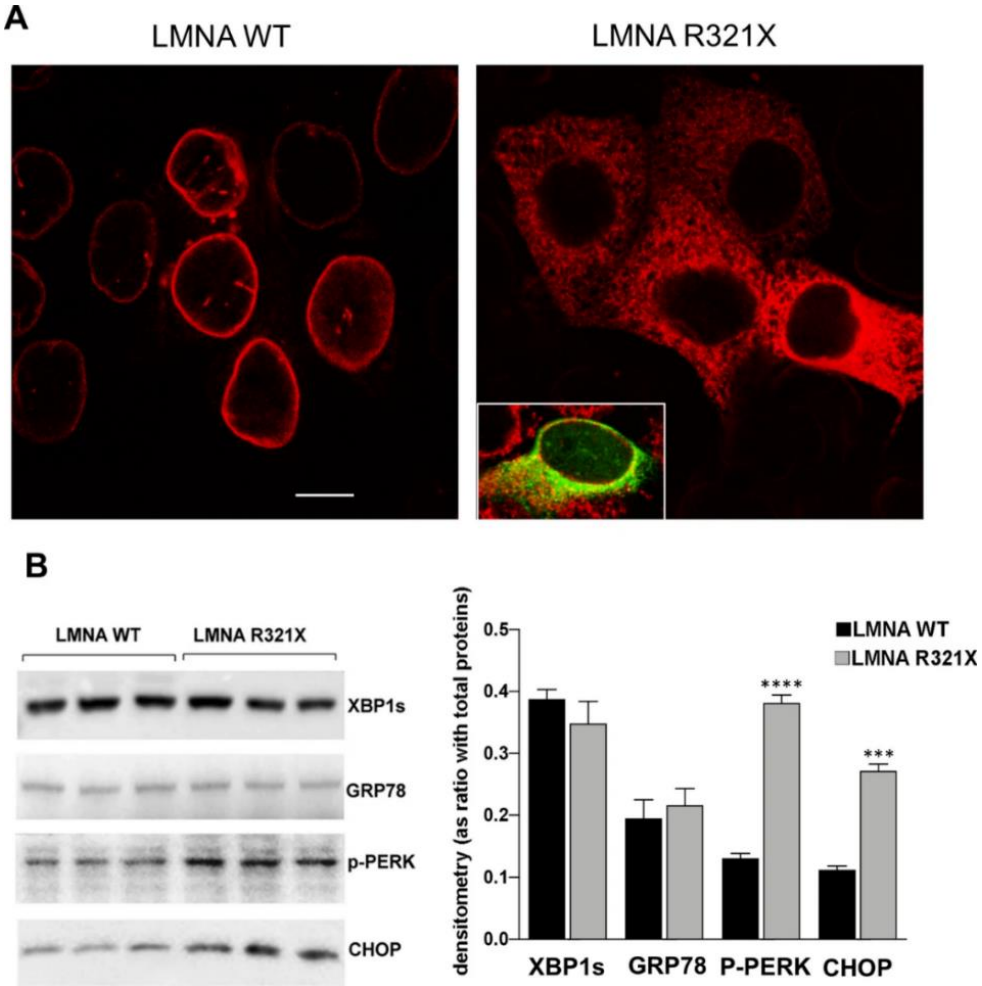

Figure 21: Expression of WT and R321X LMNA in HL-1 cardiomyocytes. (A) Confocal laser fluorescence analysis of LMNA in HL-1 clones where red signals correspond to m-Cherry tagged LMNA proteins and the green signal, in the inset, corresponds to the ER marker calnexin. Bar = 10 µm. (B) Expression of ER stress markers in WT and R321X LMNA-cardiomyocytes. Left panel: representative Western blotting of XBP1s, GRP78, p-PERK and CHOP in the two lines of cardiomyocytes (LMNA WT, LMNA R321X). The triplicate of each experimental condition in the representative western blotting corresponds to three different biological replicas. Right panel: densitometric analysis of the immunoreactive bands corresponding to the ER stress markers, normalized for total protein content. Data are represented as mean ± SEM. Statistical analysis was performed on three independent experiments and significance calculated by Student's t-test for unpaired samples. (****p = 0.0001, LMNA R321X vs LMNA WT; ***p = 0.0002, LMNA R321X vs LMNA WT).

5.4.2 Targeting eIF2α in LMNA R321X- cardiomyocytes: effect of salubrinal and guanabenz

DNA damage-inducible 34 (GADD34) protein is involved in braking PERK-CHOP arm of UPR by functioning as a protein phosphatase 1 (PP1) subunit targeting phosphorylated eIF2α. Previous evidence demonstrated that inhibition of eIF2α dephosphorylation by GADD34 deletion or using small molecule inhibitors of the GADD34–PP1 complex, prolonged eIF2α phosphorylation, subsequently leading to adaptive UPR and promoting cell survival (275).

We thus tested the effect of two inhibitors of the GADD34–PP1 complex, salubrinal and guanabenz, in inducing sustained eIF2α phosphorylation without affecting cell viability in LMNA R321X-cardiomyocytes. MTT test clearly demonstrated that cell viability was not significantly affected for concentrations below 300 μM salubrinal and 30 μM guanabenz **(Fig. 22A)**. The concentrations tested in the MTT assay have been chosen in the range of those reported in bibliography to be effective in sustaining adaptive UPR. Both compounds after 48 h of incubation at non-toxic concentrations were able to increase the phosphorylation levels of eIF2α in LMNA R321X-cardiomyocytes in a dose-dependent fashion (**Fig. 22B, C**, p-eIF2α). For the following experiments we used 200 μM salubrinal and 20 μM guanabenz for 48 h, since MTT test clearly demonstrated that cell viability was not significantly affected at these concentrations although the levels of p-eIF2α were significantly increased.

We studied the possible beneficial effect of the sustained eIF2α phosphorylation upon salubrinal and guanabenz treatment analyzing the expression levels of the major players in the PERK branch of the UPR. As shown in **Fig. 23A, B**, 48 h treatment with either salubrinal or guanabenz, significantly reduced the expression of both pro-apoptotic factor CHOP, and the caspase-dependent apoptosis marker, cleaved Poly (ADP-ribose) polymerase 1 (PARP-CL), in LMNA R321X-cardiomyocytes almost at levels of LMNA WT-cardiomyocytes (**Fig. 23A**, CHOP, PARP-CL; **Fig. 23B** CHOP expression, PARP-CL expression). The efficacy of both drugs was proved by the increased levels of p-eIF2α in treated LMNA R321X-cardiomyocytes (**Fig. 23A**, p-eIF2α; **Fig. 23B**, p-eIF2α expression). As expected, the expression of p-eIF2α downstream effector, ATF4, increased together with the sustained p-eIF2α phosphorylation under salubrinal or guanabenz treatments (**Fig. 23A**, ATF4; **Fig. 23B**, ATF4 expression). Interestingly, the phosphorylation level of the ER stress sensor PERK decreased under drug treatments in LMNA R321X-cardiomyocytes although both drugs

were targeting the downstream effector of PERK, p-eIF2α (**Fig. 23A**, p-PERK; **Fig. 23B**, p-PERK expression). This finding confirms that salubrinal and guanabenz were actually alleviating ER stress. It has been demonstrated that ER stress may also suppress AKT/TSC/mTOR signaling pathway (276,277). Accordingly, we found that phosphorylated AKT (p-AKT) was significantly downregulated in LMNA R321X-cardiomyocytes compared to their controls and that both salubrinal and guanabenz re-established the levels of p-AKT at the levels of those measured in LMNA WT-cardiomyocytes (**Fig. 23A**, p-AKT; **Fig. 23B**, p-AKT expression). The expression of the house keeping protein Na^+/K^+-ATPase α subunit was also analyzed to confirm that overall protein synthesis was not altered by the increased levels of p-eIF2α upon salubrinal and guanabenz treatments (**Fig. 23A**, Na^+/K^+-ATPase).

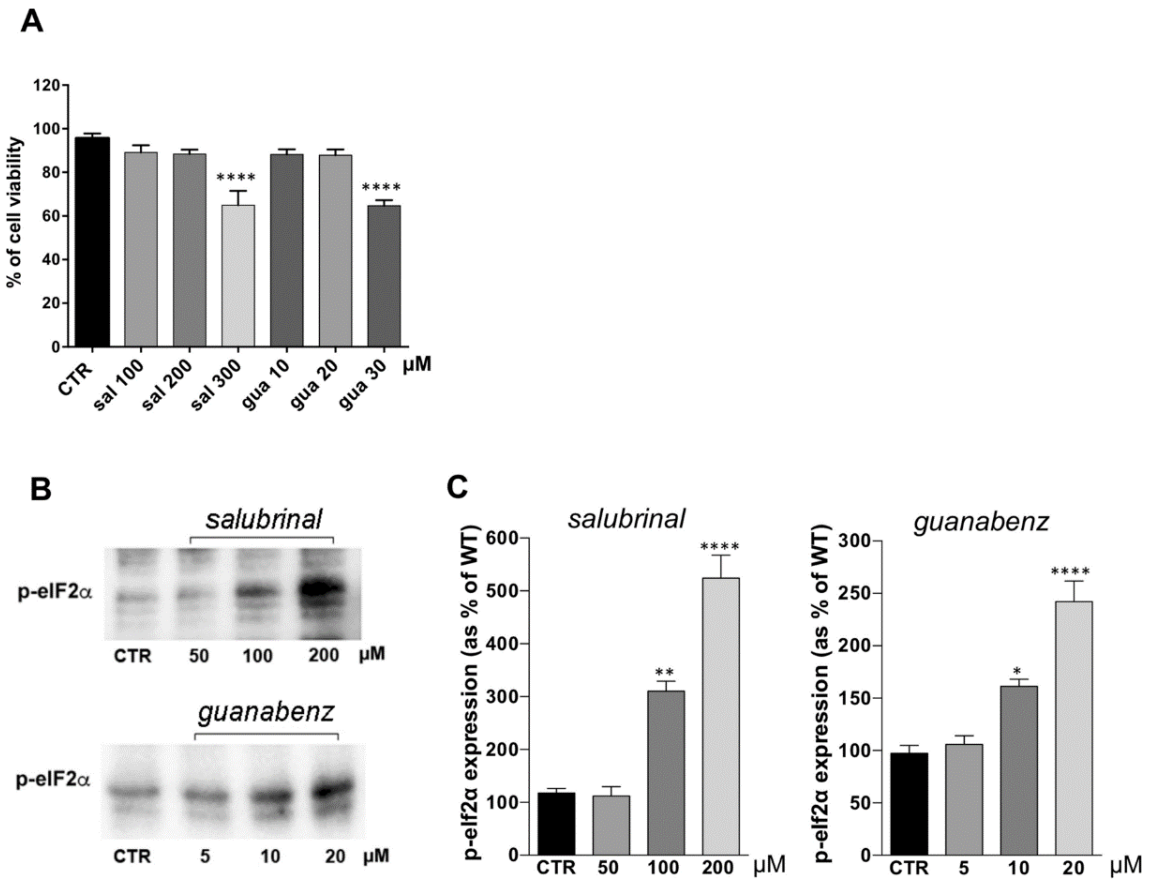

Figure 22: Effect of salubrinal and guanabenz on cell viability and eIF2α phosphorylation. (A) MTT assay performed on LMNA R321X-cardiomyocytes upon 48 h incubation with salubrinal and guanabenz at three different concentrations. Statistical analysis was performed on three independent experiments and significance calculated by one-way Anova. Significancy of untreated cardiomyocytes (CTR) vs treated cardiomyocytes is reported (****p = 0.0001). (B) Representative

Western blotting of phospho-eIF2α (p-eIF2α) performed on lysates from LMNA R321X-cardiomyocytes treated with either salubrinal or guanabenz at three different concentrations for 48 h. The triplicate of each experimental condition in the representative western blotting corresponds to three different biological replicas. (C) Densitometric analysis of the immunoreactive bands corresponding to p-eIF2α in the experimental conditions shown in A, normalized for total protein content and reported as % of the control condition. Data are represented as mean ± SEM. Statistical analysis was performed on three independent experiments and significance calculated by one-way ANOVA and Tukey's multiple comparisons test. Significancy of untreated cardiomyocytes (CTR) vs treated cardiomyocytes is reported (*p = 0.01, **p = 0.003, ****p = 0.0001).

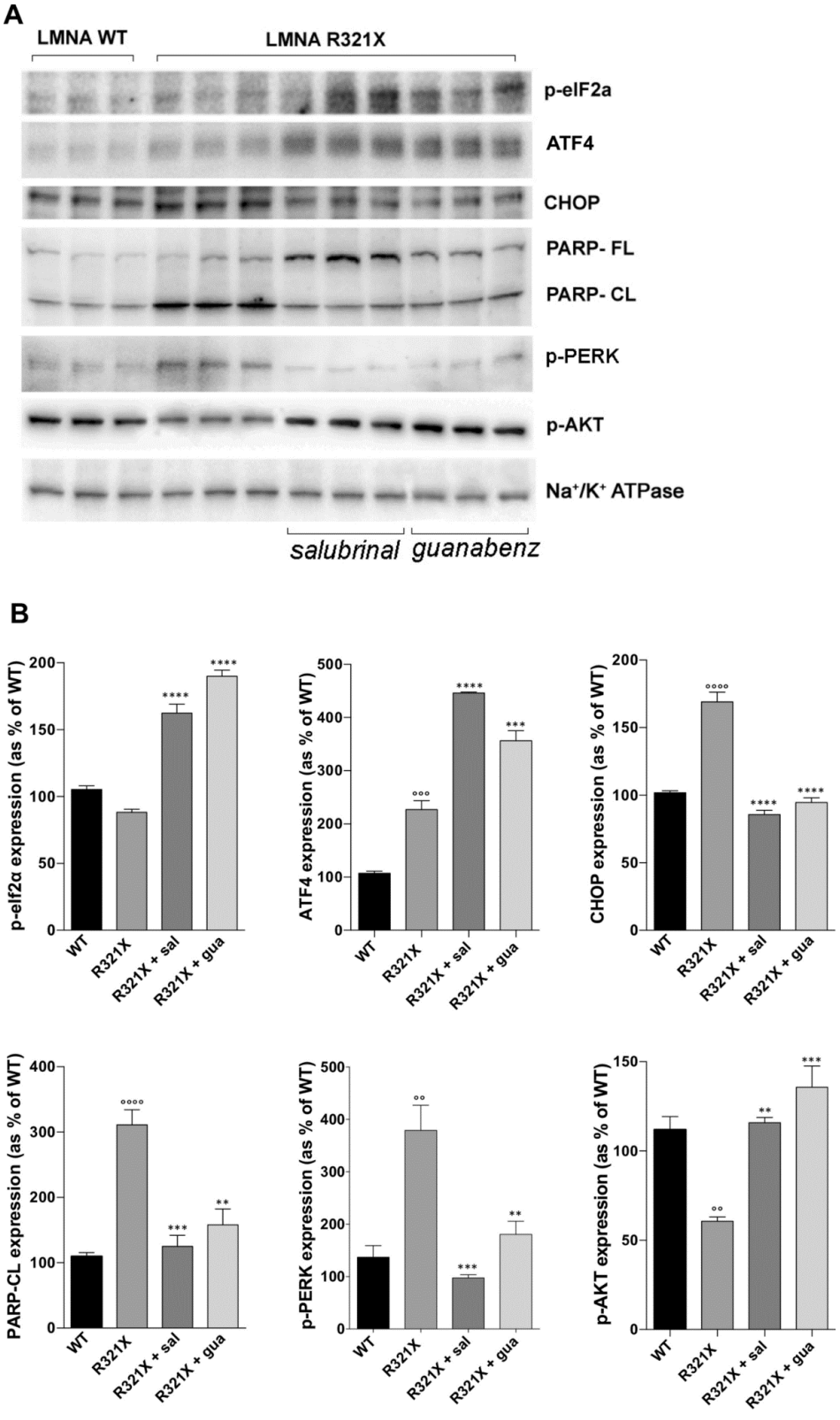

Figure 23: Effect of salubrinal and guanabenz on the expression of markers of PERK and AKT pathways in LMNA R321X-cardiomyocytes. (A) Representative Western blotting of phospho-eIF2α (p-eIF2α), ATF4, CHOP, full length PARP (PARP-FL) and cleaved PARP (PARP-CL), p-PERK and p-AKT performed on lysates from LMNA R321X-cardiomyocytes treated with either 200 µM salubrinal or 20 µM guanabenz for 48 h and from LMNA WT-cardiomyocytes as control. The

expression of Na^+/K^+-ATPase α subunit was also checked in all samples as control. The triplicate of each experimental condition in the representative western blotting corresponds to three different biological replicas. (B) Densitometric analysis of the immunoreactive bands corresponding to p-eIF2α, ATF4, CHOP, PARP-CL, p-PERK, p-AKT in the experimental conditions shown in A, normalized for total protein content and reported as % of the control condition (WT). Data are represented as mean ± SEM. Statistical analysis was performed on three independent experiments and significance calculated by one-way ANOVA and Tukey's multiple comparisons test (°°°°p = 0.0001, °°°p = 0.0003, °°p = 0.003 for WT vs R321X; **p = 0.003, ***p = 0.0003, ****p = 0.0001 for untreated R321X vs treated R321X).

5.4.3 Targeting PERK in LMNA R321X-cardiomyocytes: effect of empagliflozin

The treatment with salubrinal and guanabenz was aimed at inducing an adaptive UPR pathway, which predominantly maintains the ER function and/or ER proteostasis under ER stress conditions. However, long-term or severe ER stress could activate a maladaptive UPR pathway leading to eliminate dysfunctional cells by apoptosis or autophagy. In this scenario, shutting-down the UPR response may also results beneficial for cell survival and homeostasis. The PERK-dependent UPR pathway initiates with PERK auto-phosphorylation by its kinase domain when its cytoplasmic domain senses the accumulation of unfolded/misfolded proteins in the ER lumen. Several inhibitors of PERK catalytic domain have been developed and shown to be effective in down-regulating UPR response promoting cells survival (278). However, they resulted to have off-target effects, which limited their use in clinical practice (279).

Interestingly, empagliflozin, a selective sodium-glucose co-transporter-2 (SGLT-2) inhibitor, a new class of oral anti-diabetic agents approved for the treatment of type 2 diabetes mellitus, has been demonstrated to provide additional non-glycemic benefits, counteracting the activation of PERK-CHOP branch of the UPR in either cardiovascular or neuronal diseases (280).

We indeed, analysed the possible effect of empagliflozin in LMNA R321X-cardiomyocytes in alleviating ER disfunction. First of all we performed a cell toxicity assay incubating LMNA-cardiomyocytes with empagliflozin at 3 different concentrations for 48 h. Concentrations to be tested have been chosen in the range of those reported in bibliography

to be effective in counteracting UPR **(Fig. 24A).** In the following experiments we used 10 µM empagliflozin as the maximal dose at which cell viability was not significantly affected. As shown in **Fig. 24B, C** treatment with 10 µM empagliflozin significantly decreased the expression levels of both CHOP and PARP-CL in LMNA R321X-expressing cardiomyocytes toward those observed in LMNA WT-cardiomyocytes (**Fig. 24B**, CHOP and PARP-CL; **Fig. 24C**, CHOP expression and PARP-CL expression). The downregulation of p-PERK in empagliflozin treated LMNA R321X-cardiomyocytes clearly indicated the efficacy of this drug in braking the PERK-dependent UPR (**Fig. 24B** p-PERK; **Fig. 24C** p-PERK expression). We also checked whether empagliflozin was able to rescue the phosphorylation levels of AKT in LMNA R321X-cardiomyocytes. As shown in **Fig. 24** empagliflozin significantly increased p-AKT levels in treated LMNA R321X-cardiomyocytes toward those of LMNA WT-cardiomyocytes (**Fig. 24B**, p-AKT; **Fig. 24C**, p-AKT expression) confirming the ability of this drug to promote pro-survival pathways in cells and animal models (281).

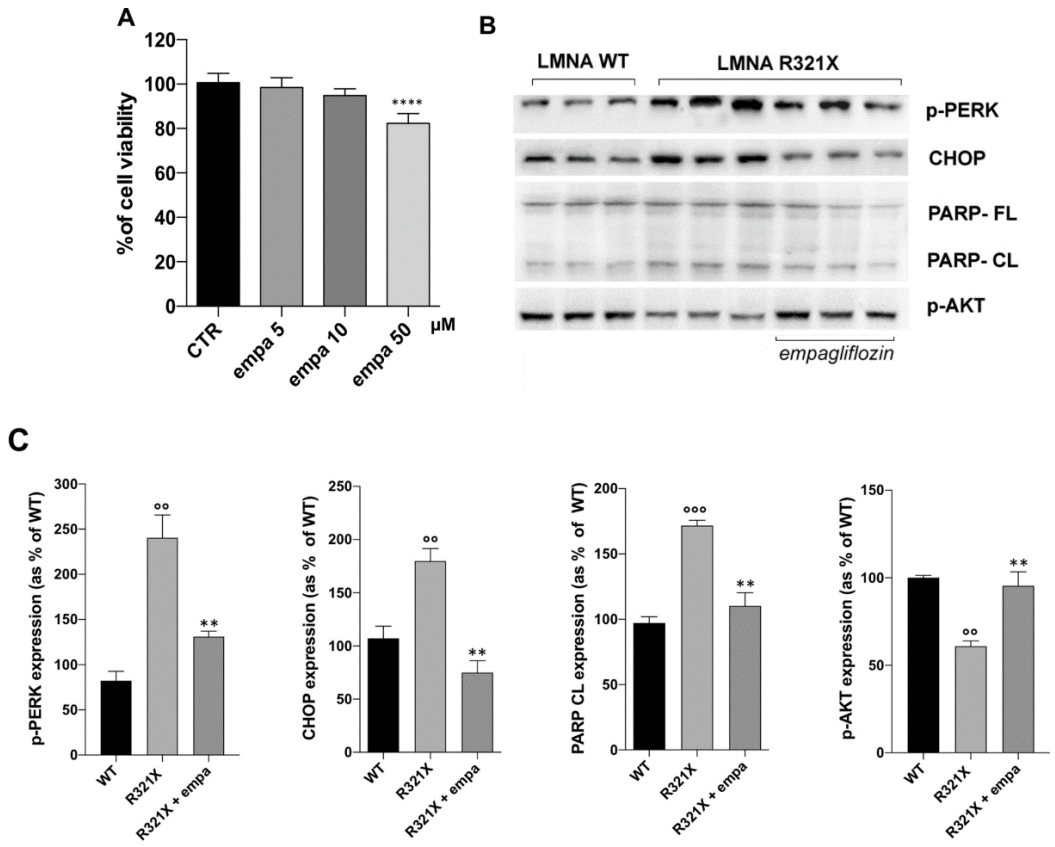

Figure 24: Effect of empagliflozin on the expression of markers of PERK and AKT pathway in LMNA R321X-cardiomyocytes. (A) MTT assay performed on LMNA R321X-cardiomyocytes upon

48 h incubation with empagliflozin at three different concentrations. Statistical analysis was performed on three independent experiments. Data reported as mean ± SEM and significance calculated by one-way Anova. (B) Representative Western blotting of p-PERK, CHOP, full length PARP (PARL-FL), cleaved PARP (PARP-CL) and p-AKT performed on lysates from LMNA R321X-cardiomyocytes treated with 10 μM empagliflozin for 48 h and from LMNA WT-cardiomyocytes as control. The triplicate of each experimental condition in the representative western blotting corresponds to three different biological replicas. (C) Densitometric analysis of the immunoreactive bands corresponding to p-PERK, CHOP, PARP-CL and p-AKT in the experimental conditions shown in B, normalized for total protein content and reported as % of the control condition (WT). Data are reported as mean ± SEM. Statistical analysis was performed on three independent experiments and significance calculated one-way ANOVA and Tukey's multiple comparisons test (°°p = 0.001 and °°°p = 0.0006 for WT vs R321X; **p = 0.007 for untreated R321X vs treated R321X).

5.4.4 Effect of all drugs tested on ER functions

We previously demonstrated in HEK-293 cells that ER stress induced ER function impairment characterized by an increased Ca^{2+} leakage from the ER and a decreased ability to restore ER luminal levels of Ca^{2+} (165).

It is well known that leaky ER induces in turn a cytosolic Ca^{2+}overload (282), which in cardiomyocytes could profoundly affect either electrical or contractile function. We indeed measured the cytosolic Ca^{2+} concentration $[Ca^{2+}]_{cyt}$ in LMNA WT and R321X-cardiomyocytes by the use of Fura2-AM fluorescent Ca^{2+} dye (see methods for details) and we found that in resting condition $[Ca^{2+}]_{cyt}$ in LMNA R321X-cardiomycytes was almost three fold higher than those measured in LMNA WT cardiomyocytes in which, in turn, was in the expected physiological range (**Fig. 25A**, WT: 197.6 ± 6.27 nM; R321X: 509.5 ± 16.16 nM). Interestingly, the treatment of LMNA R321X-cardiomyocytes with salubrinal, guanabenz or empagliflozin significantly lowered the $[Ca^{2+}]_{cyt}$ almost at levels found in controls, thus indicating that all of them were able to counteract ER Ca^{2+} leakage in these cardiomyocytes (**Fig. 25A**, R321X + sal: 240 ± 11.63 nM; R321X + gua: 242 ± 12.36 nM; R321X + empa: 236.2 ± 12.36).

It is well known that the increase in $[Ca^{2+}]_{cyt}$ induces the activation of the Ca^{2+}/calmodulin-dependent serine/threonine protein phosphatase, calcineurin, which de-phosphorylates the

nuclear factor of activated T-cells (NFAT), inducing its translocation into the nucleus (283). Moreover, UPR response may per se activate calcineurin, since its phosphatase activity on ER chaperons may relieve ER stress (284).

We have, indeed, analysed if calcineurin was activated in LMNA R321X-cardiomyocytes monitoring the nuclear translocation of a GFP-tagged version of NFAT (GFP-NFAT), when expressed in these cardiomyocytes both in resting condition and upon drugs treatments.

The subcellular localization of GFP-NFAT, expressed as the ratio between the number of cardiomyocytes expressing the probe in the nucleus (* in the inset of **Fig. 25B**) vs those expressing the probe in the cytosol (# in the inset of **Fig. 25B**), was compared in resting and treated LMNA R321X-cardiomyocytes and in LMNA WT-cardiomyocytes as control (**Fig. 25B**). Of note, we found a significant increase in NFAT-positive nuclei in LMNA R321X-cardiomyocytes, compared to LMNA WT-cardiomyocytes (**Fig. 25B**, R321X). The treatment of LMNA R321X-cardiomyocytes with salubrinal, guanabenz or empagliflozin restored the prevalent cytosolic localization of GFP-NFAT as shown by the ratio between cardiomyocytes expressing the probe in the nucleus vs those expressing the probe in the cytosol comparable to that of LMNA WT-cardiomyocytes (**Fig. 25B**, R321X + sal, R321X + gua, R321X + empa).

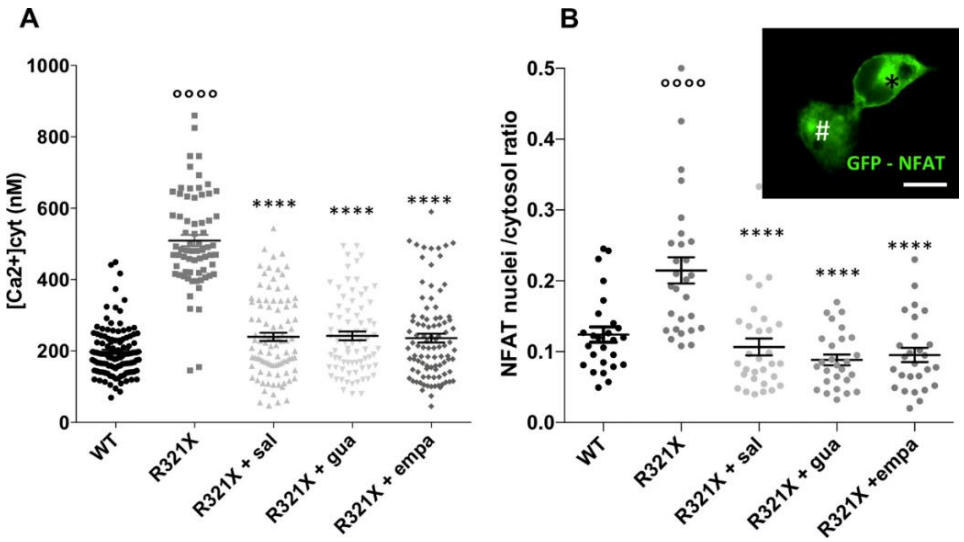

Figure 25: Effect of salubrinal, guanabenz and empagliflozin on $[Ca^{2+}]$cyt and NFAT nuclear translocation in LMNA R321X-cardiomyocytes. (A) Data plot summarizing analysis of the steady state $[Ca^{2+}]$cyt in LMNA WT and R321X-cardioyocytes (WT, n = 117; R321X, n = 68) and in treated LMNA R321X-cardiomyocytes (R321X + sal, n = 95; R321X + gua, n = 76; R321X + empa, n = 96). Data are reported as mean ± SEM. Statistical analysis was performed on three independent

experiments and significance calculated by one-way ANOVA and Tukey's multiple comparisons test (°°°°p = 0.0001 for WT vs R321X; ****p = 0.0001 for untreated R321X vs treated R321X). (B) Data plot summarizing the ratio between the number of cells expressing NFAT-GFP in the nucleus vs cells expressing the probe in the cytosol. Inset reports representative image of HL-1 cells expressing NFAT-GFP either in the cytosol (*) or in the nucleus (#). Scale bar: 20 μm. NFAT localization was evaluated both in LMNA WT and LMNA R321X-cardiomyocytes (WT, R321X) and in treated LMNA R321X-cardiomyocytes (R321X + sal, R321X + gua, R321X + empa). Data were obtained from 3 independent experiments. Ten different fields for each treatment were blindly acquired and analysed for every independent experiment. Cells analysed for each experimental condition: LMNA WT n = 2763 cells, LMNA R321X n = 2548 cells, LMNA R321X + sal n = 1941 cells, LMNA R321X + gua n = 3259 cells, LMNA R321X + empa n = 2032 cells. The plot shows mean ± SEM and significant differences, were calculated by ordinary one-way ANOVA and Tukey's multiple comparisons test (°°°°p = 0.0001 for WT vs R321X; ****p = 0.0001 for untreated R321X vs treated R321X).

We finally analysed the ability of ER to release and uptake Ca^{2+}, which is a fundamental mechanism in the electromechanical coupling in cardiomyocytes. To this end we monitored cytosolic Ca^{2+} dynamics by Fura-2AM upon ER Ca^{2+} depletion and the capacitative calcium entry (CCE) induction in the absence or presence of salubrinal, guanabenz and empagliflozin. When ER Ca^{2+} stores were depleted blocking the SERCA pump with 40 μM CPA in the absence of external Ca^{2+}, cytosolic Ca^{2+} increased transiently because of the passive diffusion of Ca^{2+} through ER leaks (**Fig. 26A, C,** first pick). After complete ER Ca^{2+} emptying (about 20 min), re-addition of 5 mM Ca^{2+} in the extracellular solution in the continuous presence of CPA, rapidly increased cytosolic Ca^{2+} due to the CCE at the plasma membrane classically triggered by Ca^{2+} store depletion (**Fig. 26A, C**, second pick). The expression of LMNA R321X reduced both ER Ca^{2+} depletion and CCE when compared to their controls (**Fig. 26A, C,** blue lines). However, the amplitude of the two Ca^{2+} responses of the same protocol was recovered upon the treatment with either salubrinal or guanabenz (**Fig. 26A**, red line and purple line) as well as after empagliflozin treatment (**Fig. 26C**, green line). The quantitative analysis of the above-described Ca^{2+} dynamics are showed in **Fig. 26B, D.** These data clearly indicated an impaired release of Ca^{2+} from the ER, likely reflecting reduced ER Ca^{2+} content and increased $[Ca^{2+}]_{cyt}$ in LMNA R321X-cardiomyocytes, which was then rescued by all drugs tested. Reduced CCE in LMNA

R321X-cardiomyocytes was also observed, which was also reversed by salubrinal, guanabenz and empligliflozin.

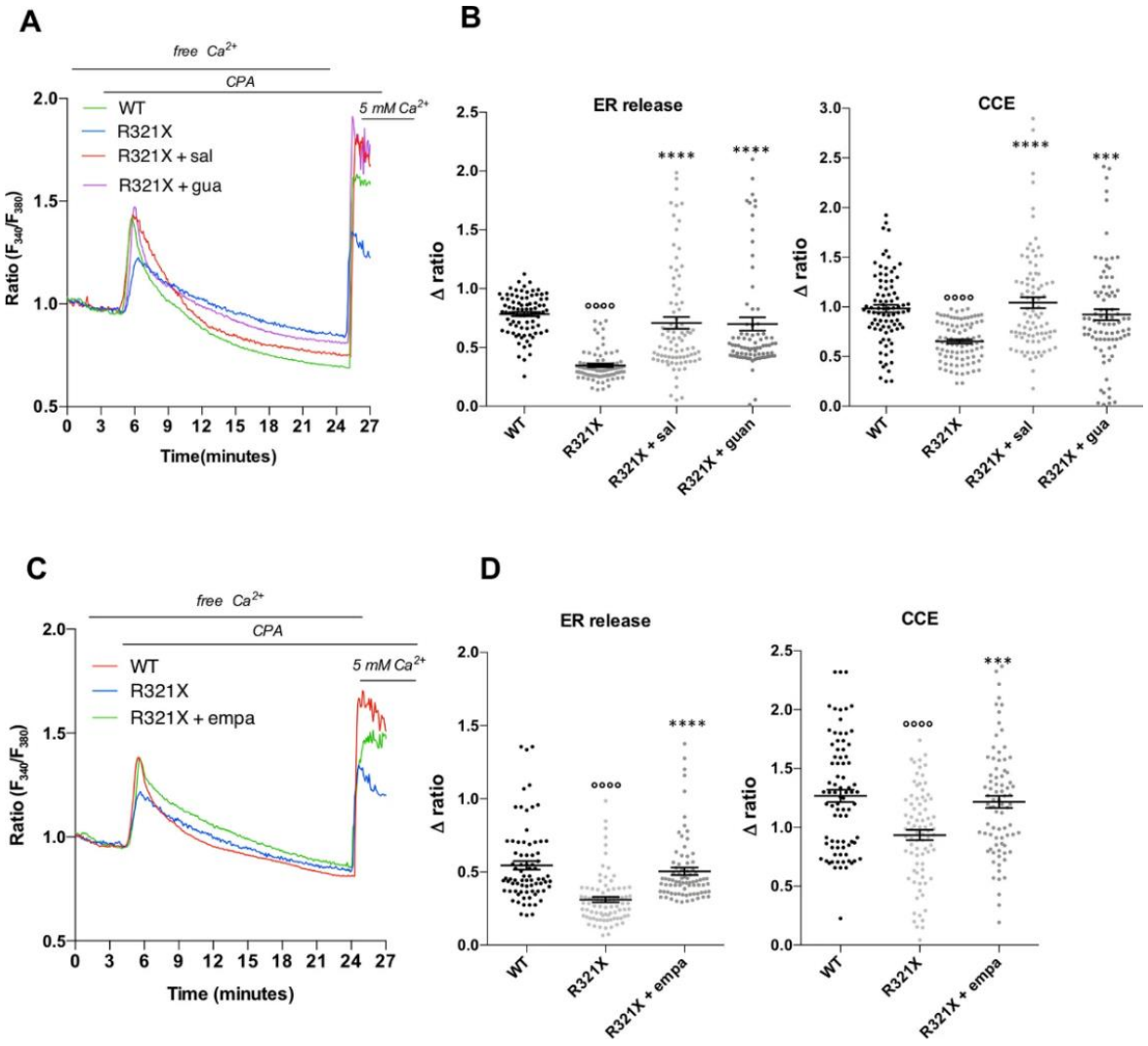

Figure 26: Effect of salubrinal, guanabenz and empagliflozin on cytosolic Ca^{2+} dynamics in LMNA R321X-cardiomyocytes. **(**A) Changes in fluorescence ratio in 4 representative Fura-2AM-loaded cardiomyocytes showing the effect of salubrinal and guanabenz. Each color line represents an individual cell and a specific cell line, as reported in the inset. Horizontal black lines report experimental conditions of the perfusion ringer (free Ca^{2+}, CPA, 5 mM Ca^{2+}). (B) Data plot summarizing the cytosolic Ca^{2+} response induced by either CPA (ER release) or by 5 mM Ca^{2+} (CCE) in the experimental conditions shown in A. Plots show mean value of Δ ratio ± SEM of all responsive cells (n = 82/82 responsive cells, in 3 independent experiments). Ordinary one-way ANOVA and Tukey's multiple comparisons test was used for statistical analysis (°°°°p = 0.0001 for WT vs R321X; ****p = 0.0001 and ***p = 0.004 for untreated R321X vs treated R321X). **(**C) Changes in fluorescence ratio in 3 representative Fura-2AM-loaded cardiomyocytes showing the effect of

empagliflozin. Each color line represents an individual cell and a specific cell line, as reported in the inset. Horizontal black lines report experimental conditions of the perfusion ringer (free Ca^{2+}, CPA, 5 mM Ca^{2+}). (D) Data plot summarizing the cytosolic Ca^{2+} response induced by either CPA (ER release) or by 5 mM Ca^{2+} (CCE) in the experimental conditions shown in **C** ($n = 80/80$ responsive cells, in 3 independent experiments). Plots show mean value of Δ ratio ± SEM of all responsive cells ($n = 80/80$ responsive cells, in 3 independent experiments). Ordinary one-way ANOVA and Tukey's multiple comparisons test was used for statistical analysis (°°°°p = 0.001 for WT vs R321X; ***p = 0.006, ****p = 0.0001 for untreated R321X vs treated R321X).

However, the knowledge of mechanisms underlying this phenomenon has required more investigation. In vertebrate the CCE is triggered mainly by the ER Ca^{2+} sensor protein STIM1, which once activated by ER Ca^{2+} depletion, oligomerizes and accumulates at ER-plasma membrane junctions where it binds, traps and opens ORAI1 pore-forming Ca^{2+} channels thus refilling ER stores. We indeed checked for the expression levels of STIM1 and ORAI1 in LMNA WT and R321X-cardiomyocytes by Western blotting. As shown in **Fig. 27**, the expression of STIM1 was downregulated in LMNA R321X-cardiomyocytes compared to their controls whereas the expression levels of ORAI1 resulted comparable in the two lines of cardiomyocytes (**Fig. 27A, B**, LMNA WT and LMNA R321X). Interestingly, the expression levels of STIM1 were recovered upon all drugs treatment (**Fig. 27A** LMNA R321X + salubrinal and guanabenz; **Fig. 27B**, LMNA R321X + empagliflozin). The quantitative analysis of the above-described phenomena clearly showed both the significant decrease of STIM1 expression in LMNA R321X-cardiomyocytes and the efficacy of all drugs in restoring the expression levels of STIM1 in these cardiomyocytes (**Fig. 27A**, low panel, WT, R321X, R321X + sal, R321X + gua; **Fig. 27B**, low panel, WT, R321X, R321X + empa).

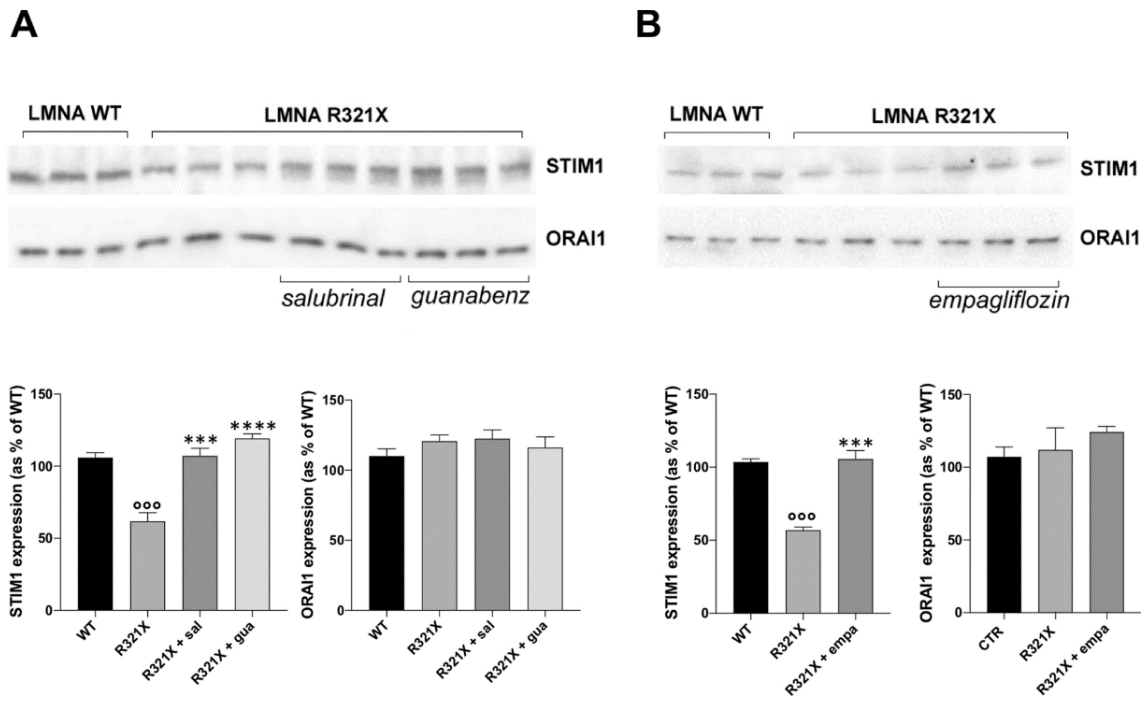

Figure 27: Effect of salubrinal, guanabenz and empagliflozin on STIM1 and ORA1 expression in LMNA R321X-cardiomyocytes. (A) Upper panel: Representative Western blotting of STIM1 and ORA1 performed on lysates from LMNA R321X-cardiomyocytes treated with either 200 µM salubrinal or 20 µM guanabenz for 48 h and from LMNA WT-cardiomyocytes as control. The triplicate of each experimental conditions in the representative western blotting corresponds to three different biological replicas. Lower panel: densitometric analysis of the immunoreactive bands corresponding to STIM1 and ORA1, in the experimental conditions shown in the upper panel, normalized for total protein content and reported as % of the control condition (WT). Data are represented as mean ± SEM. Statistical analysis was performed on three independent experiments and significance calculated by one-way ANOVA and Tukey's multiple comparisons test (°°°p = 0.0001, for WT vs R321X; ***p = 0.0003, ****p = 0.0001 for untreated R321X vs treated R321X). (B) Upper panel: Representative Western blotting of STIM1 and ORA1 performed on lysates from LMNA R321X-cardiomyocytes treated with either 10 µM empagliflozin for 48 h and from LMNA WT-cardiomyocytes as control. The triplicate of each experimental condition in the representative western blotting corresponds to three different biological replicas. Lower panel: densitometric analysis of the immunoreactive bands corresponding to STIM1 and ORA1, in the experimental conditions shown in the upper panel, normalized for total protein content and reported as % of the control condition (WT). Data are represented as mean ± SEM. Statistical analysis was performed on three independent experiments and significance calculated by one-way ANOVA and Tukey's multiple comparisons test (°°°p = 0.0001, for WT vs R321X; ***p = 0.0003, for untreated R321X vs treated R321X).

5.5 Discussion

This work represents the final step toward the definition of a possible personalized therapeutic approach in the field of cardiac laminopathies. We previously demonstrated that an Italian family affected by a severe DCM with history of sudden deaths at young age, carried a mutation in the *Lmna* gene encoding for a truncated variant of the LMNA, LMNA R321X. Interestingly, we demonstrated that such variant mis-localized and accumulated into the ER when expressed in mature cardiomyocytes, as expected from the absence of the nuclear localization sequence (NLS), inducing ER dysfunction and the up-regulation of pro-apoptotic markers. Of note, a very similar truncated variant of LMNA misplaced into the ER when expressed in cardiomyocytes but induced a severe cardiomyopathy by a different pathogenic mechanism (166). These findings clearly indicate that each *Lmna* mutation drives cardiac detriment by its own and unique pathway and that ER stress induced by the accumulation of LMNA R321X into ER might be a useful pharmacological target in the LMNA R321X associated cardiac laminopathy. Specifically, we deciphered the pathways activated in LMNA R321X-cardiomyocytes, which we summarized in the cartoon of **Fig. 28**. Once activated the PERK arm of the UPR upon the accumulation of mis-folded LMNA R321X into the ER, this results in ER Ca^{2+} leak, most likely due to the activation of calcineurin and ryanodine receptors (RyR). Interestingly, PERK/calcineurin signaling has been identified in diabetic cardiomyopathy as novel pathway regulating the intracellular Ca^{2+} dynamics and involved in the pathogenesis of the disease (285). Accordingly, we found an increased steady-state cytosolic Ca^{2+} level in LMNA R321X-cardiomyocytes, and the activation the calcineurin/NFAT pathway with NFAT translocation from cytosol to nuclei of these cardiomyocytes. Interestingly, calcineurin/NFAT pathway has been found activated in response to pathological stimulation in mice and humans, such as pressure overload or myocardial infarction and precedes the development of pathological cardiac hypertrophy, DCM and heart failure (286) thus suggesting a pivotal role in the heart function detriment when activated.

Concomitantly, STIM1 expression into ER was downregulated in LMNA R321X-cardiomyocytes, thus decreasing the Capacitive Ca^{2+} Entry (CCE), finally contributing to the ER impairment in maintaining luminal Ca^{2+} levels in these cells. The downregulation of STIM proteins with unaffected ORAI protein expression was already observed in cells under ER stress conditions (287,288), suggesting an active role of this ER protein in the initiating/sustaining ER stress and UPR signaling.

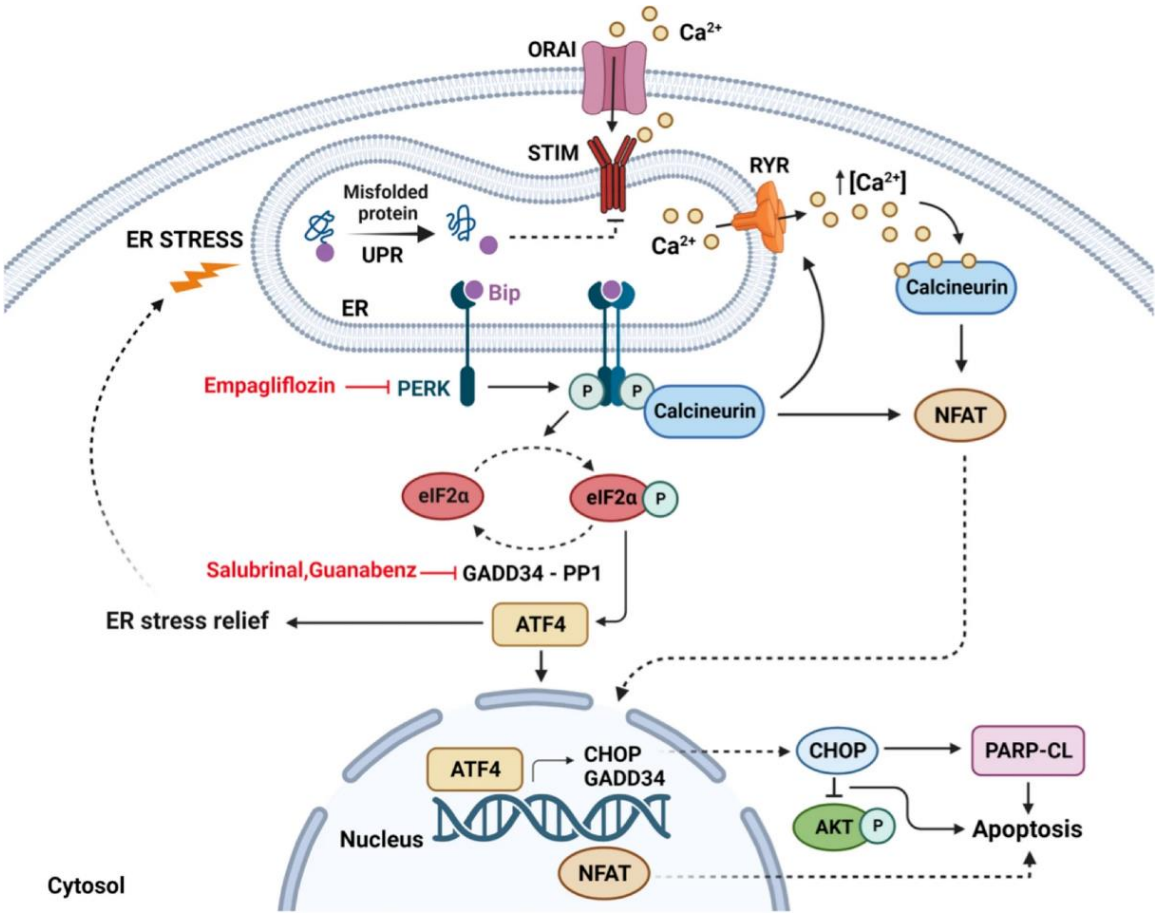

Figure 28: Proposed working model. The activation of PERK arm of UPR by PERK phosphorylation results in ER Ca^{2+} leak and increase in cytosolic Ca^{2+}, most likely due to the activation of calcineurin and Ryanodine Receptors (RyR) from p-PERK. Concomitantly, STIM1 expression is downregulated into the ER membrane of LMNA R321X-cardiomyocytes, thus decreasing the Capacitive Ca^{2+} Entry in these cells, contributing the impairment in handling Ca^{2+}(STIM-ORAI). The increase in cytosolic Ca^{2+} together with calcineurin activation induce NFAT translocation from cytosol to nuclei of these cardiomyocytes, most likely contributing to activation of pro-apoptotic pathways. In addition, PERK phosphorylation activates a downstream pathway: eiF2α phosphorylation (p-eiF2α) and ATF4 expression. ATF4 alleviates ER stress. If ER stress is persistent, ATF4 induces the expression of the pro-apoptotic factor CHOP and increases the apoptosis rate in LMNA R321X-cardiomyocytes, as shown by the caspase depended PARP-cleavage in these cardiomyocytes (PARP-CL). The activation of the CHOP-dependent pro-apoptotic pathway is also paralleled by the inhibition of the pro-survival pathway of AKT (p-AKT). Salubrinal and guanabenz act inhibiting eiF2α de-phosphorylation, sustaining ATF4 expression in the direction of ER stress alleviation. Empagliflozin, instead, acts directly inhibiting PERK activation. All drugs shutting down the PERK pathway of the UPR recover ER Ca^{2+} leaks, STIM1 downregulation, cytosolic Ca^{2+} overload and the downstream pro-apoptotic responses. The cartoon has been created with BioRender.com.

The activation of PERK-dependent arm of the UPR, induces the phosphorylation of the downstream effector eIF2α, which reduced translation of misfolded proteins thus alleviating ER workload and promoting cell survival. As the stress declines, the GADD34 protein facilitates the dephosphorylation of eIF2α by recruiting the protein phosphatase PP1 restoring normal protein synthesis (289). On the other hand, phosphorylation of eIF2α increases the expression of the transcription factor ATF4, which regulates a wide range of genes playing a crucial role in cell adaptation to stress conditions and cell survival. However, when ER stress persists p-eIF2α dephosphorylation increases again ER workload inducing a pro-apoptotic response, characterized by the expression of the pro-apoptotic factor CHOP and the caspase activation as demonstrated by the PARP cleavage. Interestingly, the activation of the CHOP-dependent pro-apoptotic pathway was also paralleled by the inhibition of the pro-survival pathway of AKT demonstrated by the decrease of AKT phosphorylation in LMNA R321X-cardiomyocytes compared to their controls. Of note, it has been demonstrated that one way by which CHOP may promote apoptosis under ER stress is inhibiting the phosphorylation and the activity of the pro-survival kinase AKT (290,291), although we cannot exclude that other mechanisms are involved in the down-regulation of AKT pathway in LMNA R321X-cardiomyocytes.

Once dissected the pathways triggered in LMNA R321X-cardiomyocytes, we analysed the effect of different drugs on these pathways. Interestingly, in 2005, Boyce and colleagues reported that a small molecule, salubrinal, acted as an inhibitor of the GADD34-PP1 complex, which dephosphorylates eIF2α (292). Thus, salubrinal was supposed to weaken the synthesis of unfolded or misfolded proteins during persistent ER stress contributing to the preservation of homeostasis in ER and saving cells from apoptosis. Accordingly, we found that salubrinal, increasing the rate of eIF2α phosphorylation in LMNA R321X-cardiomyocytes and the expression of the downstream ATF4 factor, relieved the activation of PERK pathway, downregulated the expression levels of apoptosis markers such as CHOP and PARP-CL and restored the pro-survival ATK pathway. Salubrinal was previously found to be neuroprotective in animal models of Amyotrophic Lateral Sclerosis (ALS) (293), cerebral ischemia/reperfusion (294) and traumatic brain injury (295) where ER stress was involved in the pathogenesis of the disease. In addition, salubrinal was reported to protect cardiomyocytes against apoptosis in a rat model of myocardial infarction, where ER stress was triggered by hypoxia (296). Despite the clear effect in counteracting ER stress in cell and animal models, salubrinal has never been further developed for the use in clinical

practice, most likely because of its lack of selectivity for ER-stress related phosphatases and its unstable chemical structure, making its clinical use unfeasible (292).

In contrast, guanabenz, an FDA-approved α2-adrenergic receptor agonist formerly used in clinical practice for the treatment of hypertension (297), has been found to efficiently inhibit GADD34-PP1 complex independently from α2-adrenergic agonism (298). Of note, guanabenz selectively inhibits only the stress-induced eIF2α phosphatase in stressed cells (298).

We found that guanabenz was efficient as salubrinal in restoring homeostasis in LMNA R321X-cardiomyocytes. Of note, HL-1 cardiomyocytes as well as human heart doesn't express α2-adrenergic receptors (299,300), thus confirming that guanabenz was acting on HL-1 cardiomyocytes independently from its α2-adrenergic agonism.

In agreements with our findings, guanabenz proved to efficiently rescue motoneurons function in in vitro and in vivo ALS models in which ER stress-related protein misfolding is central to the pathogenesis of the disease (301–303). Based on these results in 2017 the ProMISe trial, Phase II clinial trial, has been started treating ASL patients with guanabenz (304).

Interestingly, guanabenz was found also to interfere with ER stress and to exert protective effects in cardiac myocytes and in 3-dimensional engineered heart tissue (305).

Owing to its role on the α2-adrenergic receptors and possible effects on the cardiovascular system as a result of its activation, guanabenz could seem unsuitable for patients affected by cardiomyopathies. In fact, α2-adrenergic receptors activation decreased centrally the sympathetic outflow and blood pressure. Interestingly, the first symptomatic treatment for DCM due to *Lmna* mutations, like that affecting the family expressing LMNA R321X, is based on the use of anti-hypertensive drug such as β-blockers and ACE inhibitors (269), thus suggesting that the use of guanabenz could be in line with the currently used therapeutic management of cardiac laminopathies.

Of note, several clinical trials with patients with type 2 diabetes mellitus (T2DM) treated with inhibitors of SLGT-2, generically called gliflozins, reported unexpected beneficial effects on cardiovascular outcomes in these patients, in the absence of significant adverse effects (306–309). Subsequently, studies investigating the effect of gliflozins in patients with heart failure (HF) with either reduced or preserved ejection fraction and without T2DM were conducted. All of them demonstrated that gliflozins have a significant positive impact on HF and cardiac pathological remodeling independent from their anti-diabetic effects (310) or ejection fraction (311). The current clinical guidelines for HF, therefore, now include

SGLT2i as a Class 1A recommendation for the treatment of HF (312,313). Interestingly, gliflozins not only counteract cardiac remodeling but also arrhythmias. Although the mechanisms by which gliflozins act on the cardiovascular system have not been completely elucidated, their role in the protection against various cardiovascular diseases, especially HF, myocardial hypertrophy, myocardial infarction at the currently used dosage is undisputed.

Here we studied the ability of empagliflozin in counteracting ER stress in LMNA R321X-cardiomyocytes. 10 μM empagliflozin for 48 h was well tolerated by HL-1 cardiomyocytes and highly effective in reducing the expression of both CHOP and PARP-CL decreasing PERK phosphorylation levels and rescuing p-AKT levels. Our findings are in agreement with previous reports where gliflozins were able to inhibit the PERK-CHOP pathway of UPR acting on PERK activation itself, as shown in the brain of rat model of Parkinson's disease (280), in the heart of I/R injury mouse model (314) and in doxorubicin induced cardiac fibrosis and apoptosis in Streptozotocin (STZ) rats (315).

Interestingly, it has been demonstrated that in patients treated with dapagliflozin, compared with the untreated group, the risk of atrial fibrillation was significantly reduced a well as the total number of atrial fibrillation events (316). Moreover, a meta-analysis published recently suggested that gliflozins specifically reduced the risk of ventricular tachycardia (317). Of note, we previously shown that patients carrying the variant LMNA R321X are affected by DCM with recurrent atrial fibrillation and ventricular tachycardia (165). Thus, the use of gliflozins in these patients may be useful not only for their ability to alleviate ER stress but also for their antiarrhythmic properties.

We would also like to underlie that all drugs tested on living LMNA R321X-cardiomycytes restore the ability of the ER to correctly store Ca^{2+} and to trigger CCE. Both the ER Ca^{2+} levels and CCE in cardiomyocytes are essential in cardiomyocytes electrical and mechanical events (318,319).

5.6 Conclusion

Unlike most other forms of familial cardiomyopathies, sudden cardiac death may be the first manifestation of LMNA cardiomyopathy, even in the absence of systolic dysfunction, because of malignant arrhythmias such as ventricular tachycardia and fibrillation. Current therapy for LMNA cardiomyopathy is only symptomatic and follows the standard heart failure regimen thus making the treatment of LMNA cardiomyopathy a challenging field in the cardiovascular research and clinic. Our findings clearly demonstrated that ER stress due to LMNA R321X accumulation into the ER of cardiomyocytes was involved in the pathogenic mechanisms of the associated severe DCM. Interestingly, we found that ER stress in LMNA R321X-cardiomyocytes can be counteracted basically in two ways: (a) sustaining an adaptive UPR using molecules such as salubrinal and guanabenz or (b) blocking a maladaptive UPR with gliflozins such as empagliflozin. Some of these drugs, guanabenz and empagliflozin, are already used in the clinical practice, thus providing preclinical evidence for a possible ready-to-use therapeutic strategies in the patients expressing LMNA R321X pathogenic variant.

6. The microtubules plus-end tracking proteins CLIP-170 mediates nuclear shape in Emery-Dreifuss muscular dystrophy

6.1 Introduction

The nucleus is a dynamic structure that responds to cellular movement by changing shape. During cell division, it disassembles and reassembles, and it can undergo breakage and repair. These dynamics can be influenced by mutations in the *Lmna* gene, which encodes nuclear lamins A and C, through alternative RNA splicing events (17,320).

Several studies have shown nuclear morphological alterations in carriers of *Lmna* gene mutations, including nuclear blebs (hernias, including micronuclei), honeycomb structures, doughnut-shaped structures, or combinations of the above categories (321–324).

A cohort study of 13 patients with different forms of laminopathy found the presence of nuclear honeycomb structures and nuclear envelope (NE) vesicles in fibroblasts of *Lmna* mutation carriers (325). Furthermore, primary cultures of skin fibroblasts from three patients carrying p.R482Q or p.R482W *Lmna* mutations, which cause Dunnigan-type familial partial lipodystrophy (FPLD), exhibit dysmorphic nuclei. These nuclei are mainly composed of NE herniations (326).

In addition, Muchir et al. (327) analysed skin fibroblasts from a patient with type 1B limb-girdle muscular dystrophy (LGMD1B) and from her deceased newborn grandchild. The patient carried a heterozygous (+/ mut) *Lmna* nonsense mutation (Y259X), while the grandchild carried a homozygous (mut/mut) mutation of the same gene. In fibroblasts$^{+/mut}$, the presence of only 50% of lamins A and C does not result in any detectable abnormality. However, in fibroblasts$^{mut/mut}$, the complete absence of lamins A and C leads to abnormally shaped nuclei with lobules. These abnormalities are associated with alterations in the protein composition of the INM and aberrant localization of emerin and nesprin-1 in the ER (327).

While not all LMNA variants necessarily cause nuclear malformations, mutations in the head and tail domains of lamins A and C, as well as mutations in linkers and the lamin A coil domain, have been found to significantly impact the nuclear architecture of patients' fibroblasts (325,328,329).

Recent studies indicate that A-type lamins may facilitate connections between the nucleus and the cytoskeleton through NE nesprin and SUN proteins. Folker et al. demonstrated that

Lmna mutations causing striated muscle diseases block actin-dependent nuclear movement, whereas those affecting adipose tissue inhibit microtubule-dependent centrosome positioning (88). Interestingly, *Lmna* exon 4 mutants exhibited abnormal nuclear morphology and changes in levels and/or subcellular localization of various members of the lamin and LINC (LInker of Nucleoskeleton and Cytoskeleton) complex (330).

There is mounting evidence that *Lmna* mutations can disrupt various structural and cytoskeletal components of the cell, including microtubules, actin cytoskeleton, and intermediate filaments (272,331,332). Our recent study demonstrated that alterations in the microtubule cytoskeleton and reduced acetylation of α-tubulin, a post-translational modification, contribute to the development of LMNA cardiomyopathy in a mouse model of Emery-Dreifuss muscular dystrophy (EDMD) (144,333). As the cytoskeleton has been shown to exert sufficient force to modify nuclear morphology (334), we investigated how defects in microtubules contribute to the elongation of nuclear shape, a cellular phenotype observed in EDMD.

Microtubules are dynamic components of the cytoskeleton. CLIP-170 (also known as CAP-Gly domain–containing linker protein 1 or cytoplasmic linker protein 1 (CLIP1)) is a microtubule plus end–tracking protein (+TIP) that binds to the plus-end of microtubules (MT) to protect them from depolymerization (335–337). As a result, MT polymerization is accelerated. Conversely, removal of CLIP-170 from the plus end promotes MT depolymerization (338). Our findings indicate that in striated muscles from *Lmna*$^{H222P/H222P}$ mice, a model of EDMD, CLIP-170 displays a punctiform localization at the poles of elongated nuclei, whereas in wild-type animals, it localizes around the nuclei.

CLIP-170 has two N-terminal microtubule-binding domains, a middle coiled-coil domain and two C-terminal zinc knuckles (339). The activities of CLIP-170 are determined by conformational changes. The phosphorylated form of CLIP170 adopts a folded conformation and dissociates from microtubule plus ends. In its unphosphorylated form (extended conformation), CLIP-170 binds to microtubules (340).

We investigated the effect of a neurosteroid, referred to as the XY molecule for intellectual property purposes. Neurosteroids can activate CLIP-170 by altering its conformation (341–345). We discovered that XY molecule restores the nuclear shape in striated muscles of EDMD mice by removing CLIP-170 from the poles of elongated nuclei. These results suggest that CLIP-170 plays a critical role in modulating nuclear shape.

6.2 Methods

6.2.1 Mouse strains, husbandry, and treatments

Wild-type C57/Bl6 and *Lmna*$^{H222P/H222P}$ (346) male mice were fed standard chow and water ad libitum and housed in a disease-free barrier facility under a 12 h/12 h light/dark cycle, controlled temperature of 22 °C, and 55% humidity. All animal experiments were approved by the French Ministry of Higher Education and Research at the Centre for Research in Myology for the Care and Use of Experimental Animals. Animal experiments were performed according to the guidelines from Directive 2010/63/EU of the European Parliament regarding the protection of animals used for scientific purposes.

6.2.2 Isolation of mouse muscle fibers

WT C57/BL6J and *Lmna*$^{H222P/H222P}$ male mice aged 6 months were anaesthetised via intraperitoneal injection of sodium pentobarbital (50 mg/kg) and killed by cervical dislocation. The extensor digitorum longus (EDL) and gastrocnemius muscles were carefully dissected from the hind limbs and immediately digested for 1.5 and 3 h, respectively, in collagenase solution (DMEM, high glucose, GlutaMAX™ supplemented with 1% penicillin-streptomycin containing 2 mg/mL collagenase type II (17101015, Gibco™, Life Technologies™) in a humidified incubator (5% CO_2, 95% O_2) at 37°C. After digestion, muscles were incubated for 30 min in isolation medium (DMEM, high glucose, GlutaMAX™ supplemented with 1% penicillin-streptomycin) in a humidified incubator (5% CO_2, 95% O_2) at 37°C. After incubation, muscles were gently triturated in isolation medium to release individual myofibers using a large bore glass pipette precoated with coating solution (DMEM, high glucose, GlutaMAX™ supplemented with 1% penicillin-streptomycin and 5% horse serum (16050122, Gibco™, Life Technologies™)). Myofibers were plated on coating solution-coated 35-mm Petri dishes in culture medium (DMEM, high glucose, GlutaMAX™ supplemented with 1% penicillin-streptomycin, 10% horse serum and 0.5% chicken embryo extract (CEE) (MD-004D-UK, Life Science Production)) for 2 h in a humidified incubator (5% CO_2, 95% O_2) at 37°C. Isolated muscle fibers were either used immediately and fixed for immunostaining or treated with XY molecule.

6.2.3 Isolation of mouse cardiomyocytes

Isolation of cardiomyocytes was performed according to Ackers-Johnson's protocol (347). Briefly, WT C57/BL6J and *Lmna*$^{H222P/H222P}$ male mice aged 6 months were anaesthetised with a ketamine/xylazin mixture and the chest was opened to expose the heart. Descending aorta was cut and the heart was immediately flushed by injection of 7 mL EDTA buffer (130mM NaCl, 5mM KCl, 0.5 mM NaH_2PO_4, 10mM Hepes, 10mM Glucose, 10mM BDM, 10mM Taurine and 5mM EDTA) into the right ventricle. Ascending aorta was clamped and the heart was transferred to a petri dish containing fresh EDTA buffer. Digestion was achieved by sequential injection of 10 mL EDTA buffer (2ml/min), 3 mL perfusion buffer (130mM NaCl, 5mM KCl, 0.5 mM NaH_2PO_4, 10mM Hepes, 10mM Glucose, 10mM BDM, 10mM Taurine and 1mM $MgCl_2$) (2ml/min), and 60 to 120 mL collagenase buffer (0.5mg/ml collagenase 2, 0.5mg/ml collagenase 4 and 0.05mg/ml Protease XIV) into the left ventricle (1ml/min). Whole hearts were then gently pulled into 1-mm pieces using forceps. Cell dissociation was completed by gentle trituration, and enzyme activity was inhibited by addition of 5 mL stop buffer (Perfusion buffer containing 5% FBS). Cell suspension was passed through a 100-µm filter, and cells underwent 3 sequential rounds of gravity settling to remove non-myocyte cardiac populations and dead cells. Isolated cardiomyocytes were used immediately for proteins extraction.

6.2.4 Treatment in culture cells

Myofibers isolated from *Lmna*$^{H222P/H222P}$ male mice were treated by adding either 100 µM XY molecule (SelleckChem) or DMSO to culture medium (DMEM, high glucose, GlutaMAX™ supplemented with 1% penicillin-streptomycin, 10% horse serum and 0,5% CEE) for 2 h in a humidified incubator (5% CO_2, 95% O_2) at 37°C.

6.2.5 Protein extraction and immunoblotting

Total proteins were isolated from isolated cardiomyocytes using extraction buffer (Cell Signaling) containing protease inhibitors (25 mg/ml aprotinin, 10 mg/ml leupeptin, 1 mM 4-

[2-aminoethyl]-benzenesulfonyl fluoride hydrochloride and 2 mM Na_3VO_4). The lysates were sonicated (3 pulses of 10 s at 30% amplitude).

The protein content of the samples was determined using the bicinchoninic acid protein assay (23227, Thermo Scientific™). Protein extracts (15 µg) were analysed by SDS-PAGE on 10% gels and transferred to nitrocellulose membranes (Invitrogen). After washing with Tris-buffered saline containing 1% Tween 20 (TBS-T), the membranes were blocked with 5% BSA in TBS-T for 1 h at RT and then incubated with the appropriate antibody at 4 °C overnight. Membranes were incubated with fluorescent-conjugated anti-mouse or anti-rabbit secondary antibodies (BioRad) for 1 h at RT. Antibody detection was imaged using the ChemiDoc Imaging System and ImageLab software (Bio-Rad). Quantification was performed using ImageLab software (Bio-Rad).

6.2.6 Immunofluorescence microscopy

For immunofluorescence microscopy, isolated muscle fibers were collected in 2 mL tubes precoated with coating solution and fixed with 4% PFA for 10 min at RT. After three washes with 1X PBS, myofibers were permeabilized with 5% Triton X-100 (1610407, Bio-Rad) diluted in 1X PBS for 10 min, followed by three washes with 1X PBS. Myofibers were incubated with 0.1% glycine (G7126, Sigma-Aldrich) in 1X PBS for 20 minutes. After two washes with 1X PBS, non-specific signals were blocked with blocking solution (3% BSA, 5% goat serum, 0.5% Triton X-100 in 1X PBS) for 5-6 hours at RT with gentle shaking. Fibers were incubated with primary antibody in blocking solution overnight at 4°C with gentle agitation. After three washes in 1X PBS, myofibers were incubated with secondary antibody in blocking solution for 3 hours at RT with gentle agitation and washed three times with 1X PBS. The nuclei were counter stained with 0.10% DAPI (Hoechst 33342, Invitrogen™) in 1X PBS for 10 min, washed with 1X PBS and the slides were mounted with Fluoromount-G® (0100-01, SouthernBiotech).

Immunofluorescence microscopy was performed using a Nikon Ti2 microscope equipped with a motorised stage and coupled to a Prime 95B Scientific CMOS (sCMOS) camera at ×100 with an oil immersion objective. The microscope was controlled by MetaMorph 7.10 software (Molecular Devices) with a pixel resolution of 0.11 µm/px at 16-bit. Images were processed using FIJI/ImageJ software.

6.2.7 Antibodies

The primary antibodies used were anti-CLIP170 (sc-28325, Santa Cruz Biotechnology; #8899, Cell Signaling Technology), anti-α-actinin sarcomeric (A7732, Sigma-Aldrich), anti-α-tubulin clone YL1/2 (MAB1864, Sigma-Aldrich), anti-CLASP1 (ab108620, Abcam), anti-LIS1 (ab68598, Abcam) and anti-EB1 (sc374474, Santa Cruz Biotechnology).
The secondary antibodies for immunofluorescence were Alexa Fluor 561-conjugated goat anti-mouse IgG2b, Alexa Fluor 488-conjugated goat anti-mouse IgG, Alexa Fluor 647-conjugated goat anti-rat IgG and Alexa Fluor 647-conjugated goat anti-rabbit IgG (Life Technologies). Fluorescence-conjugated StarBright Blue 520 anti-mouse or StarBright Blue 700 anti-rabbit secondary antibodies (Bio-Rad) were used for immunoblotting. All antibodies were used at the manufacturer's recommended dilutions.

6.2.8 Nuclear shape analysis

The quantification of nuclear morphology was performed using Cellpose 2.0 (https://www.cellpose.org/) and QuPatch (https://qupath.github.io/) software, analyzing four parameters: max diameter, min diameter, circularity and eccentricity. The circularity and eccentricity values ranged from 0 to 1. A circularity value of 1 indicates a perfect circle, while an eccentricity value of 0 indicates no deviation from circularity.

6.2.9 Statistics

GraphPad Prism 8 was used for the statistical analysis and graphical representation of the data. Data are reported as median and quartiles or as mean ± SEM of three independent experiments, depending on the data set analysed.
Statistical analysis was performed using a non-parametric test, Wilcoxon-Mann-Whitney test (with $P< 0.05$ considered significant), or unpaired t test (with $P < 0.0464$ considered significant), depending on the data set analysed.

6.3 Results

6.3.1 Nuclear shape alterations in EDMD mice

We investigated the molecular mechanisms underlying nuclear deformations, a common phenotype of EDMD (96,348–351), for which there are still significant gaps in understanding. Our study utilised the knock-in *Lmna*$^{H222P/H222P}$ mouse model, which carries the LMNA p.H222P mutation and accurately replicates all EDMD features (352). EDMD is characterized by three clinical aspects: joint contractures that begin in early childhood; slowly progressive muscle weakness and wasting initially in a humero-peroneal distribution that later extends to the scapular and pelvic girdle muscles; and cardiac involvement that may manifest as palpitations, presyncope and syncope and dilated cardiomyopathy with conduction defects (DCM-CD) (352–354). This mouse model recapitulates some of the most important features of cardiac laminopathies in humans, such as left ventricular dilation and systolic dysfunction. Male mice develop the disease with faster kinetics than female mice (352).

The nuclei of *Lmna*$^{H222P/H222P}$ mice exhibit an elongated shape when compared to wild-type mice (**Fig. 29a**). To quantitatively assess the degree of irregular nuclear shape, we analysed four parameters: maximum diameter, minimum diameter, circularity, and eccentricity (**Fig. 29c**). These parameters are commonly used to analyse nuclear roundness abnormalities in 2D cell cultures. Muscle fibre nuclei isolated from *Lmna*$^{H222P/H222P}$ mice showed a significant increase in maximum diameter and a significant decrease in minimum nuclear diameter compared to muscle fibre nuclei isolated from wild-type mice (**Fig. 29b**).

Nuclear circularity was determined by calculating the ratio of 4π times nuclear area (A) to nuclear perimeter (P) squared ($4\pi A/P^2$) (**Fig. 29c**). This ratio provides measures of the roundness of the nucleus. A perfectly circular nucleus has a ratio of 1, while a more deconvoluted shape has a ratio smaller than 1 (355). Our findings indicate that the nuclei of muscle fibers isolated from mice expressing LMNA p.H222P exhibit significantly less circularity than those expressing wild-type LMNA (**Fig. 29b**). The results were confirmed by calculating a related parameter of nuclear eccentricity, which measures the shape of the boundary ellipse (eccentricity=c/a) (**Fig. 29c**). A circle has an eccentricity of 0, and a more elongated shape is associated with higher eccentricity (355). The eccentricity of muscle fibre nuclei isolated from *Lmna*$^{H222P/H222P}$ mice was close to unity and significantly lower in wild-type counterparts (**Fig. 29b**).

The analysis of nuclear morphology confirmed that muscle fibers isolated from *Lmna*$^{H222P/H222P}$ mice had more elongated nuclei than wild-type cells. This suggests that the LMNA p.H222P mutation may compromise nuclear stability, making cells more susceptible to recurrent mechanical stress and reducing mechano-transduction, as already reported for several *Lmna* gene mutations (110,356–359).

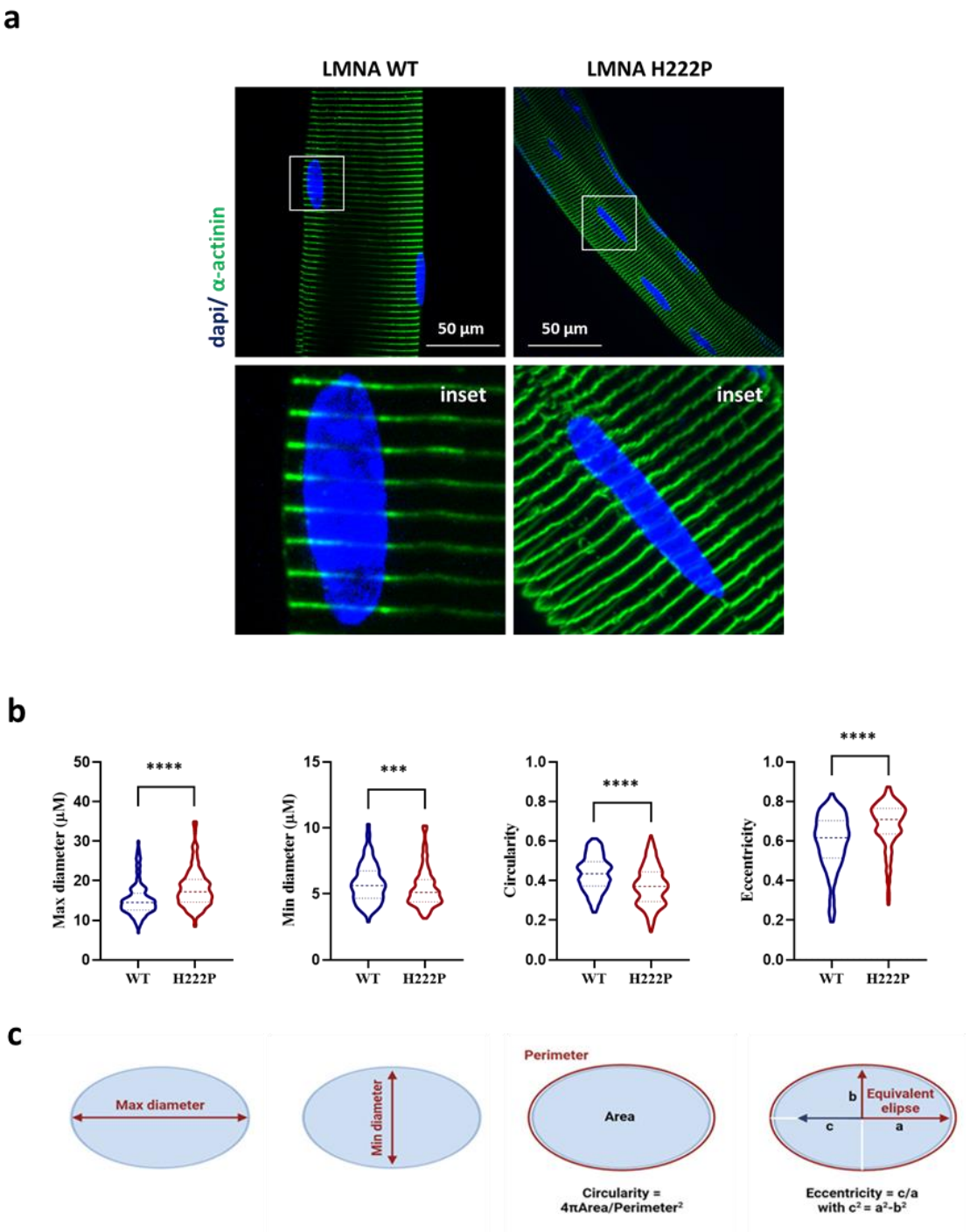

Figure 29: Nuclear shape alterations in *Lmna*$^{H222P/H222P}$ mice. (a) Immunofluorescence staining of α-actinin (green) of isolated muscle fibers from 6-month-old male *Lmna*$^{+/+}$ (LMNA WT) mice and *Lmna*$^{H222P/H222P}$ (LMNA H222P) mice. Nuclei counter-stained with dapi. Scale bar: 50 µm. The insets show a higher magnification. (b) Violin plots summarizing the quantification of nuclear shape changes of isolated muscle fibers from 6-month-old male *Lmna*$^{+/+}$ (LMNA WT) mice and *Lmna*$^{H222P/H222P}$ (LMNA H222P) mice, based on four indices: max diameter, min diameter, circularity and eccentricity, calculated by Cellpose 2.0 and QuPatch software. Data are reported as median and quartiles of three independent experiments (number of nuclei >300). Statistical analysis was performed using a non-parametric test, Wilcoxon-Mann-Whitney test (***p 0.0001, ****p<0.0001). (c) Schematic representation of parameters analysed in (b) and mathematical definition of circularity and eccentricity. Values for each of these range from 0 to 1. (Created with BioRender.com).

6.3.2 Alteration of the α-tyrosinated tubulin network in EDMD mice

We have previously demonstrated that *Lmna*$^{H222P/H222P}$ mice exhibit an alteration of the acetylated α-tubulin network, as well as reduced expression of acetylated α-tubulin. This reduction is due to decreased expression of α-tubulin acetyltransferase 1 (α-TAT1) (144,333).

In this study, we demonstrate that muscle fibers isolated from *Lmna*$^{H222P/H222P}$ mice exhibit a partial alteration in the organization in orthogonal grid of tyrosinated α-tubulin network compared to wild-type mice (**Fig. 30a**). The tyrosination cycle (detyrosination/re-tyrosination) is the most well-characterized reversible post-translational modifications (PTM) (360). The tyrosination cycle is regulated by the detyrosinating enzymatic complex formed by vasohibin (VASH) and small vasohibin-binding protein (SVBP) by cleaving the gene-encoded C-terminal tyrosine residue at α-tubulin tail, which is then re-inserted during tyrosination by the tyrosinating enzyme tubulin–tyrosine ligase (TTL) (361,362) (**Fig. 30b**). The changes in the distribution of the tyrosinated α-tubulin network, and the previously reported decrease in acetylated α-tubulin, confirm that in striated muscle of *Lmna*$^{H222P/H222P}$ mice, microtubules are predominantly in a depolarised state, altering their stabilisation and nuclear-cytoskeletal association.

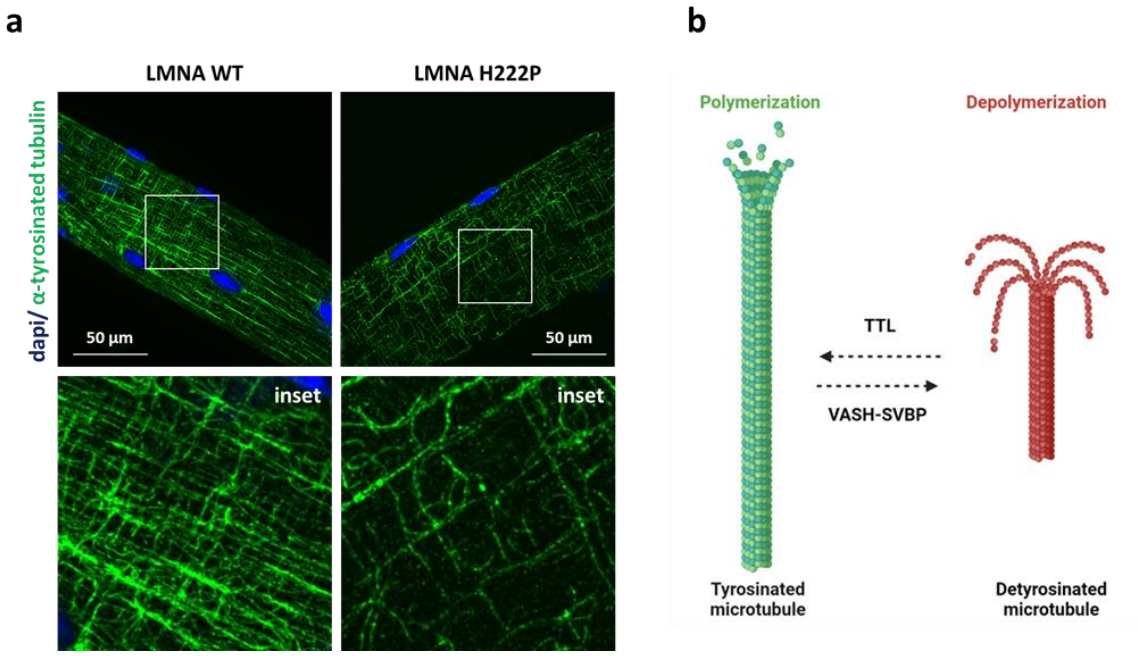

Figure 30: Alteration of the α-tyrosinated tubulin network in *Lmna*$^{H222P/H222P}$ mice. (a) Immunofluorescence staining of α-tyrosinated tubulin (green) of isolated muscle fibers from 6-month-old male *Lmna*$^{+/+}$ (LMNA WT) mice and *Lmna*$^{H222P/H222P}$ (LMNA H222P) mice. Nuclei counter-stained with dapi are also shown. Scale bar: 50 µm. The insets show a higher magnification. (b) Schematic representation of tyrosination cycle (Created with BioRender.com).

6.3.3 Microtubule-associated proteins (MAPs) expression and CLIP-170 localization in skeletal muscle cells expressing LMNA p.H222P mutation

Actin and microtubule cytoskeletons have differential effects on nuclear morphology, especially in cells that experience continuous mechanical stress, such as striated muscles (363). Microtubules (MTs) originate from their 'minus' end, which is stabilized at microtubule-organizing centres containing γ-tubulin, and grow at their 'plus' end by adding GTP-bound α/β-tubulin dimers. The GTP-tubulin 'cap' recruits various microtubule-associated proteins (MAPs) and tubulin plus-end-interacting proteins (+TIPs) that collectively determine the growth, shrinkage or stabilization of a microtubule (364,365).

The aim of this investigation was to explore the potential involvement of MAPs, specifically +TIPs, in the modification of nuclear morphology in mice with EDMD. The expression of the primary +TIPs, including CLIP-170, CLASP1 (Cytoplasmic linker associated protein 1), LIS1 (Lissencephaly 1 protein), and EB1 (end-binding protein 1), was assessed in

cardiomyocytes isolated from the hearts of male *Lmna*$^{+/+}$ (LMNA WT) mice and *Lmna*$^{H222P/H222P}$ (LMNA H222P) mice (**Fig. 31a**). Immunoblotting of lysed cells showed that the expression of CLIP-170 was significantly lower in isolated cardiomyocytes of male *Lmna*$^{H222P/H222P}$ (LMNA H222P) mice compared to wild-type mice. The expression of the other +TIPs did not differ between the two groups (**Fig. 31a, b**).

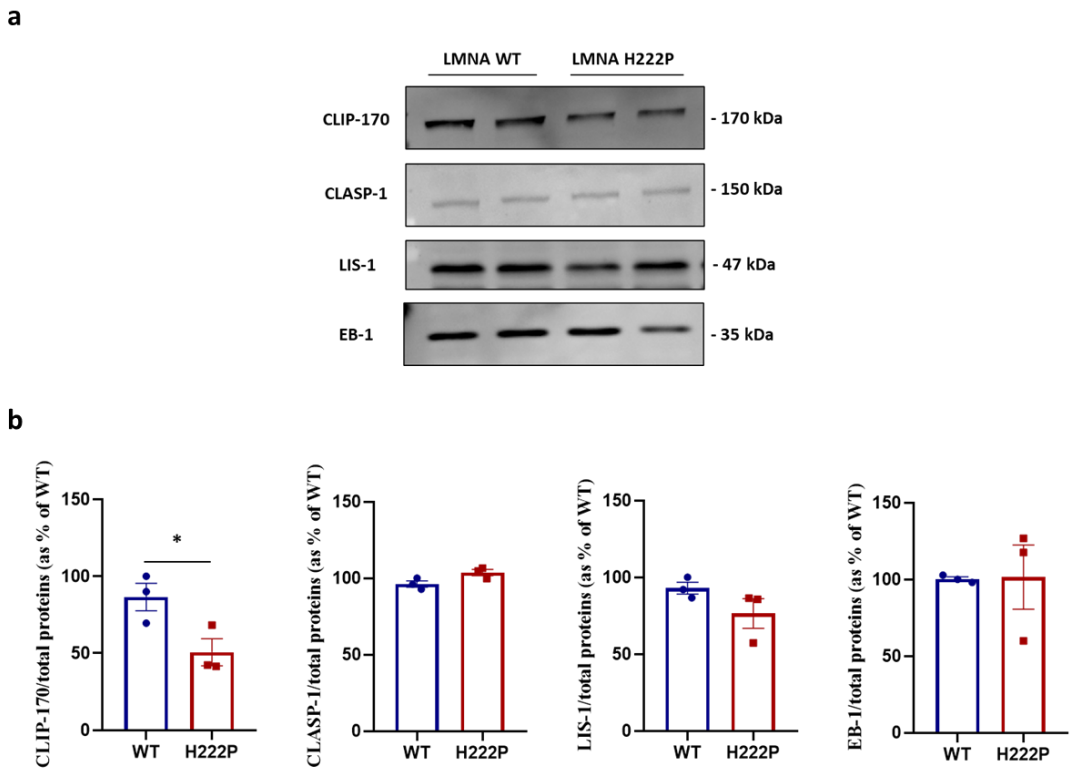

Figure 31: Expression of MAPs in cardiac cells from *Lmna*$^{H222P/H222P}$ mice. (a) Representative Western blotting of CLIP-170, CLASP-1, LIS-1, EB-1 in isolated cardiomyocytes from hearts of male *Lmna*$^{+/+}$ (LMNA WT) and *Lmna*$^{H222P/H222P}$ (LMNA H222P) mice. The duplicate of each experimental condition in the representative Western blot corresponds to two different biological replicates. (b) Densitometric analysis of immunoreactive bands corresponding to MAPs in the experimental conditions shown in (a), normalized to total protein content and expressed as % of the control condition (WT). Data are expressed as mean ± SEM. Statistical analysis was performed on three independent experiments and significance was calculated by Student's t-test for unpaired samples. (*p = 0.0464, LMNA H222P vs. LMNA WT).

Additionally, we observed that puncta of CLIP-170 (shown in red) localized at the opposite poles of elongated nuclei in isolated muscle fibers from *Lmna*$^{H222P/H222P}$ mice, whereas it localizes around the nuclei in wild-type mice (**Fig. 32**). This suggests that the instability of the cytoskeleton in mice expressing LMNA H222P may affect the localization of CLIP-170, as well as its interaction with tubulin microtubules.

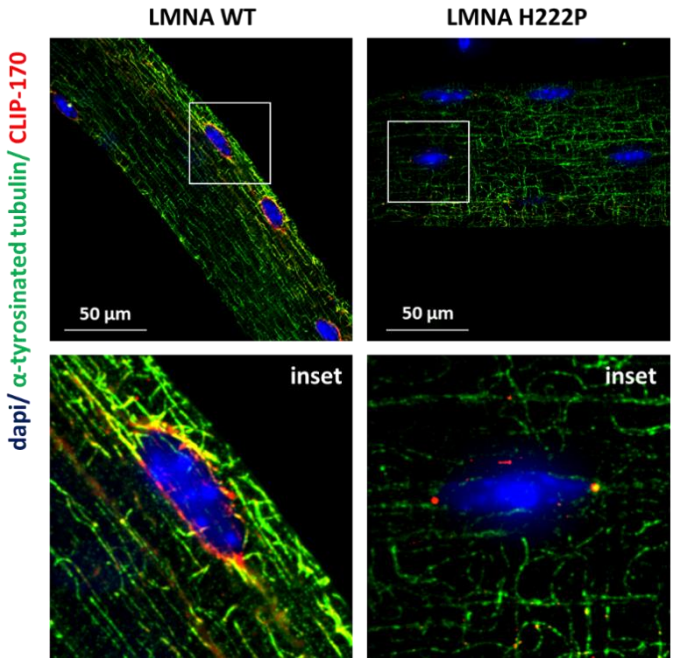

Figure 32: Abnormal CLIP-170 localization in isolated muscle fibers from *Lmna*$^{H222P/H222P}$ (LMNA H222P) mice. Immunofluorescence staining of CLIP-170 (red) and α-tyrosinated tubulin (green) of isolated muscle fibers from 6-month-old male *Lmna*$^{+/+}$ (LMNA WT) mice and *Lmna*$^{H222P/H222P}$ (LMNA H222P) mice. Nuclei counter-stained with dapi are also shown. Scale bar: 50 µm. The insets show a higher magnification.

6.3.4 XY molecule-mediated CLIP-170 activation restores its localization and rescues nuclear shape alteration in EDMD mice

The activities of CLIP170 change according to the different conformational state of the protein. When the protein is folded into a closed structure, it has reduced affinity for its binding partners and MTs, whereas an open and extended conformation activates the protein (340) (**Fig. 35**). The reduced expression and different localization of CLIP-170 in

cardiomyocytes of *Lmna*$^{H222P/H222P}$ mice suggest that the protein is mainly in a closed and inactive conformation.

A recent discovery has identified a neurosteroid that interacts with CLIP-170 at its coiled-coil domain. This neurosteroid can activate CLIP-170 promoting an open conformation of the protein which in turn increases its affinity for MTs and promotes MT polymerization (343) (**Fig. 35**). Therefore, we hypothesized that molecule XY, acting as a neurosteroid, could improve the polymerization state of the cytoskeleton by activating CLIP-170.

In order to address this issue, isolated muscle fibers from *Lmna*$^{H222P/H222P}$ mice were treated with either molecule XY or DMSO (vehicle). Treatment with XY molecule removed CLIP-170 from the poles of elongated nuclei while promoting its broader localization all around the nucleus (**Fig. 33**), as partially observed in wild-type fibers (**Fig. 32**), and along the entire muscle fibre (**Fig. 33**).

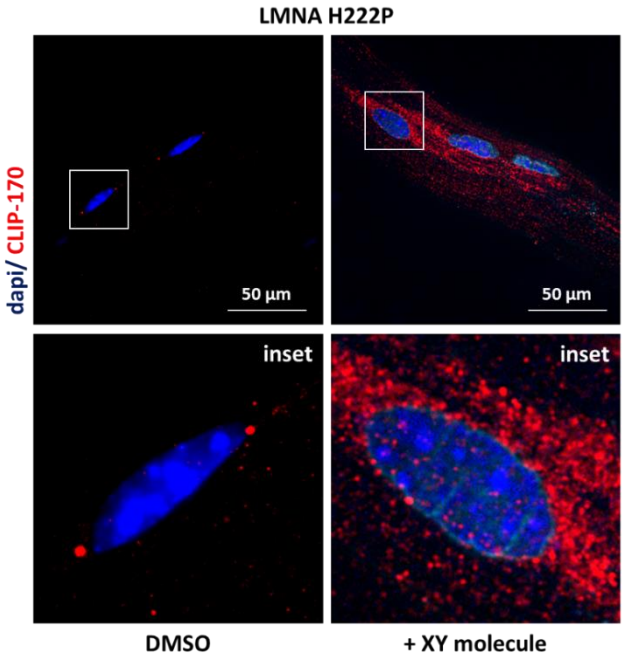

Figure 33: XY molecule-mediated CLIP-170 activation in *Lmna*$^{H222P/H222P}$. Immunofluorescence staining of CLIP-170 (red) of isolated muscle fibers from 6-month-old male *Lmna*$^{H222P/H222P}$ (LMNA H222P) mice either treated with 100 µM molecule XY or DMSO for 2 hours. Nuclei counter-stained with dapi are also shown. Scale bar: 50 µm. The insets show a higher magnification.

Furthermore, treatment of muscle fibers isolated from *Lmna*$^{H222P/H222P}$ mice with molecule XY resulted in a significant reduction in maximum diameter and nuclear eccentricity. In addition, there was a significant increase in the minimum diameter and circularity of the nuclei (**Fig. 34 a, b**), restoring them to the shape of their wild-type counterparts (**Fig. 29a**). All available data indicate that activation of CLIP-170 by molecule XY, is able to restore its localization and rescue isolated muscle fibres from the NE alterations caused by the LMNA p.H222P mutation.

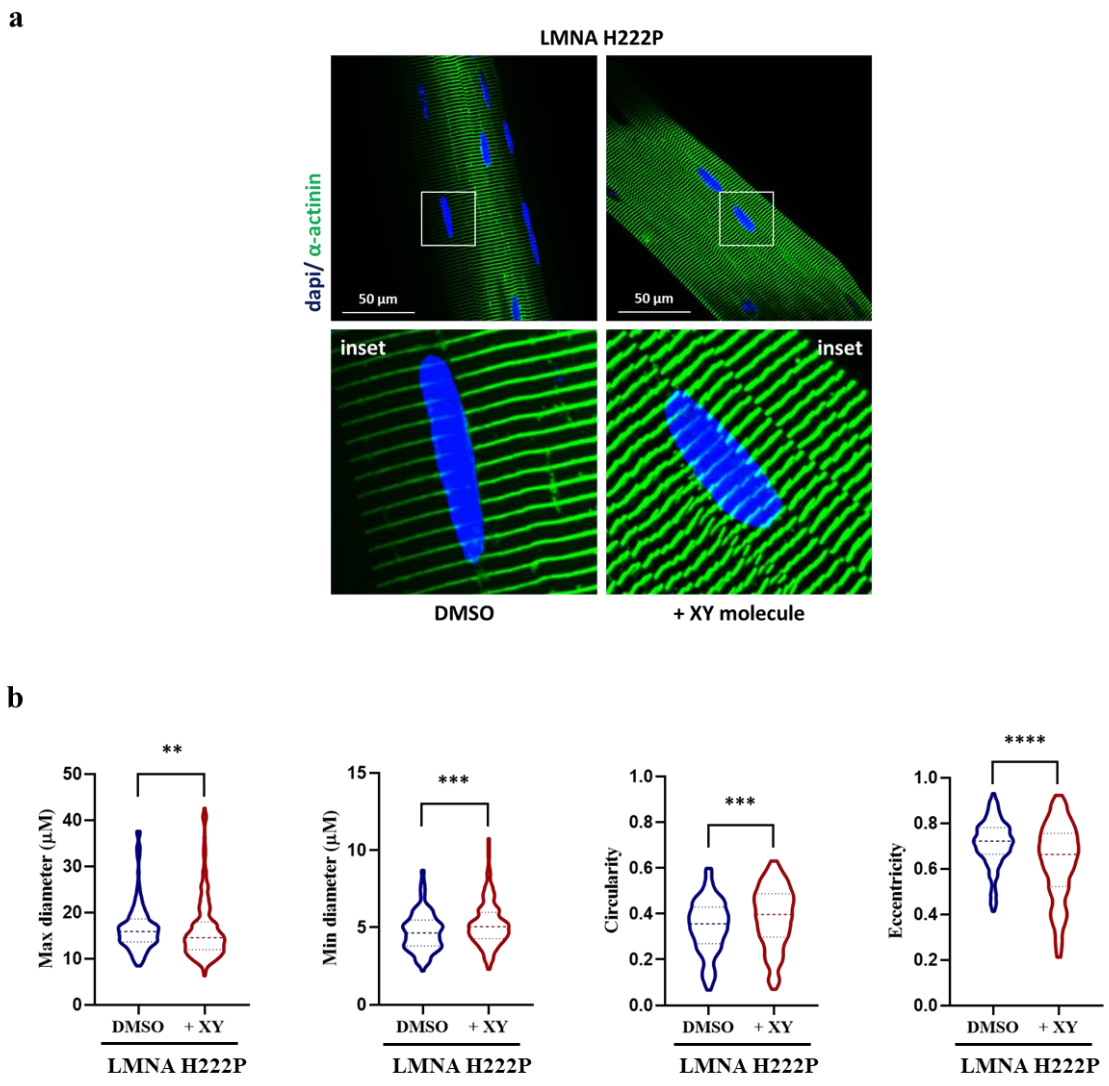

Figure 34: XY molecule-mediated CLIP-170 activation and rescues nuclear shape alteration in EDMD mice. (a) Immunofluorescence staining of α-actinin (green) of isolated muscle fibers from 6-month-old male *Lmna*$^{H222P/H222P}$ (LMNA H222P) mice either treated with 100 µM XY molecule or DMSO for 2 hours. Nuclei counter-stained with dapi. Scale bar: 50 µm. The insets show a higher magnification. (b) Violin plot summarizing the quantification of nuclear shape changes of isolated

muscle fibers from 6-month-old male *Lmna*$^{H222P/H222P}$ (LMNA H222P) mice either treated with 100 µM XY molecule or DMSO for 2 hours, based on four indices: max diameter, min diameter, circularity and eccentricity, calculated by Cellpose 2.0 and QuPatch software. Data are reported as median and quartiles of three independent experiments (number of nuclei >170 (DMSO); >300 (XY)). Statistical analysis was performed using a non-parametric test, Wilcoxon-Mann-Whitney test ((**p 0.0073 (max diameter), ***p 0.0002 (min diameter), ***p 0.0003, ****p<0.0001)).

6.4 Discussion

The various components of the NE work together to maintain the integrity of the nucleus, protecting the genome and responding to external and internal forces. The nuclear shape is not fixed and can change significantly due to forces acting on the NE, such as those from the outside (cytoskeleton) or from within, as well as tension within the envelope (7). It is important to note that changes to nuclear integrity occur at a low frequency in normal, healthy cells. However, these changes can significantly increase when the NE integrity is challenged, such as in cases of mechanical stress or when the NE structure is weakened by mutations of the *Lmna* gene, such as in EDMD (96,348–351).

We demonstrated that muscle fibre nuclei isolated from $Lmna^{H222P/H222P}$ mice have an oblong shape compared to their wild-type counterparts. This suggests that the expression of the mutated lamin causes an alteration of the NE, making it more susceptible to mechanical deformation.

Additionally, we observed a modification of the tyrosinated α-tubulin network in the muscle fibers of mice with LMNA p.H222P mutation. This finding is consistent with the results presented in our previous work, where we showed that there is a decrease in the expression of acetylated α-tubulin in cardiomyocytes isolated from $Lmna^{H222P/H222P}$ mice, which is caused by reduced expression of α-TAT1 (144,333). The mutated lamin expression leads to cytoskeleton instability, resulting in tubulin microtubule depolarization.

The addition of a carboxy-terminal tyrosine to α-tubulins is a well-researched post-translational modification (366). TTL catalyses the re-addition of a tyrosine residue to the C-terminus of detyrosinated α-tubulin as part of the evolutionarily conserved tubulin tyrosination cycle (366–368). The enzyme TTL is essential for cell and organism development. In fact, TTL-null mice die shortly after birth due to disorganized neuronal networks (369). Additionally, TTL suppression is associated with cell transformation and is correlated with poor prognosis in patients with various forms of cancer (370–373). This confirms the important role of this enzyme and the tyrosination cycle and their involvement in several pathological forms.

It is interesting to note that the tyrosination cycle regulates the interaction of cytoskeleton-associated proteins-glycine-rich (CAP-Gly) with microtubules. Indeed, CLIP-170 and the large dynactin subunit p150glued use their CAP-Gly domains to bind the C-terminal tyrosine of α-tubulin (374). Recognition of the tyrosine residue is essential for CLIP-170 and

p150glued to localize to growing microtubule tips, where they are involved in regulating microtubule dynamics and microtubule interactions with subcellular structures (375–378). CLIP-170 regulates cell migration and mitosis by controlling the linkage of microtubules to the cell border or the kinetochore and promoting microtubule assembly. It also influences the localization of dynein-dynactin motor proteins to the microtubule by recruiting the dynactin subunit p150Glued and the dynein-binding protein LIS1, which further promotes microtubule assembly (379–381) (**Fig. 35**). CLIP-170 exists in two conformations: the folded inactive form and the open active conformation that binds microtubules and the microtubule-associated proteins p150Glued and LIS1. The conformation of CLIP-170 changes from an open to a folded state upon AMPK-mediated phosphorylation at Ser311, resulting in the inhibition of its activity and dissociation from microtubules (382,383) (**Fig. 35**).

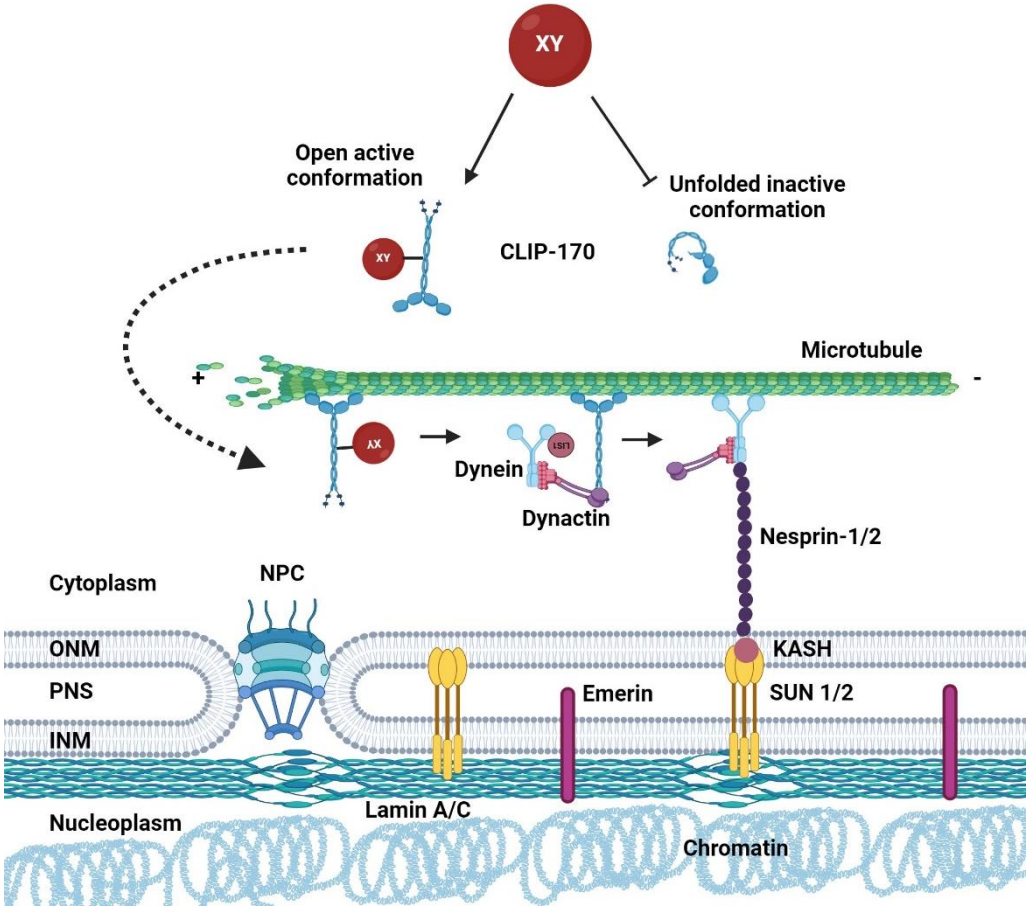

Figure 35: Schematic representation of the effect of CLIP-170 activation on microtubule dynamics mediated by the XY molecule (Created with BioRender.com).

Recent studies indicate that an activated form of AMP-activated protein kinase (AMPK) localizes to the intercalated disc in response to mechanical stress and phosphorylates the CLIP-170 to promote microtubule dynamics. Blocking CLIP-170 phosphorylation results in microtubule hyperstabilization at the intercalated disc, leading to microtubule accumulation, cardiomyocyte elongation, and cardiac dilation (338).

The decreased expression of CLIP-170 and its distinct localization in the striated muscles of *Lmna*$^{H222P/H222P}$ mice suggest that CLIP-170 may be predominantly inactive and phosphorylated. Alternatively, the different localization of CLIP-170 could be due to a reduced availability of tyrosinated α-tubulin binding sites, to which CLIP-170 binds. We have demonstrated that the activation of CLIP-170 by a neurosteroid XY restores its localization and corrects the abnormal nuclear shape in isolated muscle fibers from *Lmna*$^{H222P/H222P}$ mice.

Neurosteroids are synthesized by cytochrome P450 in the central and peripheral nervous system, glial cells, and neurons, from cholesterol or steroidal precursors imported from peripheral sources (384–388). They play a significant role in neurodevelopment and have neuroprotective effects. Neurosteroids are relevant to the pathophysiology and pharmacological treatment of various psychiatric disorders, including mood and anxiety disorders, psychotic disorders, childhood disorders, eating disorders, dementia, stress disorders, schizophrenia, and postpartum disorders (389–393).

Neurosteroids exert their effects through mechanisms other than classic nuclear receptors of steroid hormones. These mechanisms include binding to ionic receptors of neurotransmitters or directly or indirectly modulating other neurotransmitter receptors (388). A newly discovered mechanism of action in the brain involves the specific binding of steroids or their precursors to microtubule-associated proteins, resulting in increased polymerization of tubulin for microtubule assembly (384,394). In a neuronal model with mutations in the X-linked cyclin-dependent kinase-like 5 (CDKL5) gene, steroids have been shown to correct neuronal defects caused by CLIP170 dysfunction (341,342,345).

In conclusion, the present study demonstrates that molecule XY, induces CLIP-170 activation, resulting in the recovery of CLIP-170 localization and of altered nuclear morphology in mice carrying the LMNA p.H222P mutation. Further investigation is required to understand the mechanisms by which CLIP-170 modulates nuclear morphology through its association with microtubules. In conclusion, the data suggest that XY molecule, may have therapeutic effects in mice carrying the LMNA p.H222P mutation by modulating microtubule dynamics and its association with the nuclear envelope.

7. Concluding remarks

This study identifies at cellular level the pathogenetic mechanisms underlying three different *Lmna* gene mutations (Q517X, R321X, H222P) that affect striated muscles. Specifically, LMNA Q517X and LMNA R321X mutations affect the heart, resulting in the onset of DCM while LMNA p.H222P affects both the skeletal muscle and the heart causing muscular dystrophy and DCM, respectively. Cardiomyopathies caused by *Lmna* mutations have a particularly aggressive and rapid clinical course, which may result in sudden cardiac death from malignant ventricular arrhythmias and end-stage heart failure at earlier ages than other familial cardiomyopathies. Current therapies involve implantable pacemakers and defibrillators to manage arrhythmia and conduction defects to prevent sudden cardiac death (269). Pharmacological interventions for congestive heart failure typically target its symptoms. These therapies can extend the survival rate of affected patients, but they only improve cardiac function and reduce complications and secondary features of the disease, without addressing the specific mutation causing the pathology (1).

Here, we identified three pathogenic mechanisms and proposed a potential therapeutic target for each of the mutations investigated. For two of the mutations analysed (LMNA Q517X and LMNA H222P), a similar pathogenic mechanism involving post-translational modifications of tubulin and the involvement of the microtubule network's has been identified.

Therefore, the idea that *Lmna* mutations may affect striated muscle physiology through the "mechanical hypothesis" seem strongly supported by the experimental data collected in this thesis. In addition, the expression of LMNA Q517X is associated with a decreased expression of the Na^+-channel Nav1.5 at the plasma membrane of cardiomyocytes. This reveals a new mechanism through which *Lmna* mutations may regulate the electrical profile of cardiac cells leading to arrhythmogenic phenotypes. However, the functional characterization of LMNA R321X depicts a different scenario since the mutation-dependent activation of the ER stress is mostly related to the cytotoxic accumulation of the truncated mutant within the ER. Thus, the activation of a specific genetic program, known as UPR, upon *Lmna* mutation, stands for "the gene regulation hypothesis" as main molecular mechanism associated with laminopathies.

Overall, our results have significantly contributed to our understanding of the pathogenetic processes underlying *Lmna* mutations. This provides valuable insights for the development of potential new, highly effective, therapeutic targets usable to rescue cell functions that have been impaired by specific pathogenetic mechanisms.

The discovery of drugs that can alleviate the harmful effects of *Lmna* mutations, ranging from PTM of tubulin-targeting agents to UPR modulators and CLIP-170 regulators, opens new therapeutic avenues for patients affected by these conditions. It provides a solid foundation for the development of personalized therapeutic approaches, offering hope and better prospects for patients affected by these debilitating conditions.

8. References

1. Gerbino A, Procino G, Svelto M, Carmosino M. Role of Lamin A/C Gene Mutations in the signaling defects leading to cardiomyopathies. Vol. 9, Frontiers in Physiology. 2018.

2. Foisner R. Cell cycle dynamics of the nuclear envelope. Vol. 3, TheScientificWorldJournal. 2003.

3. van Heerden D, Klima S, van den Bout I. How nuclear envelope dynamics can direct laminopathy phenotypes. Curr Opin Cell Biol. 2024 Feb 1;86:102290.

4. Tiwari V, Alam MJ, Bhatia M, Navya M, Banerjee SK. The structure and function of lamin A/C: Special focus on cardiomyopathy and therapeutic interventions. Life Sci [Internet]. 2024 Mar 15 [cited 2024 Feb 19];341:122489. Available from: https://linkinghub.elsevier.com/retrieve/pii/S002432052400078X

5. Carmosino M, Torretta S, Procino G, Gerbino A, Forleo C, Favale S, et al. Role of nuclear Lamin A/C in cardiomyocyte functions. Vol. 106, Biology of the Cell. 2014.

6. Korfali N, Wilkie GS, Swanson SK, Srsen V, de las Heras J, Batrakou DG, et al. The nuclear envelope proteome differs notably between tissues. Nucleus (United States). 2012;3(6).

7. Ungricht R, Kutay U. Mechanisms and functions of nuclear envelope remodelling. Vol. 18, Nature Reviews Molecular Cell Biology. 2017.

8. Donnaloja F, Carnevali F, Jacchetti E, Raimondi MT. Lamin A/C Mechanotransduction in Laminopathies. Vol. 9, Cells. 2020.

9. Turgay Y, Eibauer M, Goldman AE, Shimi T, Khayat M, Ben-Harush K, et al. The molecular architecture of lamins in somatic cells. Nature. 2017;543(7644).

10. Gruenbaum Y, Wilson KL, Harel A, Goldberg M, Cohen M. Review: Nuclear lamins - Structural proteins with fundamental functions. J Struct Biol. 2000;129(2–3).

11. Aaronson RP, Blobel G. Isolation of nuclear pore complexes in association with a lamina. Proc Natl Acad Sci U S A. 1975;72(3).

12. Fisher DZ, Chaudhary N, Blobel G. cDNA sequencing of nuclear lamins A and C reveals primary and secondary structural homology to intermediate filament proteins. Proc Natl Acad Sci U S A. 1986;83(17).

13. Dittmer T, Misteli T. The lamin protein family. Genome Biol. 2011;12(5).

14. Ishikawa H, Bischoff R, Holtzer H. Mitosis and intermediate-sized filaments in developing skeletal muscle. J Cell Biol. 1968;38(3).

15. Moir RD, Spann TP, Lopez-Soler RI, Yoon M, Goldman AE, Khuon S, et al. Review: The dynamics of the nuclear lamins during the cell cycle - Relationship between structure and function. J Struct Biol. 2000;129(2–3).

16. Ho CY, Lammerding J. Lamins at a glance. J Cell Sci. 2012;125(9).

17. Lin F, Worman HJ. Structural organization of the human gene encoding nuclear lamin A and nuclear lamin C. Journal of Biological Chemistry. 1993;268(22).

18. Ahn J, Jo I, Kang S mi, Hong S, Kim S, Jeong S, et al. Structural basis for lamin assembly at the molecular level. Nat Commun. 2019;10(1).

19. Wu D, Flannery AR, Cai H, Ko E, Cao K. Nuclear localization signal deletion mutants of lamin A and progerin reveal insights into lamin A processing and emerin targeting. Nucleus (United States). 2014;5(1).

20. Corrigan DP, Kuszczak D, Rusinol AE, Thewke DP, Hrycyna CA, Michaelis S, et al. Prelamin A endoproteolytic processing in vitro by recombinant Zmpste24. Biochemical Journal. 2005;387(1).

21. Sinensky M, Fantle K, Trujillo M, McLain T, Kupfer A, Dalton M. The processing pathway of prelamin A. J Cell Sci. 1994;107(1).

22. Dhe-Paganon S, Werner ED, Chi YI, Shoelson SE. Structure of the globular tail of nuclear lamin. Journal of Biological Chemistry. 2002;277(20).

23. Al-Saaidi R, Bross P. Do lamin A and lamin C have unique roles? Vol. 124, Chromosoma. 2015.

24. Malashicheva A, Perepelina K. Diversity of Nuclear Lamin A/C Action as a Key to Tissue-Specific Regulation of Cellular Identity in Health and Disease. Vol. 9, Frontiers in Cell and Developmental Biology. 2021.

25. Yoo C, Pal M, Miller FR, Barder TJ, Huber C, Lubman DM. Toward high sequence coverage of proteins in human breast cancer cells using on-line monolith-based HPLC-ESI-TOF MS compared to CE MS. Electrophoresis. 2006;27(11).

26. Fong LG, Ng JK, Lammerding J, Vickers TA, Meta M, Coté N, et al. Prelamin A and lamin A appear to be dispensable in the nuclear lamina. Journal of Clinical Investigation. 2006;116(3).

27. Machowska M, Piekarowicz K, Rzepecki R. Regulation of lamin properties and functions: Does phosphorylation do it all? Open Biol. 2015;5(11).

28. Dominici S, Fiori V, Magnani M, Schena E, Capanni C, Camozzi D, et al. Different prelamin A forms accumulate in human fibroblasts: A study in experimental models and progeria. European Journal of Histochemistry. 2009;53(1).

29. Lutz RJ, Trujillo MA, Denham KS, Wenger L, Sinensky M. Nucleoplasmic localization of prelamin A: Implications for prenylation-dependent lamin A assembly into the nuclear lamina. Proc Natl Acad Sci U S A. 1992;89(7).

30. Simon DN, Wilson KL. Partners and post-translational modifications of nuclear lamins. Vol. 122, Chromosoma. 2013.

31. Prokocimer M, Davidovich M, Nissim-Rafinia M, Wiesel-Motiuk N, Bar DZ, Barkan R, et al. Nuclear lamins: Key regulators of nuclear structure and activities. J Cell Mol Med. 2009;13(6).

32. Kochin V, Shimi T, Torvaldson E, Adam SA, Goldman A, Pack CG, et al. Interphase phosphorylation of lamin A. J Cell Sci. 2014;127(12).

33. Ikegami K, Secchia S, Almakki O, Lieb JD, Moskowitz IP. Phosphorylated Lamin A/C in the Nuclear Interior Binds Active Enhancers Associated with Abnormal Transcription in Progeria. Dev Cell. 2020;52(6).

34. Zhang YQ, Sarge KD. Sumoylation regulates lamin A function and is lost in lamin A mutants associated with familial cardiomyopathies. Journal of Cell Biology. 2008;182(1).

35. Xie W, Chojnowski A, Boudier T, Lim JSY, Ahmed S, Ser Z, et al. A-type Lamins Form Distinct Filamentous Networks with Differential Nuclear Pore Complex Associations. Current Biology. 2016;26(19).

36. Shimia T, Kittisopikul M, Tran J, Goldman AE, Adam SA, Zheng Y, et al. Structural organization of nuclear lamins A, C, B1, and B2 revealed by superresolution microscopy. Mol Biol Cell. 2015;26(22).

37. Machiels BM, Zorenc AHG, Endert JM, Kuijpers HJH, Van Eys GJJM, Ramaekers FCS, et al. An alternative splicing product of the lamin A/C gene lacks exon 10. Journal of Biological Chemistry. 1996;271(16).

38. Furukawa K, Inagaki H, Hotta Y. Identification and cloning of an mRNA coding for a germ cell-specific A-type lamin in mice. Exp Cell Res. 1994;212(2).

39. Furukawa K, Hotta Y. cDNA cloning of a germ cell specific lamin B3 from mouse spermatocytes and analysis of its function by ectopic expression in somatic cells. EMBO J. 1993;12(1).

40. Harborth J, Elbashir SM, Bechert K, Tuschl T, Weber K. Identification of essential genes in cultured mammalian cells using small interfering RNAs. J Cell Sci. 2001;114(24).

41. Lee JM, Tu Y, Tatar A, Wu D, Nobumori C, Jung HJ, et al. Reciprocal knock-in mice to investigate the functional redundancy of lamin B1 and lamin B2. Mol Biol Cell. 2014;25(10).

42. Coffinier C, Jung HJ, Nobumori C, Chang S, Tu Y, Barnes RH, et al. Deficiencies in lamin B1 and lamin B2 cause neurodevelopmental defects and distinct nuclear shape abnormalities in neurons. Mol Biol Cell. 2011;22(23).

43. Vergnes L, Péterfy M, Bergo MO, Young SG, Reue K. Lamin B1 is required for mouse development and nuclear integrity. Proc Natl Acad Sci U S A. 2004;101(28).

44. Hegele RA, Cao H, Liu DM, Costain GA, Charlton-Menys V, Wilson Rodger N, et al. Sequencing of the reannotated LMNB2 gene reveals novel mutations in patients with acquired partial lipodystrophy. Am J Hum Genet. 2006;79(2).

45. Padiath QS, Saigoh K, Schiffmann R, Asahara H, Yamada T, Koeppen A, et al. Lamin B1 duplications cause autosomal dominant leukodystrophy. Nat Genet. 2006;38(10).

46. Shimi T, Butin-Israeli V, Adam SA, Hamanaka RB, Goldman AE, Lucas CA, et al. The role of nuclear lamin B1 in cell proliferation and senescence. Genes Dev. 2011;25(24).

47. Rober RA, Weber K, Osborn M. Differential timing of nuclear lamin A/C expression in the various organs of the mouse embryo and the young animal: A developmental study. Development. 1989;105(2).

48. Constantinescu D, Gray HL, Sammak PJ, Schatten GP, Csoka AB. Lamin A/C Expression Is a Marker of Mouse and Human Embryonic Stem Cell Differentiation. Stem Cells. 2006;24(1).

49. Stewart C, Burke B. Teratocarcinoma stem cells and early mouse embryos contain only a single major lamin polypeptide closely resembling lamin B. Cell. 1987;51(3).

50. Peter M, Nigg EA. Ectopic expression of an A-type lamin does not interfere with differentiation of lamin A-negative embryonal carcinoma cells. J Cell Sci. 1991;100(3).

51. Sullivan T, Escalante-Alcalde D, Bhatt H, Anver M, Bhat N, Nagashima K, et al. Loss of A-type lamin expression compromises nuclear envelope integrity leading to muscular dystrophy. Journal of Cell Biology. 1999;147(5).

52. Yang SH, Meta M, Qiao X, Frost D, Bauch J, Coffinier C, et al. A farnesyltransferase inhibitor improves disease phenotypes in mice with a Hutchinson-Gilford progeria syndrome mutation. Journal of Clinical Investigation. 2006;116(8).

53. Swift J, Ivanovska IL, Buxboim A, Harada T, Dingal PCDP, Pinter J, et al. Nuclear lamin-A scales with tissue stiffness and enhances matrix-directed differentiation. Science (1979). 2013;341(6149).

54. Gaustad KG, Boquest AC, Anderson BE, Gerdes AM, Collas P. Differentiation of human adipose tissue stem cells using extracts of rat cardiomyocytes. Biochem Biophys Res Commun. 2004;314(2).

55. Kubben N, Adriaens M, Meuleman W, Voncken JW, Steensel B Van, Misteli T. Mapping of lamin A- and progerin-interacting genome regions. Chromosoma [Internet]. 2012 Jul 19 [cited 2024 Mar 13];121(5):447–64. Available from: https://link.springer.com/article/10.1007/s00412-012-0376-7

56. Hutchison CJ. The role of DNA damage in laminopathy progeroid syndromes. In: Biochemical Society Transactions. 2011.

57. Gonzalez-Suarez I, Redwood AB, Perkins SM, Vermolen B, Lichtensztejin D, Grotsky DA, et al. Novel roles for A-type lamins in telomere biology and the DNA damage response pathway. EMBO Journal. 2009;28(16).

58. Dechat T, Shimi T, Adam SA, Rusinol AE, Andres DA, Spielmann HP, et al. Alterations in mitosis and cell cycle progression caused by a mutant lamin A known to accelerate human aging. Proc Natl Acad Sci U S A. 2007;104(12).

59. Dauer WT, Worman HJ. The Nuclear Envelope as a Signaling Node in Development and Disease. Vol. 17, Developmental Cell. 2009.

60. Gerace L, Tapia O. Messages from the voices within: regulation of signaling by proteins of the nuclear lamina. Vol. 52, Current Opinion in Cell Biology. 2018.

61. Laguri C, Gilquin B, Wolff N, Romi-Lebrun R, Courchay K, Callebaut I, et al. Structural characterization of the LEM motif common to three human inner nuclear membrane proteins. Structure. 2001;9(6).

62. Margalit A, Brachner A, Gotzmann J, Foisner R, Gruenbaum Y. Barrier-to-autointegration factor - a BAFfling little protein. Vol. 17, Trends in Cell Biology. 2007.

63. Samson C, Petitalot A, Celli F, Herrada I, Ropars V, Le Du MH, et al. Structural analysis of the ternary complex between lamin A/C, BAF and emerin identifies an interface disrupted in autosomal recessive progeroid diseases. Nucleic Acids Res. 2018;46(19).

64. Segura-Totten M, Kowalski AK, Craigie R, Wilson KL. Barrier-to-autointegration factor: Major roles in chromatin decondensation and nuclear assembly. Journal of Cell Biology. 2002;158(3).

65. Wagner N, Krohne G. LEM-Domain Proteins: New Insights into Lamin-Interacting Proteins. Vol. 261, International Review of Cytology. 2007.

66. Manilal S, Nguyen TM, Sewry CA, Morris GE. The Emery-Dreifuss muscular dystrophy protein, emerin, is a nuclear membrane protein. Hum Mol Genet. 1996;5(6).

67. Lee KK, Haraguchi T, Lee RS, Koujin T, Hiraoka Y, Wilson KL. Distinct functional domains in emerin bind lamin A and DNA-bridging protein BAF. J Cell Sci. 2001;114(24).

68. Dechat T, Vlcek S, Foisner R. Review: Lamina-associated polypeptide 2 isoforms and related proteins in cell cycle-dependent nuclear structure dynamics. J Struct Biol. 2000;129(2–3).

69. Vlcek S, Korbei B, Foisner R. Distinct functions of the unique C terminus of LAP2α in cell proliferation and nuclear assembly. Journal of Biological Chemistry. 2002;277(21).

70. Zastrow MS, Vlcek S, Wilson KL. Proteins that bind A-type lamins: Integrating isolated clues. Vol. 117, Journal of Cell Science. 2004.

71. Ishimura A, Ng JK, Taira M, Young SG, Osada SI. Man1, an inner nuclear membrane protein, regulates vascular remodeling by modulating transforming growth factor β signaling. Development. 2006;133(19).

72. Mansharamani M, Wilson KL. Direct binding of nuclear membrane protein MAN1 to emerin in vitro and two modes of binding to barrier-to-autointegration factor. Journal of Biological Chemistry. 2005;280(14).

73. Moir RD, Yoon M, Khuon S, Goldman RD. Nuclear lamins A and B1: Different pathways of assembly during nuclear envelope formation in living cells. Journal of Cell Biology. 2000;151(6).

74. Panorchan P, Schafer BW, Wirtz D, Tseng Y. Nuclear envelope breakdown requires overcoming the mechanical integrity of the nuclear lamina. Journal of Biological Chemistry. 2004;279(42).

75. Bertero A, Fields PA, Smith AST, Leonard A, Beussman K, Sniadecki NJ, et al. Chromatin compartment dynamics in a haploinsufficient model of cardiac laminopathy. Journal of Cell Biology. 2019;218(9).

76. Xanthis I, Iskratsch T. Lamin-A Mechano-Protects the Heart. Vol. 49, Developmental Cell. 2019.

77. Nikolova V, Leimena C, McMahon AC, Tan JC, Chandar S, Jogia D, et al. Defects in nuclear structure and function promote dilated cardiomyopathy in lamin A/C-deficient mice. Journal of Clinical Investigation. 2004;113(3).

78. James TN, St. Martin E, Willis PW, Lohr TO. Apoptosis as a possible cause of gradual development of complete heart block and fatal arrhythmias associated with absence of the AV node, sinus node, and internodal pathways. Circulation. 1996;93(7).

79. Olivetti G, Abbi R, Quaini F, Kajstura J, Cheng W, Nitahara JA, et al. Apoptosis in the Failing Human Heart. New England Journal of Medicine. 1997;336(16).

80. Haque F, Lloyd DJ, Smallwood DT, Dent CL, Shanahan CM, Fry AM, et al. SUN1 Interacts with Nuclear Lamin A and Cytoplasmic Nesprins To Provide a Physical Connection between the Nuclear Lamina and the Cytoskeleton. Mol Cell Biol. 2006;26(10).

81. McGee MD, Rillo R, Anderson AS, Starr DA. UNC-83 is a KASH protein required for nuclear migration and is recruited to the outer nuclear membrane by a physical interaction with the SUN protein UNC-84. Mol Biol Cell. 2006;17(4).

82. Davidson PM, Cadot B. Actin on and around the Nucleus. Vol. 31, Trends in Cell Biology. 2021.

83. Wilhelmsen K, Litjens SHM, Kuikman I, Tshimbalanga N, Janssen H, Van Bout I Den, et al. Nesprin-3, a novel outer nuclear membrane protein, associates with the cytoskeletal linker protein plectin. Journal of Cell Biology. 2005;171(5).

84. Wong X, Loo TH, Stewart CL. LINC complex regulation of genome organization and function. Vol. 67, Current Opinion in Genetics and Development. 2021.

85. Chen CY, Chi YH, Mutalif RA, Starost MF, Myers TG, Anderson SA, et al. Accumulation of the inner nuclear envelope protein Sun1 is pathogenic in progeric and dystrophic laminopathies. Cell. 2012;149(3).

86. Khatau SB, Kusuma S, Hanjaya-Putra D, Mali P, Cheng L, Lee JSH, et al. The differential formation of the LINC-mediated perinuclear actin cap in pluripotent and somatic cells. PLoS One. 2012;7(5).

87. Méjat A, Misteli T. LINC complexes in health and disease. Nucleus. 2010;1(1).

88. Folker ES, Östlund C, Luxton GWG, Worman HJ, Gundersen GG. Lamin A variants that cause striated muscle disease are defective in anchoring transmembrane actin-associated nuclear lines for nuclear movement. Proc Natl Acad Sci U S A. 2011;108(1).

89. TOKUYASU KT, MAHER PA, DUTTON AH, SINGER SJ. Intermediate Filaments in Skeletal and Cardiac Muscle Tissue in Embryonic and Adult Chicken. Ann N Y Acad Sci. 1985;455(1).

90. Sébillon P, Bouchier C, Bidot LD, Bonne G, Ahamed K, Charron P, et al. Expanding the phenotype of LMNA mutations in dilated cardiomyopathy and functional consequences of these mutations. J Med Genet. 2003;40(8).

91. Mounkes LC, Kozlov S V., Rottman JN, Stewart CL. Expression of an LMNA-N195K variant of A-type lamins results in cardiac conduction defects and death in mice. Hum Mol Genet. 2005;14(15).

92. Yang L, Munck M, Swaminathan K, Kapinos LE, Noegel AA, Neumann S. Mutations in LMNA Modulate the Lamin A - Nesprin-2 Interaction and Cause LINC Complex Alterations. PLoS One. 2013;8(8).

93. Fawcett DW. On the occurrence of a fibrous lamina on the inner aspect of the nuclear envelope in certain cells of vertebrates. American Journal of Anatomy. 1966;119(1).

94. Belmont AS, Zhai Y, Thilenius A. Lamin B distribution and association with peripheral chromatin revealed by optical sectioning and electron microscopy tomography. Journal of Cell Biology. 1993;123(6 PART 2).

95. Galiová G, Bártová E, Raška I, Krejčí J, Kozubek S. Chromatin changes induced by lamin A/C deficiency and the histone deacetylase inhibitor trichostatin A. Eur J Cell Biol. 2008;87(5).

96. Ognibene A, Sabatelli P, Petrini S, Squarzoni S, Riccio M, Santi S, et al. Nuclear changes in a case of X-linked Emery-Dreifuss muscular dystrophy. Muscle Nerve. 1999;22(7).

97. Scaffidi P, Misteli T. Lamin A-dependent nuclear defects in human aging. Science (1979). 2006;312(5776).

98. Scaffidi P, Misteli T. Reversal of the cellular phenotype in the premature aging disease Hutchinson-Gilford progeria syndrome. Nat Med. 2005;11(4).

99. Taniura H, Glass C, Gerace L. A chromatin binding site in the tail domain of nuclear lamins that interacts with core histones. Journal of Cell Biology. 1995;131(1).

100. Bruston F, Delbarre E, Östlund C, Worman HJ, Buendia B, Duband-Goulet I. Loss of a DNA binding site within the tail of prelamin A contributes to altered heterochromatin anchorage by progerin. FEBS Lett. 2010;584(14).

101. Briand N, Collas P. Lamina-associated domains: Peripheral matters and internal affairs. Vol. 21, Genome Biology. 2020.

102. Shah PP, Lv W, Rhoades JH, Poleshko A, Abbey D, Caporizzo MA, et al. Pathogenic LMNA variants disrupt cardiac lamina-chromatin interactions and de-repress alternative fate genes. Cell Stem Cell. 2021;28(5).

103. Shoeman RL, Traub P. The in vitro DNA-binding properties of purified nuclear lamin proteins and vimentin. Journal of Biological Chemistry. 1990;265(16).

104. Han X, Feng X, Rattner JB, Smith H, Bose P, Suzuki K, et al. Tethering by lamin A stabilizes and targets the ING1 tumour suppressor. Nat Cell Biol. 2008;10(11).

105. Liu B, Wang J, Chan KM, Tjia WM, Deng W, Guan X, et al. Genomic instability in laminopathy-based premature aging. Nat Med. 2005;11(7).

106. Manju K, Muralikrishna B, Parnaik VK. Expression of disease-causing lamin A mutants impairs the formation of DNA repair foci. J Cell Sci. 2006;119(13).

107. Gnocchi VF, Ellis JA, Zammit PS. Does satellite cell dysfunction contribute to disease progression in Emery-Dreifuss muscular dystrophy? In: Biochemical Society Transactions. 2008.

108. Magagnotti C, Bachi A, Zerbini G, Fattore E, Fermo I, Riba M, et al. Protein profiling reveals energy metabolism and cytoskeletal protein alterations in LMNA mutation carriers. Biochim Biophys Acta Mol Basis Dis. 2012;1822(6).

109. Lammerding J, Schulze PC, Takahashi T, Kozlov S, Sullivan T, Kamm RD, et al. Lamin A/C deficiency causes defective nuclear mechanics and mechanotransduction. Journal of Clinical Investigation. 2004;113(3).

110. Zwerger M, Jaalouk DE, Lombardi ML, Isermann P, Mauermann M, Dialynas G, et al. Myopathic lamin mutations impair nuclear stability in cells and tissue and disrupt nucleo-cytoskeletal coupling. Hum Mol Genet. 2013;22(12).

111. Andrés V, González JM. Role of A-type lamins in signaling, transcription, and chromatin organization. Vol. 187, Journal of Cell Biology. 2009.

112. Reddy KL, Zullo JM, Bertolino E, Singh H. Transcriptional repression mediated by repositioning of genes to the nuclear lamina. Nature. 2008;452(7184).

113. Malhas AN, Lee CF, Vaux DJ. Lamin B1 controls oxidative stress responses via Oct-1. Journal of Cell Biology. 2009;184(1).

114. Spann TP, Goldman AE, Wang C, Huang S, Goldman RD. Alteration of nuclear lamin organization inhibits RNA polymerase II-dependent transcription. Journal of Cell Biology. 2002;156(4).

115. Kumaran RI, Muralikrishna B, Parnaik VK. Lamin A/C speckles mediate spatial organization of splicing factor compartments and RNA polymerase II transcription. Journal of Cell Biology. 2002;159(5).

116. Gonzàlez JM, Navarro-Puche A, Casar B, Crespo P, Andrès V. Fast regulation of AP-1 activity through interaction of lamin A/C, ERK1/2, and c-Fos at the nuclear envelope. Journal of Cell Biology. 2008;183(4).

117. Markiewicz E, Dechat T, Foisner R, Quinlan RA, Hutchison CJ. Lamin A/C binding protein LAP2α Is required for nuclear anchorage of retinoblastoma protein. Mol Biol Cell. 2002;13(12).

118. Mancini MA, Shan B, Nickerson JA, Penman S, Lee WH. The retinoblastoma gene product is a cell cycle-dependent, nuclear matrix-associated protein. Proc Natl Acad Sci U S A. 1994;91(1).

119. Dreuillet C, Tillit J, Kress M, Ernoult-Lange M. In vivo and in vitro interaction between human transcription factor MOK2 and nuclear lamin A/C. Nucleic Acids Res. 2002;30(21).

120. Arranz V, Harper F, Florentin Y, Puvion E, Kress M, Ernoult-Lange M. Human and Mouse MOK2 Proteins Are Associated with Nuclear Ribonucleoprotein Components

and Bind Specifically to RNA and DNA through Their Zinc Finger Domains. Mol Cell Biol. 1997;17(4).

121. Ivorra C, Kubicek M, González JM, Sanz-González SM, Álvarez-Barrientos A, O'Connor JE, et al. A mechanism of AP-1 suppression through interaction of c-Fos with lamin A/C. Genes Dev. 2006;20(3).

122. Shaulian E, Karin M. AP-1 as a regulator of cell life and death. Vol. 4, Nature Cell Biology. 2002.

123. Eferl R, Wagner EF. AP-1: A double-edged sword in tumorigenesis. Vol. 3, Nature Reviews Cancer. 2003.

124. Lloyd DJ, Trembath RC, Shackleton S. A novel interaction between lamin A and SREBP1: Implications for partial lipodystrophy and other laminopathies. Hum Mol Genet. 2002;11(7).

125. Arimura T, Helbling-Leclerc A, Massart C, Varnous S, Niel F, Lacène E, et al. Mouse model carrying H222P-Lmna mutation develops muscular dystrophy and dilated cardiomyopathy similar to human striated muscle laminopathies. Hum Mol Genet. 2005;14(1).

126. Muchir A, Pavlidis P, Decostre V, Herron AJ, Arimura T, Bonne G, et al. Activation of MAPK pathways links LMNA mutations to cardiomyopathy in Emery-Dreifuss muscular dystrophy. Journal of Clinical Investigation. 2007;117(5).

127. Muchir A, Reilly SA, Wu W, Iwata S, Homma S, Bonne G, et al. Treatment with selumetinib preserves cardiac function and improves survival in cardiomyopathy caused by mutation in the lamin A/C gene. Cardiovasc Res. 2012;93(2).

128. Wu W, Iwata S, Homma S, Worman HJ, Muchir A. Depletion of extracellular signal-regulated kinase 1 in mice with cardiomyopathy caused by lamin A/C gene mutation partially prevents pathology before isoenzyme activation. Hum Mol Genet. 2014;23(1).

129. Wu W, Chordia MD, Hart BP, Kumarasinghe ES, Ji MK, Bhargava A, et al. Macrocyclic MEK1/2 inhibitor with efficacy in a mouse model of cardiomyopathy caused by lamin A/C gene mutation. Bioorg Med Chem. 2017;25(3).

130. Wu W, Muchir A, Shan J, Bonne G, Worman HJ. Mitogen-Activated Protein Kinase Inhibitors Improve Heart Function and Prevent Fibrosis in Cardiomyopathy Caused by Mutation in Lamin A/C Gene. Circulation [Internet]. 2011 Jan 4 [cited 2024 Mar 12];123(1):53–61. Available from: https://www.ahajournals.org/doi/abs/10.1161/CIRCULATIONAHA.110.970673

131. Chatzifrangkeskou M, Yadin D, Marais T, Chardonnet S, Cohen-Tannoudji M, Mougenot N, et al. Cofilin-1 phosphorylation catalyzed by ERK1/2 alters cardiac actin dynamics in dilated cardiomyopathy caused by lamin A/C gene mutation. Hum Mol Genet. 2018;27(17).

132. Gillespie-Brown J, Fuller SJ, Bogoyevitch MA, Cowley S, Sugden PH. The mitogen-activated protein kinase kinase MEK1 stimulates a pattern of gene expression typical of the hypertrophic phenotype in rat ventricular cardiomyocytes. Journal of Biological Chemistry. 1995;270(47).

133. Thorburn J, Carlson M, Mansour SJ, Chien KR, Ahn NG, Thorburn A. Inhibition of a signaling pathway in cardiac muscle cells by active mitogen-activated protein kinase kinase. Mol Biol Cell. 1995;6(11).

134. Rosenkranz S. TGF-h 1 and angiotensin networking in cardiac remodeling. [cited 2024 Mar 12]; Available from: https://academic.oup.com/cardiovascres/article/63/3/423/344762

135. Huang H, Tang Y, Wu G, Mei Y, Liu W, Liu X, et al. ALK7 protects against pathological cardiac hypertrophy in mice. Cardiovasc Res. 2015;108(1).

136. Choi JC, Wu W, Muchir A, Iwata S, Homma S, Worman HJ. Dual specificity phosphatase 4 mediates cardiomyopathy caused by lamin A/C (LMNA) gene mutation. Journal of Biological Chemistry. 2012;287(48).

137. Choi JC, Wu W, Phillips E, Plevin R, Sera F, Homma S, et al. Elevated dual specificity protein phosphatase 4 in cardiomyopathy caused by lamin A/C gene mutation is primarily ERK1/2-dependent and its depletion improves cardiac function and survival. Hum Mol Genet. 2018;27(13).

138. Le Dour C, Macquart C, Sera F, Homma S, Bonne G, Morrow JP, et al. Decreased WNT/β-catenin signalling contributes to the pathogenesis of dilated cardiomyopathy caused by mutations in the lamin a/C gene. Hum Mol Genet. 2017;26(2).

139. Eisenberg T, Knauer H, Schauer A, Büttner S, Ruckenstuhl C, Carmona-Gutierrez D, et al. Induction of autophagy by spermidine promotes longevity. Nat Cell Biol. 2009;11(11).

140. Morselli E, Maiuri MC, Markaki M, Megalou E, Pasparaki A, Palikaras K, et al. Caloric restriction and resveratrol promote longevity through the Sirtuin-1-dependent induction of autophagy. Cell Death Dis. 2010;1(1).

141. Choi JC, Muchir A, Wu W, Iwata S, Homma S, Morrow JP, et al. Temsirolimus activates autophagy and ameliorates cardiomyopathy caused by lamin A/C gene mutation. Vol. 4, Science Translational Medicine. 2012.

142. Muchir A, Wu W, Choi JC, Iwata S, Morrow J, Homma S, et al. Abnormal p38α mitogen-activated protein kinase signaling in dilated cardiomyopathy caused by lamin A/C gene mutation. Hum Mol Genet. 2012;21(19).

143. Chen SC, Kennedy BK, Lampe PD. Phosphorylation of connexin43 on S279/282 may contribute to laminopathy-associated conduction defects. Exp Cell Res. 2013;319(6).

144. Macquart C, Jüttner R, Morales Rodriguez B, Le Dour C, Lefebvre F, Chatzifrangkeskou M, et al. Microtubule cytoskeleton regulates Connexin 43 localization and cardiac conduction in cardiomyopathy caused by mutation in A-type lamins gene. Hum Mol Genet. 2019;28(24).

145. Rodriguez BM, Khouzami L, Decostre V, Varnous S, Pekovic-Vaughan V, Hutchison CJ, et al. N-acetyl cysteine alleviates oxidative stress and protects mice from dilated cardiomyopathy caused by mutations in nuclear A-type lamins gene. Hum Mol Genet. 2018;27(19).

146. Olson EN, Nordheim A. Linking actin dynamics and gene transcription to drive cellular motile functions. Vol. 11, Nature Reviews Molecular Cell Biology. 2010.

147. Parmacek MS. Myocardin-related transcription factors: Critical coactivators regulating cardiovascular development and adaptation. Vol. 100, Circulation Research. 2007.

148. Miralles F, Posern G, Zaromytidou AI, Treisman R. Actin dynamics control SRF activity by regulation of its coactivator MAL. Cell. 2003;113(3).

149. Mouilleron S, Guettler S, Langer CA, Treisman R, McDonald NQ. Molecular basis for G-actin binding to RPEL motifs from the serum response factor coactivator MAL. EMBO Journal. 2008;27(23).

150. Hirano H, Matsuura Y. Sensing actin dynamics: Structural basis for G-actin-sensitive nuclear import of MAL. Biochem Biophys Res Commun. 2011;414(2).

151. Pawłowski R, Rajakylä EK, Vartiainen MK, Treisman R. An actin-regulated importin α/β-dependent extended bipartite NLS directs nuclear import of MRTF-A. EMBO Journal. 2010;29(20).

152. Vartiainen MK, Guettler S, Larijani B, Treisman R. Nuclear actin regulates dynamic subcellular localization and activity of the SRF cofactor MAL. Science (1979). 2007;316(5832).

153. Balza RO, Misra RP. Role of the serum response factor in regulating contractile apparatus gene expression and sarcomeric integrity in cardiomyocytes. Journal of Biological Chemistry. 2006;281(10).

154. Ho CY, Jaalouk DE, Vartiainen MK, Lammerding J. Lamin A/C and emerin regulate MKL1-SRF activity by modulating actin dynamics. Nature. 2013;497(7450).

155. Sen-Chowdhry S, McKenna WJ. Sudden death from genetic and acquired cardiomyopathies. Circulation. 2012;125(12).

156. James TN. Normal and abnormal consequences of apoptosis in the human heart: From postnatal morphogenesis to paroxysmal arrhythmias. Vol. 90, Circulation. 1994.

157. Basso C, Bauce B, Corrado D, Thiene G. Pathophysiology of arrhythmogenic cardiomyopathy. Vol. 9, Nature Reviews Cardiology. 2012.

158. Fatkin D, MacRae C, Sasaki T, Wolff MR, Porcu M, Frenneaux M, et al. Missense Mutations in the Rod Domain of the Lamin A/C Gene as Causes of Dilated Cardiomyopathy and Conduction-System Disease. New England Journal of Medicine. 1999;341(23).

159. Arbustini E, Pilotto A, Repetto A, Grasso M, Negri A, Diegoli M, et al. Autosomal dominant dilated cardiomyopathy with atrioventricular block: A lamin A/C defect-related disease. J Am Coll Cardiol. 2002;39(6).

160. van Tintelen JP, Tio RA, Kerstjens-Frederikse WS, van Berlo JH, Boven LG, Suurmeijer AJH, et al. Severe Myocardial Fibrosis Caused by a Deletion of the 5' End of the Lamin A/C Gene. J Am Coll Cardiol. 2007;49(25).

161. Lu D, Lian H, Zhang X, Shao H, Huang L, Qin C, et al. LMNA E82K mutation activates FAS and mitochondrial pathways of apoptosis in heart tissue specific transgenic mice. PLoS One. 2010;5(12).

162. Wolf CM, Wang L, Alcalai R, Pizard A, Burgon PG, Ahmad F, et al. Lamin A/C haploinsufficiency causes dilated cardiomyopathy and apoptosis-triggered cardiac conduction system disease. J Mol Cell Cardiol. 2008;44(2).

163. Herdegen T, Waetzig V. AP-1 proteins in the adult brain: Facts and fiction about effectors of neuroprotection and neurodegeneration. Vol. 20, Oncogene. 2001.

164. Forleo C, Carmosino M, Resta N, Rampazzo A, Valecce R, Sorrentino S, et al. Clinical and functional characterization of a novel mutation in lamin a/C gene in a multigenerational family with arrhythmogenic cardiac laminopathy. PLoS One. 2015;10(4).

165. Carmosino M, Gerbino A, Schena G, Procino G, Miglionico R, Forleo C, et al. The expression of Lamin A mutant R321X leads to endoplasmic reticulum stress with aberrant Ca2+ handling. J Cell Mol Med. 2016;20(11).

166. Gerbino A, Bottillo I, Milano S, Lipari M, De Zio R, Morlino S, et al. Functional Characterization of a Novel Truncating Mutation in Lamin A/C Gene in a Family with a Severe Cardiomyopathy with Conduction Defects. Cellular Physiology and Biochemistry. 2017;44(4).

167. Pietrafesa G, De Zio R, Scorza SI, Armentano MF, Pepe M, Forleo C, et al. Targeting unfolded protein response reverts ER stress and ER Ca2+ homeostasis in cardiomyocytes expressing the pathogenic variant of Lamin A/C R321X. J Transl Med [Internet]. 2023 Dec 1 [cited 2024 Feb 5];21(1):1–18. Available from: https://translational-medicine.biomedcentral.com/articles/10.1186/s12967-023-04170-y

168. Bonne G, Di Barletta MR, Varnous S, Bécane HM, Hammouda EH, Merlini L, et al. Mutations in the gene encoding lamin A/C cause autosomal dominant Emery-Dreifuss muscular dystrophy. Nat Genet. 1999;21(3).

169. Lattanzi G, Maggi L, Araujo-Vilar D. Laminopathies. Nucleus [Internet]. 2018 [cited 2024 Apr 15];9(1):543. Available from: /pmc/articles/PMC7000148/

170. Di Barletta MR, Ricci E, Galluzzi G, Tonali P, Mora M, Morandi L, et al. Different mutations in the LMNA gene cause autosomal dominant autosomal recessive Emery-Dreifuss muscular dystrophy. Am J Hum Genet. 2000;66(4).

171. Muchir A, Bonne G, Van Der Kool AJ, Van Meegen M, Baas F, Bolhuis PA, et al. Identification of mutations in the gene encoding lamins A/C in autosomal dominant limb girdle muscular dystrophy with atrioventricular conduction disturbances (LGMD1B). Hum Mol Genet. 2000;9(9).

172. Quijano-Roy S, Mbieleu B, Bönnemann CG, Jeannet PY, Colomer J, Clarke NF, et al. De novo LMNA mutations cause a new form of congenital muscular dystrophy. Ann Neurol. 2008;64(2).

173. Lu JT, Muchir A, Nagy PL, Worman HJ. LMNA cardiomyopathy: cell biology and genetics meet clinical medicine. Dis Model Mech [Internet]. 2011 Aug 2 [cited 2024 Mar 14];4(5):562–8. Available from: https://www.ncbi.nlm.nih.gov/pmc/articles/pmid/21810905/?tool=EBI

174. Cao H, Hegele RA. Nuclear lamin A/C R482Q mutation in Canadian kindreds with Dunnigan-type familial partial lipodystrophy. Hum Mol Genet. 2000;9(1).

175. Shackleton S, Lloyd DJ, Jackson SNJ, Evans R, Niermeijer MF, Singh BM, et al. LMNA, encoding lamin A/C, is mutated in partial lipodystrophy. Nat Genet. 2000;24(2).

176. Caux F, Dubosclard E, Lascols O, Buendia B, Chazouillères O, Cohen A, et al. A new clinical condition linked to a novel mutation in lamins A and C with generalized lipoatrophy, insulin-resistant diabetes, disseminated leukomelanodermic papules, liver steatosis, and cardiomyopathy. Journal of Clinical Endocrinology and Metabolism. 2003;88(3).

177. De Sandre-Giovannoli A, Chaouch M, Kozlov S, Vallat JM, Tazir M, Kassouri N, et al. Homozygous defects in LMNA, encoding lamin A/C nuclear-envelope proteins, cause autosomal recessive axonal neuropathy in human (Charcot-Marie-Tooth disorder type 2) and mouse. Am J Hum Genet. 2002;70(3).

178. De Sandre-Giovannoli A, Bernard R, Cau P, Navarro C, Amiel J, Boccaccio I, et al. Lamin A truncation in Hutchinson-Gilford progeria. Science (1979). 2003;300(5628).

179. Eriksson M, Brown WT, Gordon LB, Glynn MW, Singer J, Scott L, et al. Recurrent de novo point mutations in lamin A cause Hutchinson-Gilford progeria syndrome. Nature. 2003;423(6937).

180. Chen L, Lee L, Kudlow BA, Dos Santos HG, Sletvold O, Shafeghati Y, et al. LMNA mutations in atypical Werner's syndrome. Lancet [Internet]. 2003 Aug 9 [cited 2024 Mar 13];362(9382):440–5. Available from: http://www.thelancet.com/article/S014067360314069X/fulltext

181. Navarro CL, De Sandre-Giovannoli A, Bernard R, Boccaccio I, Boyer A, Geneviève D, et al. Lamin A and ZMPSTE24 (FACE-1) defects cause nuclear disorganization and identify restrictive dermopathy as a lethal neonatal laminopathy. Hum Mol Genet. 2004;13(20).

182. Van Esch H, Agarwal AK, Debeer P, Fryns JP, Garg A. Brief report: A homozygous mutation in the lamin A/C gene associated with a novel syndrome of arthropathy, tendinous calcinosis, and progeroid features. Journal of Clinical Endocrinology and Metabolism. 2006;91(2).

183. Novelli G, Muchir A, Sangiuolo F, Helbling-Leclerc A, D'apice MR, Massart C, et al. Mandibuloacral dysplasia is caused by a mutation in LMNA-encoding lamin A/C. Am J Hum Genet. 2002;71(2).

184. Chatzifrangkeskou M, Bonne G, Muchir A. Nuclear envelope and striated muscle diseases. Curr Opin Cell Biol. 2015 Feb 1;32:1–6.

185. Worman HJ. Cell signaling abnormalities in cardiomyopathy caused by lamin A/C gene mutations. Vol. 46, Biochemical Society Transactions. 2018.

186. Mozzetta C, Tedesco FS. Challenging the "chromatin hypothesis" of cardiac laminopathies with LMNA mutant iPS cells. Vol. 218, Journal of Cell Biology. 2019.

187. Kervella M, Jahier M, Meli AC, Muchir A. Genome organization in cardiomyocytes expressing mutated A-type lamins. Vol. 10, Frontiers in Cell and Developmental Biology. 2022.

188. van Steensel B, Belmont AS. Lamina-Associated Domains: Links with Chromosome Architecture, Heterochromatin, and Gene Repression. Vol. 169, Cell. 2017.

189. Briand N, Collas P. Laminopathy-causing lamin A mutations reconfigure lamina-associated domains and local spatial chromatin conformation. Vol. 9, Nucleus. 2018.

190. Perovanovic J, Dell'Orso S, Gnochi VF, Jaiswal JK, Sartorelli V, Vigouroux C, et al. Laminopathies disrupt epigenomic developmental programs and cell fate. Sci Transl Med. 2016;8(335).

191. Lee J, Termglinchan V, Diecke S, Itzhaki I, Lam CK, Garg P, et al. Activation of PDGF pathway links LMNA mutation to dilated cardiomyopathy. Nature. 2019;572(7769).

192. Elliott P, Andersson B, Arbustini E, Bilinska Z, Cecchi F, Charron P, et al. Classification of the cardiomyopathies: a position statement from the european society of cardiology working group on myocardial and pericardial diseases. Eur Heart J [Internet]. 2008 Jan 1 [cited 2024 Mar 16];29(2):270–6. Available from: https://dx.doi.org/10.1093/eurheartj/ehm342

193. Mestroni L, Taylor MRG. Lamin A/C Gene and the Heart. How Genetics May Impact Clinical Care. Vol. 52, Journal of the American College of Cardiology. 2008.

194. Hershberger RE, Cowan J, Morales A, Siegfried JD. Progress with genetic cardiomyopathies; Screening, counseling, and testing in dilated, hypertrophic, and arrhythmogenic right ventricular dysplasia/cardiomyopathy. Vol. 2, Circulation: Heart Failure. 2009.

195. Goidescu CM. Dilated cardiomyopathy produced by lamin A/C gene mutations. Clujul Med. 2013;86(4).

196. Van Berlo JH, De Voogt WG, Van Der Kooi AJ, Van Tintelen JP, Bonne G, Yaou R Ben, et al. Meta-analysis of clinical characteristics of 299 carriers of LMNA gene mutations: Do lamin A/C mutations portend a high risk of sudden death? Vol. 83, Journal of Molecular Medicine. 2005.

197. Taylor MRG, Fain PR, Sinagra G, Robinson ML, Robertson AD, Carniel E, et al. Natural history of dilated cardiomyopathy due to lamin A/C gene mutations. J Am Coll Cardiol. 2003;41(5).

198. Van Berlo JH. When lamin A/C fails, the heart suffers. Vol. 14, Netherlands Heart Journal. 2006.

199. Brodt C, Siegfried JD, Hofmeyer M, Martel J, Rampersaud E, Li D, et al. Temporal relationship of conduction system disease and ventricular dysfunction in LMNA cardiomyopathy. J Card Fail. 2013;19(4).

200. Pasotti M, Klersy C, Pilotto A, Marziliano N, Rapezzi C, Serio A, et al. Long-Term Outcome and Risk Stratification in Dilated Cardiolaminopathies. J Am Coll Cardiol. 2008;52(15).

201. Meune C, Van Berlo JH, Anselme F, Bonne G, Pinto YM, Duboc D. Primary Prevention of Sudden Death in Patients with Lamin A/C Gene Mutations. New England Journal of Medicine. 2006;354(2).

202. van Rijsingen IAW, Nannenberg EA, Arbustini E, Elliott PM, Mogensen J, Hermans-van Ast JF, et al. Gender-specific differences in major cardiac events and mortality in lamin A/C mutation carriers. Eur J Heart Fail. 2013;15(4).

203. Arimura T, Onoue K, Takahashi-Tanaka Y, Ishikawa T, Kuwahara M, Setou M, et al. Nuclear accumulation of androgen receptor in gender difference of dilated cardiomyopathy due to lamin A/C mutations. Cardiovasc Res. 2013;99(3).

204. Quarta G, Syrris P, Ashworth M, Jenkins S, Zuborne Alapi K, Morgan J, et al. Mutations in the Lamin A/C gene mimic arrhythmogenic right ventricular cardiomyopathy. Eur Heart J. 2012;33(9).

205. Hermida-Prieto M, Monserrat L, Castro-Beiras A, Laredo R, Soler R, Peteiro J, et al. Familial dilated cardiomyopathy and isolated left ventricular noncompaction associated with lamin A/C gene mutations. American Journal of Cardiology. 2004;94(1).

206. Van Rijsingen IAW, Bakker A, Azim D, Hermans-Van Ast JF, Van Der Kooi AJ, Van Tintelen JP, et al. Lamin A/C mutation is independently associated with an increased risk of arterial and venous thromboembolic complications. Int J Cardiol. 2013;168(1).

207. Arbustini E, Narula N, Dec GW, Reddy KS, Greenberg B, Kushwaha S, et al. The MOGE(S) classification for a phenotype-genotype nomenclature of cardiomyopathy: Endorsed by the world heart federation. Glob Heart. 2013;8(4).

208. Narula N, Favalli V, Tarantino P, Grasso M, Pilotto A, Bellazzi R, et al. Quantitative Expression of the Mutated Lamin A/C Gene in Patients With Cardiolaminopathy. J Am Coll Cardiol. 2012 Nov 6;60(19):1916–20.

209. Luk A, Ahn E, Soor GS, Butany J. Dilated cardiomyopathy: A review. Vol. 62, Journal of Clinical Pathology. 2009.

210. Mestroni L, Maisch B, McKenna WJ, Schwartz K, Charron P, Rocco C, et al. Guidelines for the study of familial dilated cardiomyopathies. Collaborative Research Group of the European Human and Capital Mobility Project on Familial Dilated Cardiomyopathy. Eur Heart J. 1999;20(2).

211. Hershberger RE, Siegfried JD. Update 2011: Clinical and genetic issues in familial dilated cardiomyopathy. Vol. 57, Journal of the American College of Cardiology. 2011.

212. Hershberger RE, Parks SB, Kushner JD, Li D, Ludwigsen S, Jakobs P, et al. Coding sequence mutations identified in MYH7, TNNT2, SCN5A, CSRP3, LBD3, and TCAP from 313 patients with familial or idiopathic dilated cardiomyopathy. Clin Transl Sci. 2008;1(1).

213. Ollila LH, Nikus K, Parikka H, Weckström S, Tiina H. Timing of pacemaker and ICD implantation in LMNA mutation carriers. Open Heart. 2021;8(1).

214. Maron BJ, Towbin JA, Thiene G, Antzelevitch C, Corrado D, Arnett D, et al. Contemporary definitions and classification of the cardiomyopathies: An American Heart Association Scientific Statement from the Council on Clinical Cardiology, Heart Failure and Transplantation Committee; Quality of Care and Outcomes Research and Functional Genomics and Translational Biology Interdisciplinary Working Groups; and Council on Epidemiology and Prevention. Circulation. 2006;113(14).

215. Van Rijsingen IAW, Arbustini E, Elliott PM, Mogensen J, Hermans-Van Ast JF, Van Der Kooi AJ, et al. Risk factors for malignant ventricular arrhythmias in Lamin A/C mutation carriers: A European cohort study. J Am Coll Cardiol. 2012;59(5).

216. Anselme F, Moubarak G, Savouré A, Godin B, Borz B, Drouin-Garraud V, et al. Implantable cardioverter-defibrillators in lamin A/C mutation carriers with cardiac conduction disorders. Heart Rhythm. 2013;10(10).

217. Al-Khatib SM, Stevenson WG, Ackerman MJ, Bryant WJ, Callans DJ, Curtis AB, et al. 2017 AHA/ACC/HRS Guideline for Management of Patients With Ventricular Arrhythmias and the Prevention of Sudden Cardiac Death: A Report of the American College of Cardiology/American Heart Association Task Force on Clinical Practice Guidelines and the Heart Rhythm Society. J Am Coll Cardiol. 2018;72(14).

218. Benedetti S, Menditto I, Degano M, Rodolico C, Merlini L, D'Amico A, et al. Phenotypic clustering of lamin A/C mutations in neuromuscular patients. Vol. 69, Neurology. 2007.

219. Van der Kooi AJ, Bonne G, Eymard B, Duboc D, Talim B, Van der Valk M, et al. Lamin A/C mutations with lipodystrophy, cardiac abnormalities, and muscular dystrophy. Neurology. 2002;59(4).

220. Goizet C, Yaou R Ben, Demay L, Richard P, Bouillot S, Rouanet M, et al. A new mutation of the lamin A/C gene leading to autosomal dominant axonal neuropathy, muscular dystrophy, cardiac disease, and leuconychia. Vol. 41, Journal of medical genetics. 2004.

221. Ramos FJ, Chen SC, Garelick MG, Dai DF, Liao CY, Schreiber KH, et al. Rapamycin reverses elevated mTORC1 signaling in lamin A/C-deficient mice, rescues cardiac and skeletal muscle function, and extends survival. Sci Transl Med. 2012;4(144).

222. Egesipe AL, Blondel S, Cicero A Lo, Jaskowiak AL, Navarro C, De Sandre-Giovannoli A, et al. Metformin decreases progerin expression and alleviates pathological defects of hutchinson–gilford progeria syndrome cells. NPJ Aging Mech Dis. 2016;2(1).

223. Balmus G, Larrieu D, Barros AC, Collins C, Abrudan M, Demir M, et al. Targeting of NAT10 enhances healthspan in a mouse model of human accelerated aging syndrome. Nat Commun. 2018;9(1).

224. Lee YK, Lau YM, Cai ZJ, Lai WH, Wong LY, Tse HF, et al. Modeling treatment response for Lamin A/C related dilated cardiomyopathy in human induced pluripotent stem cells. J Am Heart Assoc. 2017;6(8).

225. Sayed N, Liu C, Ameen M, Himmati F, Zhang JZ, Khanamiri S, et al. Clinical trial in a dish using iPSCs shows lovastatin improves endothelial dysfunction and cellular cross-talk in LMNA cardiomyopathy. Sci Transl Med. 2020;12(554).

226. Lee SJ, Jung YS, Yoon MH, Kang SM, Oh AY, Lee JH, et al. Interruption of progerin-lamin A/C binding ameliorates Hutchinson-Gilford progeria syndrome phenotype. Journal of Clinical Investigation. 2016;126(10).

227. Osorio FG, Navarro CL, Cadiñanos J, López-Mejía IC, Quirós PM, Bartoli C, et al. Hutchinson-Gilford progeria: Splicing-directed therapy in a new mouse model of human accelerated aging. Sci Transl Med. 2011;3(106).

228. Harhouri K, Navarro C, Baquerre C, Da Silva N, Bartoli C, Casey F, et al. Antisense-based progerin downregulation in HGPS-like patients' cells. Vol. 5, Cells. 2016.

229. Jung HJ, Coffinier C, Choe Y, Beigneux AP, Davies BSJ, Yang SH, et al. Regulation of prelamin A but not lamin C by miR-9, a brain-specific microRNA. Proc Natl Acad Sci U S A. 2012;109(7).

230. Beyret E, Liao HK, Yamamoto M, Hernandez-Benitez R, Fu Y, Erikson G, et al. Single-dose CRISPR–Cas9 therapy extends lifespan of mice with Hutchinson–Gilford progeria syndrome. Nat Med. 2019;25(3).

231. Santiago-Fernández O, Osorio FG, Quesada V, Rodríguez F, Basso S, Maeso D, et al. Development of a CRISPR/Cas9-based therapy for Hutchinson–Gilford progeria syndrome. Nat Med. 2019;25(3).

232. Sánchez-López A, Espinós-Estévez C, González-Gómez C, Gonzalo P, Andrés-Manzano MJ, Fanjul V, et al. Cardiovascular Progerin Suppression and Lamin A Restoration Rescue Hutchinson-Gilford Progeria Syndrome. Circulation. 2021;144(22).

233. Gete YG, Koblan LW, Mao X, Trappio M, Mahadik B, Fisher JP, et al. Mechanisms of angiogenic incompetence in Hutchinson–Gilford progeria via downregulation of endothelial NOS. Aging Cell. 2021;20(7).

234. Koblan LW, Erdos MR, Wilson C, Cabral WA, Levy JM, Xiong ZM, et al. In vivo base editing rescues Hutchinson–Gilford progeria syndrome in mice. Nature. 2021;589(7843).

235. Hasselberg NE, Haland TF, Saberniak J, Brekke PH, Berge KE, Leren TP, et al. Lamin A/C cardiomyopathy: Young onset, high penetrance, and frequent need for heart transplantation. Eur Heart J. 2018;39(10).

236. Gerbino A, Forleo C, Milano S, Piccapane F, Procino G, Pepe M, et al. Pro-inflammatory cytokines as emerging molecular determinants in cardiolaminopathies. J Cell Mol Med. 2021;25(23).

237. Borin D, Peña B, Chen SN, Long CS, Taylor MRG, Mestroni L, et al. Altered microtubule structure, hemichannel localization and beating activity in cardiomyocytes expressing pathologic nuclear lamin A/C. Heliyon. 2020;6(1).

238. Olaopa MA, Spoonamore KG, Bhakta D, Chen Z, Celestino-Soper PBS, Chen PS, et al. Lamin-A/C Variants Found in Patients with Cardiac Conduction Disease Reduce Sodium Currents. Cardiogenetics. 2018;8(1).

239. Liu Z, Shan H, Huang J, Li N, Hou C, Pu J. A novel lamin A/C gene missense mutation (445 v > E) in immunoglobulin-like fold associated with left ventricular non-compaction. Europace. 2016;18(4).

240. Han M, Zhao M, Cheng C, Huang Y, Han S, Li W, et al. Lamin A mutation impairs interaction with nucleoporin NUP155 and disrupts nucleocytoplasmic transport in atrial fibrillation. Hum Mutat. 2019;40(3).

241. Salvarani N, Crasto S, Miragoli M, Bertero A, Paulis M, Kunderfranco P, et al. The K219T-Lamin mutation induces conduction defects through epigenetic inhibition of SCN5A in human cardiac laminopathy. Nat Commun. 2019;10(1).

242. Markandeya YS, Tsubouchi T, Hacker TA, Wolff MR, Belardinelli L, Balijepalli RC. Inhibition of late sodium current attenuates ionic arrhythmia mechanism in ventricular myocytes expressing LaminA-N195K mutation. Heart Rhythm. 2016;13(11).

243. Stallmeyer B, Koopmann M, Schulze-Bahr E. Identification of novel mutations in LMNA associated with familial forms of dilated cardiomyopathy. Genet Test Mol Biomarkers. 2012;16(6).

244. Nishiuchi S, Makiyama T, Aiba T, Nakajima K, Hirose S, Kohjitani H, et al. Gene-Based Risk Stratification for Cardiac Disorders in LMNA Mutation Carriers. Circ Cardiovasc Genet. 2017;10(6).

245. Claycomb WC, Lanson NA, Stallworth BS, Egeland DB, Delcarpio JB, Bahinski A, et al. HL-1 cells: A cardiac muscle cell line that contracts and retains phenotypic characteristics of the adult cardiomyocyte. Proc Natl Acad Sci U S A. 1998;95(6).

246. Yang Z, Murray KT. Ionic Mechanisms of Pacemaker Activity in Spontaneously-contracting Atrial HL-1 Cells.

247. Strege P, Beyder A, Bernard C, Crespo-Diaz R, Behfar A, Terzic A, et al. Ranolazine inhibits shear sensitivity of endogenous Na+ current and spontaneous action potentials in HL-1 cells. Channels. 2012;6(6).

248. De Zio R, Gerbino A, Forleo C, Pepe M, Milano S, Favale S, et al. Functional study of a KCNH2 mutant: Novel insights on the pathogenesis of the LQT2 syndrome. J Cell Mol Med. 2019;23(9).

249. Gerbino A, Schena G, Milano S, Milella L, Franco Barbosa A, Armentano F, et al. Spilanthol from Acmella oleracea lowers the intracellular levels of cAMP impairing NKCC2 phosphorylation and water channel AQP2 membrane expression in mouse kidney. PLoS One. 2016;11(5).

250. Carmosino M, Giménez I, Caplan M, Forbush B. Exon loss accounts for differential sorting of Na-K-Cl cotransporters in polarized epithelial cells. Mol Biol Cell. 2008;19(10).

251. Janke C, Bulinski JC. Post-translational regulation of the microtubule cytoskeleton: Mechanisms and functions. Vol. 12, Nature Reviews Molecular Cell Biology. 2011.

252. Casini S, Tan HL, Demirayak I, Remme CA, Amin AS, Scicluna BP, et al. Tubulin polymerization modifies cardiac sodium channel expression and gating. Cardiovasc Res. 2010;85(4).

253. Stimers JR, Song L, Rusch NJ, Rhee SW. Overexpression of the large-conductance, Ca2+-activated K+(BK) channel shortens action potential duration in HL-1 cardiomyocytes. PLoS One. 2015;10(6).

254. Deftereos S, Giannopoulos G, Papoutsidakis N, Panagopoulou V, Kossyvakis C, Raisakis K, et al. Colchicine and the heart: Pushing the envelope. Vol. 62, Journal of the American College of Cardiology. 2013.

255. Middlekauff HR, Stevenson WG, Stevenson LW. Prognostic significance of atrial fibrillation in advanced heart failure: A study of 390 patients. Circulation. 1991;84(1).

256. Mamas MA, Caldwell JC, Chacko S, Garratt CJ, Fath-Ordoubadi F, Neyses L. A meta-analysis of the prognostic significance of atrial fibrillation in chronic heart failure. Eur J Heart Fail. 2009;11(7).

257. Olson TM, Michels V V., Ballew JD, Reyna SP, Karst ML, Herron KJ, et al. Sodium channel mutations and susceptibility to heart failure and atrial fibrillation. JAMA. 2005;293(4).

258. Darbar D, Kannankeril PJ, Donahue BS, Kucera G, Stubblefield T, Haines JL, et al. Cardiac sodium channel (SCN5A) variants associated with atrial fibrillation. Circulation. 2008;117(15).

259. McNair WP, Ku L, Taylor MRG, Fain PR, Dao D, Wolfel E, et al. SCN5A mutation associated with dilated cardiomyopathy, conduction disorder, and arrhythmia. Circulation. 2004;110(15).

260. Steele DF, Fedida D. Cytoskeletal roles in cardiac ion channel expression. Vol. 1838, Biochimica et Biophysica Acta - Biomembranes. 2014.

261. Chinnakkannu P, Samanna V, Cheng G, Ablonczy Z, Baicu CF, Bethard JR, et al. Site-specific microtubule-associated protein 4 dephosphorylation causes microtubule network densification in pressure overload cardiac hypertrophy. Journal of Biological Chemistry. 2010;285(28).

262. Portran D, Schaedel L, Xu Z, Théry M, Nachury M V. Tubulin acetylation protects long-lived microtubules against mechanical ageing. Nat Cell Biol. 2017;19(4).

263. Giustiniani J, Daire V, Cantaloube I, Durand G, Poüs C, Perdiz D, et al. Tubulin acetylation favors Hsp90 recruitment to microtubules and stimulates the signaling function of the Hsp90 clients Akt/PKB and p53. Cell Signal. 2009;21(4).

264. Seidman R, Gitelman I, Sagi O, Horwitz SB, Wolfson M. The role of ERK 1/2 and p38 MAP-kinase pathways in Taxol-induced apoptosis in human ovarian carcinoma cells. Exp Cell Res. 2001;268(1).

265. Klein LE, Freeze BS, Smith AB, Horwitz SB. The microtubule stabilizing agent discodermolide is a potent inducer of accelerated cell senescence. Cell Cycle. 2005;4(3).

266. Prins KW, Tian L, Wu D, Thenappan T, Metzger JM, Archer SL. Colchicine depolymerizes microtubules, increases junctophilin-2, and improves right ventricular function in experimental pulmonary arterial hypertension. J Am Heart Assoc. 2017;6(6).

267. Scarborough EA, Uchida K, Vogel M, Erlitzki N, Iyer M, Phyo SA, et al. Microtubules orchestrate local translation to enable cardiac growth. Nat Commun. 2021;12(1).

268. Fiolet ATL, Opstal TSJ, Mosterd A, Eikelboom JW, Jolly SS, Keech AC, et al. Efficacy and safety of low-dose colchicine in patients with coronary disease: a systematic review and meta-analysis of randomized trials. Vol. 42, European Heart Journal. 2021.

269. Peretto G, Sala S, Benedetti S, Di Resta C, Gigli L, Ferrari M, et al. Updated clinical overview on cardiac laminopathies: An electrical and mechanical disease. Vol. 9, Nucleus. 2018.

270. Muchir A, Kim YJ, Reilly SA, Wu W, Choi JC, Worman HJ. Inhibition of extracellular signal-regulated kinase 1/2 signaling has beneficial effects on skeletal muscle in a mouse model of Emery-Dreifuss muscular dystrophy caused by lamin A/C gene mutation. Skelet Muscle. 2013;3(1).

271. Muchir A, Shan J, Bonne G, Lehnart SE, Worman HJ. Inhibition of extracellular signal-regulated kinase signaling to prevent cardiomyopathy caused by mutation in the gene encoding A-type lamins. Hum Mol Genet. 2009;18(2).

272. De Zio R, Pietrafesa G, Milano S, Procino G, Bramerio M, Pepe M, et al. Role of Nuclear Lamin A/C in the Regulation of Nav1.5 Channel and Microtubules: Lesson From the Pathogenic Lamin A/C Variant Q517X. Front Cell Dev Biol. 2022;10.

273. Hetz C. The unfolded protein response: Controlling cell fate decisions under ER stress and beyond. Vol. 13, Nature Reviews Molecular Cell Biology. 2012.

274. Shoulders MD, Ryno LM, Genereux JC, Moresco JJ, Tu PG, Wu C, et al. Stress-Independent Activation of XBP1s and/or ATF6 Reveals Three Functionally Diverse ER Proteostasis Environments. Cell Rep. 2013;3(4).

275. Novoa I, Zeng H, Harding HP, Ron D, Neibert DW, Hollander MC, et al. Feedback Inhibition of the Unfolded Protein Response by GADD34-mediated Dephosphorylation of eIF2. J Cell Biol [Internet]. 2001 [cited 2024 Mar 12];153(5):4196–203. Available from: http://www.jcb.org/cgi/content/full/153/5/1011

276. Yung HW, Charnock-Jones DS, Burton GJ. Regulation of AKT phosphorylation at Ser473 and Thr308 by endoplasmic reticulum stress modulates substrate specificity in a severity dependent manner. PLoS One. 2011;6(3).

277. Qin L, Wang Z, Tao L, Wang Y. ER stress negatively regulates AKT/TSC/mTOR pathway to enhance autophagy. Autophagy. 2010;6(2).

278. Axten JM, Medina JR, Feng Y, Shu A, Romeril SP, Grant SW, et al. Discovery of 7-methyl-5-(1-{[3-(trifluoromethyl)phenyl]acetyl}-2,3-dihydro- 1H-indol-5-yl)-7H-pyrrolo[2,3-d]pyrimidin-4-amine (GSK2606414), a potent and selective first-in-class inhibitor of protein kinase R (PKR)-like endoplasmic reticulum kinase (PERK). J Med Chem. 2012;55(16).

279. Rojas-Rivera D, Delvaeye T, Roelandt R, Nerinckx W, Augustyns K, Vandenabeele P, et al. When PERK inhibitors turn out to be new potent RIPK1 inhibitors: Critical issues on the specificity and use of GSK2606414 and GSK2656157. Cell Death Differ. 2017;24(6).

280. Motawi TK, Al-Kady RH, Abdelraouf SM, Senousy MA. Empagliflozin alleviates endoplasmic reticulum stress and augments autophagy in rotenone-induced Parkinson's disease in rats: Targeting the GRP78/PERK/eIF2α/CHOP pathway and miR-211-5p. Chem Biol Interact. 2022 Aug 1;362:110002.

281. Madonna R, Doria V, Minnucci I, Pucci A, Pierdomenico DS, De Caterina R. Empagliflozin reduces the senescence of cardiac stromal cells and improves cardiac function in a murine model of diabetes. J Cell Mol Med. 2020;24(21).

282. Hamilton S, Terentyev D. Altered Intracellular Calcium Homeostasis and Arrhythmogenesis in the Aged Heart. Vol. 20, International journal of molecular sciences. 2019.

283. Klee CB, Ren H, Wang X. Regulation of the calmodulin-stimulated protein phosphatase, calcineurin. Vol. 273, Journal of Biological Chemistry. 1998.

284. Bollo M, Paredes RM, Holstein D, Zheleznova N, Camacho P, Lechleiter JD. Calcineurin interacts with PERK and dephosphorylates calnexin to relieve ER stress in mammals and frogs. PLoS One. 2010;5(8).

285. Liu Z, Cai H, Zhu H, Toque H, Zhao N, Qiu C, et al. Protein kinase RNA-like endoplasmic reticulum kinase (PERK)/calcineurin signaling is a novel pathway regulating intracellular calcium accumulation which might be involved in ventricular arrhythmias in diabetic cardiomyopathy. Cell Signal. 2014;26(12).

286. Heineke J, Ritter O. Cardiomyocyte calcineurin signaling in subcellular domains: From the sarcolemma to the nucleus and beyond. Vol. 52, Journal of Molecular and Cellular Cardiology. 2012.

287. Zhu J, Zhang X, Xie H, Wang Y, Zhang X, Lin Z. Cardiomyocyte stim1 deficiency exacerbates doxorubicin cardiotoxicity by magnification of endoplasmic reticulum stress. J Inflamm Res. 2021;14.

288. Kono T, Tong X, Taleb S, Bone RN, Iida H, Lee CC, et al. Impaired Store-Operated Calcium Entry and STIM1 Loss Lead to Reduced Insulin Secretion and Increased Endoplasmic Reticulum Stress in the Diabetic b-Cell. 2018 [cited 2024 Mar 12]; Available from: http://diabetes.diabetesjournals.org/lookup/suppl/doi:10.2337/db17-1351/-/DC1.

289. Choy MS, Yusoff P, Lee IC, Newton JC, Goh CW, Page R, et al. Structural and Functional Analysis of the GADD34:PP1 eIF2α Phosphatase. CellReports [Internet]. 2015 [cited 2024 Mar 12];11:1885–91. Available from: http://dx.doi.org/10.1016/j.celrep.2015.05.043http://dx.doi.org/10.1016/j.celrep.2015.05.043

290. Wang W, Cheng J, Sun A, Lv S, Liu H, Liu X, et al. TRB3 mediates renal tubular cell apoptosis associated with proteinuria. Clin Exp Med. 2015 May 1;15(2):167–77.

291. Du K, Herzig S, Kulkarni RN, Montminy M. TRB3: A tribbles homolog that inhibits Akt/PKB activation by insulin in liver. Science (1979). 2003;300(5625).

292. Boyce M, Bryant KF, Jousse C, Long K, Harding HP, Scheuner D, et al. A selective inhibitor of eIF2α dephosphorylation protects cells from ER stress. Science (1979) [Internet]. 2005 Feb 11 [cited 2024 Mar 12];307(5711):935–9. Available from: https://www.science.org/doi/10.1126/science.1101902

293. Huang X, Chen Y, Zhang H, Ma Q, Zhang Y wu, Xu H. Salubrinal attenuates β-amyloid-induced neuronal death and microglial activation by inhibition of the NF-κB pathway. Neurobiol Aging. 2012 May 1;33(5):1007.e9-1007.e17.

294. Saxena S, Cabuy E, Caroni P. A role for motoneuron subtype-selective ER stress in disease manifestations of FALS mice. Nat Neurosci. 2009;12(5).

295. Rubovitch V, Barak S, Rachmany L, Goldstein RB, Zilberstein Y, Pick CG. The Neuroprotective Effect of Salubrinal in a Mouse Model of Traumatic Brain Injury. Neuromolecular Med. 2015 Mar 1;17(1):58–70.

296. Li RJ, He KL, Li X, Wang LL, Liu CL, He YY. Salubrinal protects cardiomyocytes against apoptosis in a rat myocardial infarction model via suppressing the dephosphorylation of eukaryotic translation initiation factor 2α. Mol Med Rep. 2015 Jul 1;12(1):1043–9.

297. Holmes B, Brogden RN, Heel RC, Speight TM, Avery GS. Guanabenz: A Review of its Pharmacodynamic Properties and Therapeutic Efficacy in Hypertension. Drugs [Internet]. 1983 Oct 15 [cited 2024 Mar 12];26(3):212–29. Available from: https://link.springer.com/article/10.2165/00003495-198326030-00003

298. Tsaytler P, Harding HP, Ron D, Bertolotti A. Selective inhibition of a regulatory subunit of protein phosphatase 1 restores proteostasis. Science (1979) [Internet]. 2011 Apr 1 [cited 2024 Mar 12];332(6025):91–4. Available from: https://www.science.org/doi/10.1126/science.1201396

299. Philipp M, Brede M, Hein L. Physiological significance of α2-adrenergic receptor subtype diversity: One receptor is not enough. Am J Physiol Regul Integr Comp Physiol [Internet]. 2002 [cited 2024 Mar 12];283(2 52-2):287–95. Available from: https://journals.physiology.org/doi/10.1152/ajpregu.00123.2002

300. White SM, Constantin PE, Claycomb WC. Cardiac physiology at the cellular level: Use of cultured HL-1 cardiomyocytes for studies of cardiac muscle cell structure and function. Am J Physiol Heart Circ Physiol [Internet]. 2004 [cited 2024 Mar 12];286(3 55-3). Available from: https://journals.physiology.org/doi/10.1152/ajpheart.00986.2003

301. Wang L, Popko B, Tixier E, Roos RP. Guanabenz, which enhances the unfolded protein response, ameliorates mutant SOD1-induced amyotrophic lateral sclerosis. Neurobiol Dis. 2014 Nov 1;71:317–24.

302. Jiang HQ, Ren M, Jiang HZ, Wang J, Zhang J, Yin X, et al. Guanabenz delays the onset of disease symptoms, extends lifespan, improves motor performance and attenuates motor neuron loss in the SOD1 G93A mouse model of amyotrophic lateral sclerosis. Neuroscience. 2014 Sep 26;277:132–8.

303. Das I, Krzyzosiak A, Schneider K, Wrabetz L, D'Antonio M, Barry N, et al. Preventing proteostasis diseases by selective inhibition of a phosphatase regulatory subunit. Science (1979) [Internet]. 2015 Apr 10 [cited 2024 Mar 12];348(6231):239–42. Available from: https://www.science.org/doi/10.1126/science.aaa4484

304. Bella ED, Tramacere I, Antonini G, Borghero G, Capasso M, Caponnetto C, et al. Protein misfolding, amyotrophic lateral sclerosis and guanabenz: protocol for a phase II RCT with futility design (ProMISe trial). BMJ Open [Internet]. 2017 Aug 1 [cited 2024 Mar 12];7(8):e015434. Available from: https://bmjopen.bmj.com/content/7/8/e015434

305. Neuber C, Uebeler J, Schulze T, Sotoud H, El-Armouche A, Eschenhagen T. Guanabenz interferes with ER stress and exerts protective effects in cardiac myocytes. PLoS One. 2014 Jun 3;9(6).

306. Steiner S. Empagliflozin, cardiovascular outcomes, and mortality in type 2 diabetes. Zeitschrift fur Gefassmedizin [Internet]. 2016 Nov 26 [cited 2024 Mar 12];13(1):17–8. Available from: https://www.nejm.org/doi/full/10.1056/NEJMoa1504720

307. Packer M, Anker SD, Butler J, Filippatos G, Pocock SJ, Carson P, et al. Cardiovascular and Renal Outcomes with Empagliflozin in Heart Failure. New England Journal of Medicine [Internet]. 2020 Oct 8 [cited 2024 Mar 12];383(15):1413–24. Available from: https://www.nejm.org/doi/full/10.1056/NEJMoa2022190

308. Wiviott SD, Raz I, Bonaca MP, Mosenzon O, Kato ET, Cahn A, et al. Dapagliflozin and Cardiovascular Outcomes in Type 2 Diabetes. New England Journal of Medicine [Internet]. 2019 Jan 24 [cited 2024 Mar 12];380(4):347–57. Available from: https://www.nejm.org/doi/full/10.1056/NEJMoa1812389

309. McMurray JJV, Solomon SD, Inzucchi SE, Køber L, Kosiborod MN, Martinez FA, et al. Dapagliflozin in Patients with Heart Failure and Reduced Ejection Fraction. https://doi.org/101056/NEJMoa1911303 [Internet]. 2019 Sep 19 [cited 2024 Mar 12];381(21):1995–2008. Available from: https://www.nejm.org/doi/full/10.1056/NEJMoa1911303

310. Dyck JRB, Sossalla S, Hamdani N, Coronel R, Weber NC, Light PE, et al. Cardiac mechanisms of the beneficial effects of SGLT2 inhibitors in heart failure: Evidence for potential off-target effects. J Mol Cell Cardiol. 2022 Jun 1;167:17–31.

311. Butler J, Filippatos G, Jamal Siddiqi T, Brueckmann M, Böhm M, Chopra VK, et al. Empagliflozin, Health Status, and Quality of Life in Patients With Heart Failure and Preserved Ejection Fraction: The EMPEROR-Preserved Trial. Circulation [Internet]. 2022 Jan 18 [cited 2024 Mar 12];145(3):184–93. Available from: https://www.ahajournals.org/doi/abs/10.1161/CIRCULATIONAHA.121.057812

312. Maddox TM, Januzzi JL, Allen LA, Breathett K, Butler J, Davis LL, et al. 2021 Update to the 2017 ACC Expert Consensus Decision Pathway for Optimization of Heart Failure Treatment: Answers to 10 Pivotal Issues About Heart Failure With Reduced Ejection Fraction: A Report of the American College of Cardiology Solution Set Oversight Committee. J Am Coll Cardiol [Internet]. 2021 Feb 16 [cited 2024 Mar 12];77(6):772–810. Available from: https://www.jacc.org/doi/10.1016/j.jacc.2020.11.022

313. Seferović PM, Fragasso G, Petrie M, Mullens W, Ferrari R, Thum T, et al. Sodium–glucose co-transporter 2 inhibitors in heart failure: beyond glycaemic control. A position paper of the Heart Failure Association of the European Society of Cardiology. Eur J Heart Fail. 2020 Sep 1;22(9):1495–503.

314. Wang CC, Li Y, Qian XQ, Zhao H, Wang D, Zuo GX, et al. Empagliflozin alleviates myocardial I/R injury and cardiomyocyte apoptosis via inhibiting ER stress-induced autophagy and the PERK/ATF4/Beclin1 pathway. J Drug Target [Internet]. 2022 [cited 2024 Mar 12];30(8):858–72. Available from: https://www.tandfonline.com/doi/abs/10.1080/1061186X.2022.2064479

315. Chang WT, Lin YW, Ho CH, Chen ZC, Liu PY, Shih JY. Dapagliflozin suppresses ER stress and protects doxorubicin-induced cardiotoxicity in breast cancer patients. Arch

Toxicol [Internet]. 2021 Feb 1 [cited 2024 Mar 12];95(2):659–71. Available from: https://link.springer.com/article/10.1007/s00204-020-02951-8

316. Zelniker TA, Bonaca MP, Furtado RHM, Mosenzon O, Kuder JF, Murphy SA, et al. Effect of Dapagliflozin on Atrial Fibrillation in Patients with Type 2 Diabetes Mellitus: Insights from the DECLARE-TIMI 58 Trial. Circulation. 2020;141(15).

317. Li HL, Lip GYH, Feng Q, Fei Y, Tse YK, Wu M zhen, et al. Sodium-glucose cotransporter 2 inhibitors (SGLT2i) and cardiac arrhythmias: a systematic review and meta-analysis. Cardiovasc Diabetol [Internet]. 2021 Dec 1 [cited 2024 Mar 12];20(1):1–13. Available from: https://link.springer.com/articles/10.1186/s12933-021-01293-8

318. Avila-Medina J, Mayoral-Gonzalez I, Dominguez-Rodriguez A, Gallardo-Castillo I, Ribas J, Ordoñez A, et al. The complex role of store operated calcium entry pathways and related proteins in the function of cardiac, skeletal and vascular smooth muscle cells. Front Physiol [Internet]. 2018 Mar 21 [cited 2024 Mar 12];9(MAR):347990. Available from: www.frontiersin.org

319. Bahar E, Kim H, Yoon H. ER Stress-Mediated Signaling: Action Potential and Ca2+ as Key Players. International Journal of Molecular Sciences 2016, Vol 17, Page 1558 [Internet]. 2016 Sep 15 [cited 2024 Mar 12];17(9):1558. Available from: https://www.mdpi.com/1422-0067/17/9/1558/htm

320. van Heerden D, Klima S, van den Bout I. How nuclear envelope dynamics can direct laminopathy phenotypes. Curr Opin Cell Biol. 2024 Feb 1;86:102290.

321. van Tienen FHJ, Lindsey PJ, Kamps MAF, Krapels IP, Ramaekers FCS, Brunner HG, et al. Assessment of fibroblast nuclear morphology aids interpretation of LMNA variants. European Journal of Human Genetics. 2019;27(3).

322. Pho M, Berrada Y, Gunda A, Stephens AD. Nuclear shape is affected differentially by loss of lamin A, lamin C, or both lamin A and C. MicroPubl Biol [Internet]. 2024 [cited 2024 Apr 6];2024. Available from: /pmc/articles/PMC10910297/

323. Nmezi B, Xu J, Fu R, Armiger TJ, Rodriguez-Bey G, Powell JS, et al. Concentric organization of A- and B-type lamins predicts their distinct roles in the spatial organization and stability of the nuclear lamina. Proc Natl Acad Sci U S A. 2019;116(10).

324. Chen NY, Kim P, Weston TA, Edillo L, Tu Y, Fong LG, et al. Fibroblasts lacking nuclear lamins do not have nuclear blebs or protrusions but nevertheless have frequent nuclear membrane ruptures. Proc Natl Acad Sci U S A [Internet]. 2018 Oct 2 [cited 2024 Apr 6];115(40):10100–5. Available from: https://www.pnas.org/doi/abs/10.1073/pnas.1812622115

325. Muchir A, Medioni J, Laluc M, Massart C, Arimura T, Van Der Kooi AJ, et al. Nuclear envelope alterations in fibroblasts from patients with muscular dystrophy, cardiomyopathy, and partial lipodystrophy carrying lamin A/C gene mutations. Muscle Nerve. 2004;30(4).

326. Vigouroux C, Auclair M, Dubosclard E, Pouchelet M, Capeau J, Courvalin JC, et al. Nuclear envelope disorganization in fibroblasts from lipodystrophic patients with heterozygous R482Q/W mutations in the lamin A/C gene. J Cell Sci. 2001;114(24).

327. Muchir A, Van Engelen BG, Lammens M, Mislow JM, McNally E, Schwartz K, et al. Nuclear envelope alterations in fibroblasts from LGMD1B patients carrying nonsense Y259X heterozygous or homozygous mutation in lamin A/C gene. Exp Cell Res. 2003;291(2).

328. Decaudain A, Vantyghem MC, Guerci B, Hécart AC, Auclair M, Reznik Y, et al. New Metabolic Phenotypes in Laminopathies: LMNA Mutations in Patients with Severe Metabolic Syndrome. J Clin Endocrinol Metab [Internet]. 2007 Dec 1 [cited 2024 Apr 6];92(12):4835–44. Available from: https://dx.doi.org/10.1210/jc.2007-0654

329. van Tienen FHJ, Lindsey PJ, Kamps MAF, Krapels IP, Ramaekers FCS, Brunner HG, et al. Assessment of fibroblast nuclear morphology aids interpretation of LMNA variants. European Journal of Human Genetics 2018 27:3 [Internet]. 2018 Nov 12 [cited 2024 Apr 6];27(3):389–99. Available from: https://www.nature.com/articles/s41431-018-0294-0

330. Gómez-Domínguez D, Epifano C, de Miguel F, Castaño AG, Vilaplana-Martí B, Martín A, et al. Consequences of lmna exon 4 mutations in myoblast function. Cells. 2020;9(5).

331. Chatzifrangkeskou M, Dour C Le, Muchir A. Modulation of cytoskeleton in cardiomyopathy caused by mutations in LMNA gene. Vol. 324, American Journal of Physiology - Cell Physiology. 2023.

332. Meinke P, Mattioli E, Haque F, Antoku S, Columbaro M, Straatman KR, et al. Muscular Dystrophy-Associated SUN1 and SUN2 Variants Disrupt Nuclear-Cytoskeletal Connections and Myonuclear Organization. PLoS Genet. 2014;10(9).

333. Le Dour C, Chatzifrangkeskou M, Macquart C, Magiera MM, Peccate C, Jouve C, et al. Actin-microtubule cytoskeletal interplay mediated by MRTF-A/SRF signaling promotes dilated cardiomyopathy caused by LMNA mutations. Nat Commun. 2022;13(1).

334. Srivastava N, Nader GP de F, Williart A, Rollin R, Cuvelier D, Lomakin A, et al. Nuclear fragility, blaming the blebs. Vol. 70, Current Opinion in Cell Biology. 2021.

335. Pierre P, Pepperkok R, Kreis TE. Molecular characterization of two functional domains of CLIP-170 in vivo. J Cell Sci. 1994;107(7).

336. Folker ES, Baker BM, Goodson H V. Interactions between CLIP-170, tubulin, and microtubules: Implications for the mechanism of CLIP-170 plus-end tracking behavior. Mol Biol Cell. 2005;16(11).

337. Akhmanova A, Mausset-Bonnefont AL, Van Cappellen W, Keijzer N, Hoogenraad CC, Stepanova T, et al. The microtubule plus-end-tracking protein CLIP-170 associates with the spermatid manchette and is essential for spermatogenesis. Genes Dev. 2005;19(20).

338. Yashirogi S, Nagao T, Nishida Y, Takahashi Y, Qaqorh T, Yazawa I, et al. AMPK regulates cell shape of cardiomyocytes by modulating turnover of microtubules through CLIP-170. EMBO Rep. 2021;22(1).

339. Galjart N. CLIPs and CLASPs and cellular dynamics. Vol. 6, Nature Reviews Molecular Cell Biology. 2005.

340. Lansbergen G, Komarova Y, Modesti M, Wyman C, Hoogenraad CC, Goodson H V., et al. Conformational changes in CLIP-170 regulate its binding to microtubules and dynactin localization. Journal of Cell Biology. 2004;166(7).

341. Barbiero I, Peroni D, Siniscalchi P, Rusconi L, Tramarin M, De Rosa R, et al. Pregnenolone and pregnenolone-methyl-ether rescue neuronal defects caused by dysfunctional CLIP170 in a neuronal model of CDKL5 Deficiency Disorder. Neuropharmacology. 2020;164.

342. Barbiero I, Zamberletti E, Tramarin M, Gabaglio M, Peroni D, De Rosa R, et al. Pregnenolone-methyl-ether enhances CLIP170 and microtubule functions improving spine maturation and hippocampal deficits related to CDKL5 deficiency. Hum Mol Genet. 2022;31(16).

343. Weng JH, Liang MR, Chen CH, Tong SK, Huang TC, Lee SP, et al. Pregnenolone activates CLIP-170 to promote microtubule growth and cell migration. Nat Chem Biol. 2013;9(10).

344. Murugan S, Jakka P, Namani S, Mujumdar V, Radhakrishnan G. The neurosteroid pregnenolone promotes degradation of key proteins in the innate immune signaling to suppress inflammation. Journal of Biological Chemistry. 2019;294(12).

345. Barbiero I, Peroni D, Tramarin M, Chandola C, Rusconi L, Landsberger N, et al. The neurosteroid pregnenolone reverts microtubule derangement induced by the loss of a functional CDKL5-IQGAP1 complex. Hum Mol Genet. 2017;26(18).

346. Vignier N, Mougenot N, Bonne G, Muchir A. Effect of genetic background on the cardiac phenotype in a mouse model of Emery-Dreifuss muscular dystrophy. Biochem Biophys Rep. 2019;19.

347. Ackers-Johnson M, Li PY, Holmes AP, O'Brien SM, Pavlovic D, Foo RS. A Simplified, Langendorff-Free Method for Concomitant Isolation of Viable Cardiac Myocytes and Nonmyocytes from the Adult Mouse Heart. Circ Res. 2016;119(8).

348. Earle AJ, Kirby TJ, Fedorchak GR, Isermann P, Patel J, Iruvanti S, et al. Mutant lamins cause nuclear envelope rupture and DNA damage in skeletal muscle cells. Nat Mater. 2020;19(4).

349. Lammerding J, Hsiao J, Schulze PC, Kozlov S, Stewart CL, Lee RT. Abnormal nuclear shape and impaired mechanotransduction in emerin-deficient cells. Journal of Cell Biology. 2005;170(5).

350. Sabatelli P, Lattanzi G, Ognibene A, Columbaro M, Capanni C, Merlini L, et al. Nuclear alterations in autosomal-dominant emery-dreifuss muscular dystrophy. Muscle Nerve. 2001;24(6).

351. Fidziańska A, Hausmanowa-Petrusewicz I. Architectural abnormalities in muscle nuclei. Ultrastructural differences between X-linked and autosomal dominant forms of EDMD. J Neurol Sci. 2003;210(1–2).

352. Vignier N, Mougenot N, Bonne G, Muchir A. Effect of genetic background on the cardiac phenotype in a mouse model of Emery-Dreifuss muscular dystrophy. Biochem Biophys Rep [Internet]. 2019 Sep 1 [cited 2024 Mar 28];19:100664. Available from: /pmc/articles/PMC6630059/

353. Bonne G, Leturcq F, Yaou R Ben. Emery-Dreifuss Muscular Dystrophy. Current Clinical Neurology [Internet]. 2019 Aug 15 [cited 2024 Mar 28];Part F2297:159–74. Available from: https://www.ncbi.nlm.nih.gov/books/NBK1436/

354. Vignier N, Muchir A. An omics view of emery–dreifuss muscular dystrophy. J Pers Med. 2020;10(2).

355. Janssen AFJ, Breusegem SY, Larrieu D. Current Methods and Pipelines for Image-Based Quantitation of Nuclear Shape and Nuclear Envelope Abnormalities. Vol. 11, Cells. 2022.

356. Pho M, Berrada Y, Gunda A, Stephens AD. Nuclear shape is affected differentially by loss of lamin A, lamin C, or both lamin A and C. MicroPubl Biol [Internet]. 2024 [cited 2024 Apr 13];2024. Available from: /pmc/articles/PMC10910297/

357. Veltrop RJA, Kukk MM, Topouzidou K, Didden L, Muchir A, van Steenbeek FG, et al. From gene to mechanics: a comprehensive insight into the mechanobiology of LMNA mutations in cardiomyopathy. Vol. 22, Cell Communication and Signaling. 2024.

358. Hah J, Kim DH. Deciphering Nuclearmechanobiology in Laminopathy. Vol. 8, Cells. 2019.

359. Broers JLV, Peeters EAG, Kuijpers HJH, Endert J, Bouten CVC, Oomens CWJ, et al. Decreased mechanical stiffness in LMNA-/- cells is caused by defective nucleo-cytoskeletal integrity: Implications for the development of laminopathies. Hum Mol Genet. 2004;13(21).

360. Barra HS, Rodriguez JA, Arce CA, Caputto R. A SOLUBLE PREPARATION FROM RAT BRAIN THAT INCORPORATES INTO ITS OWN PROTEINS

[14C]ARGININE BY A RIBONUCLEASE-SENSITIVE SYSTEM AND [14C]TYROSINE BY A RIBONUCLEASE-INSENSITIVE SYSTEM. J Neurochem. 1973;20(1).

361. Gadadhar S, Bodakuntla S, Natarajan K, Janke C. The tubulin code at a glance. J Cell Sci. 2017;130(8).

362. Liu C, Chen Y, Xie Y, Xiang M. Tubulin Post-translational Modifications: Potential Therapeutic Approaches to Heart Failure. Vol. 10, Frontiers in Cell and Developmental Biology. 2022.

363. Ramdas NM, Shivashankar G V. Cytoskeletal control of nuclear morphology and chromatin o1rganization. J Mol Biol. 2015;427(3).

364. Gudimchuk NB, McIntosh JR. Regulation of microtubule dynamics, mechanics and function through the growing tip. Vol. 22, Nature Reviews Molecular Cell Biology. 2021.

365. Caporizzo MA, Prosser BL. The microtubule cytoskeleton in cardiac mechanics and heart failure. Vol. 19, Nature Reviews Cardiology. 2022.

366. Westermann S, Weber K. Post-translational modifications regulate microtubule function. Vol. 4, Nature Reviews Molecular Cell Biology. 2003.

367. Murofushi H. Purification and characterization of tubulin-tyrosine ligase from porcine brain. J Biochem. 1980;87(3).

368. Ersfeld K, Wehland J, Plessmann U, Dodemont H, Gerke V, Weber K. Characterization of the tubulin-tyrosine ligase. Journal of Cell Biology. 1993;120(3).

369. Erck C, Peris L, Andrieux A, Meissirel C, Gruber AD, Vernet M, et al. A vital role of tubulin-tyrosine-ligase for neuronal organization. Proc Natl Acad Sci U S A. 2005;102(22).

370. Lafanechère L, Courtay-Cahen C, Kawakami T, Jacrot M, Rüdiger M, Wehland J, et al. Suppression of tubulin tyrosine ligase during tumor growth. J Cell Sci. 1998;111(2).

371. Mialhe A, Lafanechère L, Job D, Treilleux I, Peloux N, Dumontet C, et al. Tubulin detyrosination is a frequent occurrence in breast cancers of poor prognosis. Cancer Res. 2001;61(13).

372. Kato C, Miyazaki K, Nakagawa A, Ohira M, Nakamura Y, Ozaki T, et al. Low expression of human tubulin tyrosine ligase and suppressed tubulin tyrosination/detyrosination cycle are associated with impaired neuronal differentiation in neuroblastomas with poor prognosis. Int J Cancer. 2004;112(3).

373. Whipple RA, Matrone MA, Cho EH, Balzer EM, Vitolo MI, Yoon JR, et al. Epithelial-to-mesenchymal transition promotes tubulin detyrosination and microtentacles that enhance endothelial engagement. Cancer Res. 2010;70(20).

374. Steinmetz MO, Akhmanova A. Capturing protein tails by CAP-Gly domains. Vol. 33, Trends in Biochemical Sciences. 2008.

375. Badin-Larçon AC, Boscheron C, Soleilhac JM, Piel M, Mann C, Denarier E, et al. Suppression of nuclear oscillations in Saccharomyces cerevisiae expressing Glu tubulin. Proc Natl Acad Sci U S A. 2004;101(15).

376. Bieling P, Kandels-Lewis S, Telley IA, Van Dijk J, Janke C, Surrey T. CLIP-170 tracks growing microtubule ends by dynamically recognizing composite EB1/tubulinbinding sites. Journal of Cell Biology. 2008;183(7).

377. Peris L, Thery M, Fauré J, Saoudi Y, Lafanechère L, Chilton JK, et al. Tubulin tyrosination is a major factor affecting the recruitment of CAP-Gly proteins at microtubule plus ends. Journal of Cell Biology. 2006;174(6).

378. Prota AE, Magiera MM, Kuijpers M, Bargsten K, Frey D, Wieser M, et al. Structural basis of tubulin tyrosination by tubulin tyrosine ligase. Journal of Cell Biology. 2013;200(3).

379. Coquelle FM, Caspi M, Cordelières FP, Dompierre JP, Dujardin DL, Koifman C, et al. LIS1, CLIP-170's Key to the Dynein/Dynactin Pathway. Mol Cell Biol. 2002;22(9).

380. Watson P, Stephens DJ. Microtubule plus-end loading of p150Glued is mediated by EB1 and CLIP-170 but is not required for intracellular membrane traffic in mammalian cells. J Cell Sci. 2006;119(13).

381. Lomakin AJ, Semenova I, Zaliapin I, Kraikivski P, Nadezhdina E, Slepchenko BM, et al. CLIP-170-Dependent Capture of Membrane Organelles by Microtubules Initiates Minus-End Directed Transport. Dev Cell. 2009;17(3).

382. Lee HS, Komarova YA, Nadezhdina ES, Anjum R, Peloquin JG, Schober JM, et al. Phosphorylation controls autoinhibition of cytoplasmic linker protein-170. Mol Biol Cell. 2010;21(15).

383. Nakano A, Kato H, Watanabe T, Min KD, Yamazaki S, Asano Y, et al. AMPK controls the speed of microtubule polymerization and directional cell migration through CLIP-170 phosphorylation. Nat Cell Biol. 2010;12(6).

384. Baulieu EE, Robel P, Schumacher M. Neurosteroids: Beginning of the story. Vol. 46, International Review of Neurobiology. 2001.

385. Compagnone NA, Mellon SH. Neurosteroids: Biosynthesis and function of these novel neuromodulators. Front Neuroendocrinol. 2000;21(1).

386. Shibuya K, Takata N, Hojo Y, Furukawa A, Yasumatsu N, Kimoto T, et al. Hippocampal cytochrome P450s synthesize brain neurosteroids which are paracrine neuromodulators of synaptic signal transduction. In: Biochimica et Biophysica Acta - General Subjects. 2003.

387. Vallée M. Neurosteroids and potential therapeutics: Focus on pregnenolone. Vol. 160, Journal of Steroid Biochemistry and Molecular Biology. 2016.

388. Mellon SH, Griffin LD, Compagnone NA. Biosynthesis and action of neurosteroids. In: Brain Research Reviews. 2001.

389. Strous RD, Maayan R, Weizman A. The relevance of neurosteroids to clinical psychiatry: From the laboratory to the bedside. Vol. 16, European Neuropsychopharmacology. 2006.

390. Luchetti S, Bossers K, Van de Bilt S, Agrapart V, Morales RR, Frajese GV, et al. Neurosteroid biosynthetic pathways changes in prefrontal cortex in Alzheimer's disease. Neurobiol Aging. 2011;32(11).

391. Schverer M, Lanfumey L, Baulieu EE, Froger N, Villey I. Neurosteroids: non-genomic pathways in neuroplasticity and involvement in neurological diseases. Vol. 191, Pharmacology and Therapeutics. 2018.

392. Vallée M, Mayo W, Le Moal M. Role of pregnenolone, dehydroepiandrosterone and their sulfate esters on learning and memory in cognitive aging. In: Brain Research Reviews. 2001.

393. Ritsner MS, Gibel A, Shleifer T, Boguslavsky I, Zayed A, Maayan R, et al. Pregnenolone and dehydroepiandrosterone as an adjunctive treatment in schizophrenia and schizoaffective disorder: An 8-week, double-blind, randomized, controlled, 2-center, parallel-group trial. Journal of Clinical Psychiatry. 2010;71(10).

394. Murakami K, Fellous A, Baulieu EE, Robel P. Pregnenolone binds to microtubule-associated protein 2 and stimulates microtubule assembly. Proc Natl Acad Sci U S A. 2000;97(7).

La borsa di dottorato è stata cofinanziata con risorse del
Programma Operativo Nazionale Ricerca e Innovazione 2014-2020 (CCI 2014IT16M2OP005),
Fondo Sociale Europeo, Azione I.1 “Dottorati Innovativi con caratterizzazione Industriale”

UNIONE EUROPEA
Fondo Sociale Europeo

Ministero dell'Università e della Ricerca